Adaptive Resolution Simulations: Combining Multi-Particle-Collision Dynamics and Molecular Dynamics Simulations for Fluids

Uliana Alekseeva

Summary

In soft matter physics there is a variety of systems where phenomena occur on different time- and length scales which are inherently coupled. Examples of such systems are colloidal suspensions, polymer solutions or biological macromolecules. To simulate such systems, it is necessary to consistently take into account atomistic and hydrodynamic interactions within one computational scheme, which is feasible from the requirements of memory consumption and CPU time usage. The hybrid simulation approach presented in this work solves this problem by coupling of Molecular Dynamics and Multi-Particle Collision dynamics simulations. It allows to change the representation of the molecules composing the fluid on the fly, taking into account the atomistic details where it is needed, while keeping the description of the rest of the fluid on the mesoscale level. Due to the application of such hybrid coupling between fine- and coarse-grained description, it is possible to simulate larger systems for longer times efficiently, while taking into account solvent properties and hydrodynamics.

The main goal of this work is to construct a hybrid description of the solvent in such a way that hydrodynamic interactions are properly accounted for. To reveal the hydrodynamic properties of the hybrid fluid, a number of correlations functions for various systems with different hybrid states were calculated. It was found that transverse current correlation functions related to the viscosity coefficient are equal for all states of the fluid, i.e. pure MD, pure MPC and all mixed state systems. The same applies to the properties of long tile tails in the velocity autocorrelation function, which is influencing the diffusion coefficient of the fluid. Therefore, these results show that the transport properties of the fluid are not altered throughout the hybrid description. In order to verify that hydrodynamics is maintained in the hybrid system, several test flow simulations such as Poiseuille flow, shear flow, and Couette flow were performed. They have shown that the behavior of the hybrid system under flow resembles that of a fluid modeled by a mono-scale method, and it could be shown that the deviation of the velocity profile from the theoretically predicted one is less than 2%.

Although the full thermodynamic equilibrium is impossible due the fundamental differences between MD and MPC methods, the hybrid MD/MPC scheme presented in this work is proved to be a very promising approach for simulation of complex fluids. By applying the restraining force in the buffer zone it is possible to maintain dynamical equilibrium throughout the hybrid system. It was shown that the transport properties of the hybrid fluid are conserved across the transition zone between the two fluid rep-

resentations in one simulation, allowing the consistent description of hydrodynamics in the whole coupled system. By changing the representation of the molecules on the fly, the hybrid MD/MPC approach allows to couple within a single simulation atomistic and mesoscale representation of fluids, providing a valuable tool for many problems in soft matter science.

Zusammenfassung

Viele Phänomene in den komplexen Flüssigkeiten, die man im Rahmen der Physik der weichen Materie erforscht, finden auf verschiedenen Zeit- und Längenskalen statt. Beispiele für solche Systeme sind Suspensionen von Kolloiden, Polymerlösungen oder biologische Makromoleküle. Um solche Systeme simulieren zu können, müssen numerische Modelle entwickelt werden, die sowohl atomistische als auch hydrodynamische Wechselwirkungen beschreiben können und deren Kosten für CPU-Zeit oder Speicherbedarf nicht übermäßig sind. Der in dieser Arbeit dargestellte Hybrid-Simulaitons-Ansatz löst dieses Problem durch eine Kopplung zwischen Molekulardynamik- und Multi-Particle-Collision Dynamics Simulation. In diesem Simulationsschema ist es möglich, die Darstellung von Teilchen on the fly anzupassen, damit die detaillierte atomistische Beschreibung nur in einem begrenzten Raumbereich notwendig ist und für den Rest der Flüssigkeit ein kostengünstiges Mesoskalen-Modell verwendet wird. Dank der Anwendung einer solchen Hybrid-Kopplung ist es möglich, größere Systeme für längere Zeiten effektiv zu simulieren und dabei die Eigenschaften und die Hydrodynamik des Lösungsmittels adäquat zu berücksichtigen.

Hauptziel dieser Arbeit ist die Entwicklung einer Hybrid-Beschreibung des Lösungsmittels, die hydrodynamische Wechselwirkungen zwischen gelösten Teilchen richtig erfasst. Um hydrodynamische Eigenschaften der Hybrid-Flüssigkeit zu analysieren, werden mehrere Korrelationsfunktionen für verschiedene Systeme in unterschiedlichem Hybrid - Zustand gerechnet. Es zeigt sich, dass transversale Stromkorrelationsfunktionen, die mit der Viskosität verbunden sind, gleich für alle Hybrid-Zustände der Flüssigkeit sind, d.h. reine MD, reines MPC und alle Systeme mit gemischtem Zustand. Dasselbe gilt für Eigenschaften des Long-time tails der Geschwindigkeits-Korrelationsfunktion, die den Diffusionskoeffizienten beeinflusst. Diese Ergebnisse zeigen, dass die Transporteigenschaften in der Hybrid-Beschreibung nicht geändert werden. Um zu prüfen, dass Hydrodynamik des Hybrid - Systems erhalten ist, werden mehrere einfache Strömungs - Simulationen, wie z.B. Poiseuille Strömung, Scherströmung oder Couette Strömung durchgeführt. Sie zeigen, dass das Strömungsverhalten der Hybrid - Flssigkeit das Strömungsverhalten der reinen Flüssigkeit reproduziert, und dass das Geschwindigkeitsprofil, das aus Simulationsdaten erhalten wird, weniger als 2% von der Theorie abweicht.

Ein vollständiges thermodynamisches Gleichgewicht ist in der Kopplung aufgrund fundamentaler Unterschiede zwischen MD und MPC Modellen nicht erreichbar. Das in dieser Arbeit dargestellte Hybrid-MD/MPC-Verfahren erweist sich aber als eine vielver-

sprechende Methode für die Simulation von komplexen Flüssigkeiten. Die Anwendung einer externen Kraft zwischen den gekoppelten Systemen ermöglicht einen stationären Zustand mit konstanter Dichte im gesamten Hybrid-System. Es zeigt sich, dass die Transporteigenschaften der Hybrid-Flüssigkeit über den Kopplungsbereich zwischen den verschiedenen Flüssigkeitsmodellen erhalten sind, was eine konsequente Beschreibung der Hydrodynamik im ganzen System ermöglicht. Durch die adaptive Anpassung der Moleküle ermöglicht der Hybrid-MD / MPC Ansatz eine Kopplung zwischen einer atomistischen und mesoskaligen Darstellung von Flüssigkeiten und bietet ein wertvolles Werkzeug für viele Probleme im Gebiet der Physik der weichen Materie.

Contents

List of Figures

Frequently used symbols and notations

MD	Molecular Dynamics
LJ	Lennard-Jones
MPC	Multi-Particle Collision dynamics
LGA	Lattice Gas Automata method
LB	Lattice Boltzmann method
SPH	Smoothed-Particle Hydrodynamics
QM/MD	Quantum-Mechanical/Molecular-Mechanical method
DSMC	Direct Simulation Monte-Carlo
MP2C	Massively Parallel Multi-Particle Collision dynamics
m	mass of the particle
σ	diameter of the particle
ϵ	potential well depth of the LJ potential
λ	mean free path
Δt	MPC time step
α	rotation angle
a	cell size
N_c	number of particles in a cell
M	average number of particles in a cell
$\sigma_{\alpha\beta}$	stress tensor
ρ	density
D	diffusion coefficient
η	viscosity
P	pressure
μ	chemical potential
$w(x)$	switching function
$g(r)$	pair distribution function
$c_{vv}(t)$	velocity autocorrelation function
$S(\mathbf{k}, w)$	structure factor
$J_{\alpha\beta}(\mathbf{k},\mathrm{t})$	current correlation function
$J_l(\mathbf{k},\mathrm{t})$	longitudinal current correlation function
$J_{\alpha\beta}(\mathbf{k},\mathrm{t})$	transverse current correlation function

1. Introduction

Complex molecular systems are typically characterized by properties which are inherently multi-scale. In complex fluids such as polymer solutions, colloidal suspensions, biological macromolecules and membranes atomistic and hydrodynamic phenomena are strongly coupled: the dynamics is often governed by the hydrodynamics of the solvent; the long time behavior of the whole fluid depends on the microscopic interaction between solvent molecules and the constituents of the embedded macromolecule. Examples of such phenomena are self-assembling or diffusion in a complex geometry. Since the phenomena of interest cover a very broad range of length (from Angstroms to micrometer) and time scales (from femtoseconds to milliseconds), computer simulations of such systems with atomistic representation of the solvent are very costly in time.

Numerical modeling of complex fluid systems is very important, since it provides a bridge between experiments and general theoretical considerations. Although experimental techniques are sophisticated and theoretical descriptions are well developed, some specific aspects of those systems are only possible to be investigated via simulations. With a properly constructed model one can test proposed theories and provide some reference parameters for experiments. Sometimes, if the experiment is rather costly, it is necessary to perform preliminary simulations, to estimate the potential outcome of the forethought experiment.

To bridge the gap between micro- and macroscales, several mesoscale techniques have been developed in recent years. In particular, Lattice Gas Automata (LGA) [13,14], Lattice Boltzmann (LB) [15,16], Smoothed-Particle Hydrodynamics (SPH) [17,18], Dissipative Particles Dynamics (DPD) [19–21], Direct Simulation Monte Carlo (DSMC) [22–24], Fluid Particle Dynamics [25], and Multi-Particle Collision dynamics (MPC) [26–28, 30, 31] have been investigated. All these simulation techniques utilize one common principle: in order to obtain the hydrodynamic behavior of the solvent on a mesoscale, the whole detailed atomistic description of the interaction between solvent molecules is not needed. As long as mass and momentum conservation laws are satisfied, the dynamics of the solvent can be simplified. The different methods listed above differ in the way the solvent dynamics is simplified.

For the problems under study which require a detailed description in a certain area of the system, the hybrid methods can be used, where two or more levels of system representation are combined. The main idea of such simulations is to use an expensive

high-resolution model within the regions in which it is needed, while using a simpler, less expensive method, for the rest of the computational domain. Over the last ten years there has been much effort to devise such methods for various systems coupling different algorithms. As examples of such hybrid schemes one can mention the Quantum-Mechanical / Molecular-Mechanical method (QM/MM) [53], coupling between full atomistic Molecular Dynamics simulations (MD) [55] and coarse-grained or continuum fluid descriptions [61, 64], and coupling of Direct Simulation Monte Carlo(DSMC) with continuum fluid methods [58, 59].

Hybrid schemes are designed for systems, in which physical processes occurring on various length and time scales are strongly coupled. Therefore, it is crucially important to consider these processes simultaneously, but the separation of scales are so large, that the single algorithm can not cover it: the mesoscale method alone can not resolve important atomistic details, but the full atomistic description is computationally too expensive. For example, if one wishes to model colloidal particles in a solvent via Molecular Dynamics simulations, one would need 100-1000 solvent molecules for every colloidal particle, depending on how tightly packed the particles are. Thus, in order to simulate several thousand colloids in solution, still a tiny block of material, one has to track more than a million entities. With modern parallel computers such simulations are possible, but only for time scales up to nanoseconds. If the hydrodynamic phenomena are of interest, the simulations should be run on the mesoscopic time scales, thousands of time longer than the longest molecular simulations can provide.

The main idea of a hybrid scheme is to keep a detailed description where it is needed while using a less expensive coarse-grained method in the rest of the system. In this work we couple Molecular Dynamics simulations (MD) on a atomistic scale with a mesoscale approach. Since the hybrid scheme is designed for mesoscale systems, e.g. macromolecules dissolved in a solution, it is important to resolve the atomistic interactions between solute and solvent particles. For the solvent at a whole, the detailed microscopic information is superfluous and unnecessary, because we are interested in the collective motion of a fluid.

In the ideal case, the mesoscale surroundings does not bring any influence to the inner subsystem with detailed description: particles of the latter do not “notice” the presence of the outer “bath”. On the other hand, hydrodynamic interactions throughout the system should not be disturbed, that means that thermal fluctuations are to be taken into account. To assure this coherence of the different representation regions, there has to be free particle exchange between them.

In this work the multi-particle collision method is chosen as a coarse-grained description of a fluid. First, it is convenient to construct a coupling between MD and MPC by allowing the solvent particle to change a location within the whole system and adapt

its "identity" accordingly: in the MD region it is an MD particle, in the MPC region it is an MPC particle, in the buffer layer between them it is a particle with mixed "identity". Second, it is possible to calculate transport properties of the MPC analytically with great accuracy, which allows to adjust the hydrodynamic properties of mesoscale medium to the properties of the given microscopic representation.

The aim of this work is to investigate the hybrid MD/MPC algorithm. The challenge is to construct a hybrid approach in a such a way that each of two coupled regions are not distorted, i.e. particles inhabiting one region should not "feel" the presence of the other. In order to achieve this, there should be a free exchange of the particles through the buffer zone. Since the smoothness of the transition is crucial, the important aspect in the present work is to elucidate to what extent hydrodynamics is maintained across the coupling zone between two representations including transport properties, hydrodynamic interactions and hydrodynamic modes. Also mechanical, thermodynamical and thermal equilibrium throughout the whole system should be assured.

The structure of the present work is as follows. In chapter 2 two particle-based simulation methods, i.e. Molecular Dynamics and multi-particle collision dynamics, are described. The main features, implementation and transport properties of both models are discussed. MPC is a mesoscale simulation method, and a short overview of other mesoscale simulations techniques also can be found in this chapter.

In chapter 3 the hybrid MD/MPC scheme is presented. After a short overview of other hybrid simulation techniques, two different approaches to the construction of a particle-based hybrid model, energy-based and force-based, are discussed. Both MD and MPC models should describe the same fluid, that is why the main characteristics of these models ought to be matched. Due to the fundamental differences between MD and MPC fluids, the equilibrium throughout whole hybrid system can not be achieved without external restraining force in the buffer zone.

In chapter 4 structure and dynamics of the hybrid fluid is investigated. To understand the physics occurring in the buffer zone of the hybrid system, we first studied a set of systems exclusively composed of hybrid particles with a fixed "identity". A number of static and dynamic correlation functions calculated for this set of systems is presented and discussed.

The details of implementation can be found in chapter 5. The implementation of the hybrid MD/MPC scheme was made on the basis of the program MP2C (Massively Parallel Multi-Particle Collision Dynamics).

In chapter 6 several test simulations with the hybrid system are presented. In order to check whether hydrodynamic interactions between regions with different representations

are altered by coupling, the following flow simulations were performed: poiseuille flow, shear flow and couette flow. The results obtained for the hybrid system are compared with theory and analogous simulations with systems consisting only of MPC or MD particles.

Conclusions and future directions can be found in chapter 7.

2. Particle-based fluid models

Two particle-based simulation approaches for fluids, Molecular Dynamics (MD) and multi-particle collision dynamics methods (MPC) will be presented in this chapter. Molecular Dynamics simulations are used to describe the fluid on an atomistic level, with pair interactions between all particles. MPC is a mesoscale simulation method, with a coarse-grained description of the fluid. The main features, implementation and transport coefficient of both methods will be discussed.

2.1. Molecular Dynamics simulations

In Molecular Dynamics simulations [6], particles' motion is governed by classical (Newton's) equations of motion. The equations of motion may be written down in various ways, for example in Hamiltonian form:

$$\begin{aligned} \dot{\mathbf{q}}_i &= \delta\hat{H}/\delta\mathbf{p}_i, \\ \dot{\mathbf{p}}_i &= -\delta\hat{H}/\delta\mathbf{q}_i, \end{aligned} \tag{2.1}$$

where $i = 1, ..., N$, $\mathbf{p}_i$ and $\mathbf{q}_i$ are momentum and coordinate of ith particle, and $\hat{H}$ is the Hamiltonian. The solution of the equations of motion (2.1) yields the full dynamics of the system.

For MD simulations, the following aspects have to be taken into account:

- A model for the interactions between system components (atoms, molecules, surfaces etc.) is needed, i.e., the Hamiltonian has to be specified. The model has to be tested against experiment and theory: it should reproduce or approximate experimental results, like distribution functions or phase diagrams, and it should obey certain fundamental laws, for example energy and momentum conservation. It is often assumed that the particles interact only pairwise, which reduces greatly the computational effort and the implementation work.

- The integration algorithm has to be specified, which updates particle coordinates and velocities from a time t to $t + \delta t$. The equations of motion (2.1) are integrated using a finite difference method, and the time step δt has to be properly chosen to guarantee stability of the integrator.

- A statistical ensemble has to be chosen, where thermodynamic quantities like pressure, temperature or the number of particles are controlled. In MD simulations, the natural choice is the microcanonical ensemble (NVE) for systems without external potentials or the canonical ensemble (NVT) if the temperature of the system is controlled.

2.1.1. Hamiltonian

An interaction model should provide the complete description of the system from the physical point of view. All simulated objects (atoms, molecules, surfaces etc.) and the way they interact are to be defined. If a precise knowledge of interactions between the components of the system is available, then the model captures the main features of some observables.

In classical simulations particles are described as point-like centers which interact via pair- or multi-body potentials. Instead of a detailed description of atoms and their electron dynamics, one uses an effective representation, where the main features like the hard core of a particle, electric multipoles or internal degrees of freedom are modeled by a set of parameters or analytical functions, which depend on the distance from the particle.

An MD system is completely determined by its Hamiltonian $\hat{H} = \hat{H}_0 + \hat{H}_1$, where $\hat{H}_0$ is the internal part of the Hamiltonian, given as

$$\hat{H}_0 = \sum_{(i=1)}^{N} \frac{\mathbf{p}_i^2}{2m_i} + \sum_{i<j}^{N} u(\mathbf{q_i}, \mathbf{q_j}) + \sum_{i<j}^{N} u^{(3)}(\mathbf{q_i}, \mathbf{q_j}, \mathbf{q_k}) + \dots , \tag{2.2}$$

where m_i is the mass of the i-th particle, and u and $u^{(3)}$ are pair and three-body interaction potentials. $\hat{H}_1$ is an external part, which can include time dependent effects and external forces.

There are some important issues to be noted for the potentials from the computational point of view. First, it is a big difference between a pair potential and a multi-body potential. If the system has no constrains, interactions are usually described by pair potentials, which is quite simple to implement into a program. If one have to take into account multi-body potentials, the counting of interacting partners becomes much more complex and the execution of the program slows down dramatically. Only if the interacting partners are known in advance (for example, for torsion and bending potentials in a molecule), the calculation can be performed effectively by a neighbor list or by introducing a special way of indexing the molecular sites.

The second aspect is the spatial extent of the potential. If the potential drops to zero faster than r^{-d}, where r is the distance between two particles and d the dimension of the system, it is called short ranged, otherwise it is long ranged. To understand the difference between them better, consider the integral

$$I = \int^{infty} \frac{d^d r}{r^n} = \begin{cases} \infty & , \quad n \leq d \\ finite & , \quad n > d \end{cases} . \tag{2.3}$$

Hence, to calculate the potential energy for a particle interacting via a long range potential, one has to take into account contributions from all particles in the universe, while the analogous calculation for a particles interacting via short range potentials could be confined in a certain area. The possibility to neglect all interactions beyond this area (usually modeled as a sphere of radius r_c, which is called the cut-off radius) is a major advantage of short range potentials.

To compensate for the neglect of explicit calculations, one may use a long range correction to the potential

$$U_{lrc} = 2\pi N \rho^* \int_{R_c}^{\infty} dr\ r^2 g(r) u(r), \tag{2.4}$$

where ρ^* is the number density of the particles in the system and $g(r)$ is the pair distribution function. The whole short range potential may then be written as

$$U = \sum_{i<j}^{N} u(r_{ij} | r_{ij} < R_c) + U_{lrc}. \tag{2.5}$$

The intermolecular pair potential often separates in a natural way into two parts: a strong repulsion at very close distances and a smoothly varying attraction [1, 2, 7]. This separation is employed in many empirical representations of the intermolecular forces. A steep repulsive potential represent finite diameters of the particles. A very simple approximation, hard-sphere potential, models the interaction by the infinitely steep repulsion at very close distances

$$U_{ij} = \begin{cases} 0 & , \quad r_{ij} \geq \sigma \\ \infty & , \quad r_{ij} < \sigma \end{cases} , \tag{2.6}$$

where σ characterizes the size of the particle and r_{ij} is the distance between ith and jth particle.

The attractive part of the potential arises from van der Waals' interactions. For neutral particles these are the London forces caused by induced dipole interactions. Fluctuations of the electron distribution of a particle give rise to fluctuating dipole moments, which on average compensate to zero. But the instantaneous created dipoles induce also dipoles

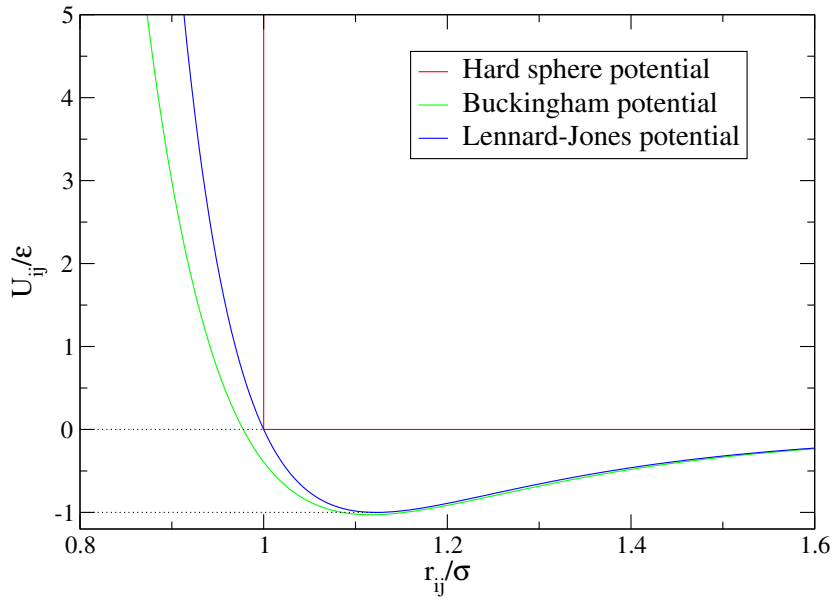

Figure 2.1.: *Comparison between a hard sphere-, a Buckingham-, and a Lennard-Jones potentials. The hard sphere potential models the interaction between particles i and j by the infinitely steep repulsion at the distances less than the particle diameter σ. The Buckingham and Lennard-Jones potential take into account both repulsive and attractive part of the interaction. Though the description of the repulsion by the exponential function (as in the Buckingham potential) is more physical, the Lennard-Jones form of the potential is often more convenient due to the simple physical interpretation of its parameters: ϵ is a minimum potential energy and σ is the diameter of the particle.*

on neighbored particles which attract each other with the force proportional r^{-6}. Two common forms of the intermolecular potential are the Buckingham potential

$$U_{ij}^{B} = A\exp(-Br_{ij}) - \frac{D}{r_{ij}^{6}}, \tag{2.7}$$

and the Lennard-Jones (LJ) potential

$$U_{ij} = 4\epsilon\left(\left(\frac{\sigma}{r_{ij}}\right)^{12} - \left(\frac{\sigma}{r_{ij}}\right)^{6}\right). \tag{2.8}$$

The parameters A, B, D, ϵ, and σ characterize the interaction. For the Lennard Jones potential the parameters have a simple physical interpretation: ϵ is a minimum potential energy, located at $r = 2^{1/6}\sigma$ and σ is the diameter of the particle, since for $r < \sigma$ the potential becomes repulsive. The comparison between hard sphere, Buckingham, and Lennard-Jones potentials is shown in the Fig. 2.1. Although the r^{-12} repulsive term has no theoretical justification, the LJ potential often gives a reasonable approximation

of a true potential. In our simulations particles are interacting via the Lennard-Jones potential.

2.1.2. Integrator

The accuracy and stability of simulation results depend strongly on the integration scheme. Since the finite difference method is the approximation of continuous propagation of the system in time, there are always errors not only due to a finite number representation, but also due to a approximative nature of the integrator itself. The requirements for the integrator therefore are:

- *accurate*, i.e. it should approximate the true trajectory very well. It could be checked with simple system, for which an analytical solution exist.
- *stable*, i.e. energy should be conserved, and small perturbation should not lead to instabilities,
- *robust*, i.e. it should be possible to use large time steps to propagate the system through phase space efficiently.

The choice of the time step can depend on the integration scheme, but it has to be significantly smaller then the typical time taken for a molecule to travel its own size. Since δt can not be too large, it imposes restrictions on the accessibility of long times and large length scales. Usually, the classical Molecular Dynamics simulations cover the range of $1-10nm$ and $1-10^4ps$. Since equations of motion (2.1) are time-reversible and conserves the phase-space volume, an integration algorithm ought to be time-reversible and symplectic in order to be stable and accurate in large-scale and long-time MD simulations.

Perhaps the most widely used method for integrating the equations of motion, a modification of which is also used in this work, is the Verlet algorithm [6, 12]. Using the explicit form of the Hamiltonian (2.2) and the fact that force acting on the ith particle is $\mathbf{f}_i = -\nabla_i u$ one can easily rewrite the equations of motion the system (2.1) in the form

$$m_i \ddot{\mathbf{r}}_i = m_i \mathbf{a}_i = \mathbf{F}_i, \tag{2.9}$$

where $\mathbf{a}_i$ is the acceleration and $\mathbf{r}_i$ is the Cartesian coordinate of the ith particle. The Verlet method is a direct solution of these equations. There are various forms of the Verlet algorithm, which differ in how and which order positions $\mathbf{r}_i(t)$, velocities $\mathbf{v}_i(t)$ and forces $\mathbf{F}_i(t)$ are calculated. The modification used in this work is the so-called velocity Verlet algorithm. First, the velocities at mid-step are computed using

$$\mathbf{v}_i(t + \frac{\delta t}{2}) = \mathbf{v}_i(t) + \frac{\delta t}{2}\mathbf{a}_i(t). \tag{2.10}$$

Then the new positions are calculated using the mid-step velocities

$$\mathbf{r}_i(t + \delta t) = \mathbf{r}_i(t) + \mathbf{v}_i(t + \frac{\delta t}{2})\delta t. \tag{2.11}$$

The forces and accelerations at time $t + \delta t$ follow then

$$\mathbf{a}_i(t + \delta t) = \frac{1}{m_i}\mathbf{F}_i(t + \delta t) = \frac{1}{m_i}\sum_{j \neq i}\mathbf{F}_{ij}(t + \delta t), \tag{2.12}$$

where $\mathbf{F}_{ij}$ is a pair force between particles i and j. Finally,the velocity are

$$\mathbf{v}_i(t + \delta t) = \mathbf{v}_i(t + \frac{\delta t}{2}) + \frac{\delta t}{2}\mathbf{a}_i(t + \delta t). \tag{2.13}$$

At this point, the kinetic energy at time $t + \delta t$ is available. The potential energy at this time can be evaluated in the force loop.

It is understandable that the performance of the particle dynamics simulation strongly depends on the available computer facilities. The first studies using the MD simulation technique were performed in 1957 by B.J.Adler and T.E.Wainwright [10] who modeled the phase transition of a system of hard spheres. In this early simulation, which was run at an IBM-704, up to 500 particles could be simulated, for which 500 collisions per hour could be calculated. Taking into account 200000 collisions for a production run, these simulations lasted for more than two weeks.

The first simulation which was applied to atoms interacting via a continuous potential was performed by A.Rahman in 1964 [11]. In this case, a model system for Argon was simulated. The interactions were modeled by a Lennard-Jones potential and the equations of motion were integrated with a finite difference scheme. This work can be considered as cornerstone for dynamical calculations. It was the first simulations where an exact method (within numerical precision) was used to calculate dynamical quantities like the autocorrelation function and transport coefficients, like the diffusion coefficient for a realistic system. The calculation were performed for 864 particles on a CDC 3600, where the propagation of all particles for one time step took about 45 seconds. That means, the calculation of 50000 time steps then took more than three weeks. Today on a standard PC this calculation may be done within one hour.

With the development of faster and bigger massively parallel computer architectures the accessible time and length scales increase. It is now possible to probe systems of more than 10^6 particles on time scales of $\sim 100ns$. Recent algorithmic and hardware developments have allowed MD studies to be extended to multi-million atom systems [51, 52].

Current supercomputers, such as for example the "JUQUEEN" at Research Center Jülich, assemble more then 400000 cores and its performance reaches 5.0 Petaflops. However, the challenge for MD, and other applications, is to achieve an efficient scaling, i.e., the simulations are limited by the parallel efficiency of the MD algorithms.

Classical Molecular Dynamics methods are nowadays applied to a huge class of problems, e.g. properties of liquids, defects in solids, fracture, surface properties, friction, molecular clusters and biomolecules. Due to the large area of applicability, there are a lot of different codes developed by many groups.

2.2. Transport properties of fluids

The transport properties of simulated fluids are of crucial importance in our case. The proper hydrodynamics should be maintained over the whole hybrid system, and it is the transport properties, which define how the fluid responses to fluctuations or external perturbations. For example, the diffusion coefficient relates the particle flux to a concentration gradient, while the shear viscosity is a measure of the shear stress induced by an applied velocity gradient.

Diffusion is a process whereby an initially nonuniform concentration profile is smoothed in the absence of flow. It is caused by the molecular motion of the particles. In the phenomenological macroscopic approach, according to the Fick's law, the diffusion flux is proportional to the negative gradient of concentration:

$$\mathbf{j} = -D\nabla c(\mathbf{r}), \tag{2.14}$$

where D, the constant of proportionality, is the diffusion coefficient. We are interested in a special case of self-diffusion of identical molecules.

Combining Fick's law (2.14) with the continuity equation

$$\frac{\partial c(\mathbf{r},t)}{\partial t} + \nabla \mathbf{j}(\mathbf{r},t) = 0, \tag{2.15}$$

one obtains the diffusion coefficient

$$D = \lim_{t\to\infty} \frac{1}{6t} \Big\langle \big[\mathbf{r}_i(t) - \mathbf{r}_i(0)\big]^2 \Big\rangle, \tag{2.16}$$

where $\mathbf{r}_i(0)$ and $\mathbf{r}_i(t)$ are the initial and current coordinates of the ith particle [1]. This relation was first derived by Einstein. Using this expression, one can directly measure the diffusion coefficient D in a simulation. For every particle, the distance travelled in

time t is measured, and then the mean square displacement is plotted as a function of time t:

$$\left\langle \Delta r(t)^2 \right\rangle = \frac{1}{N} \sum_{i=1}^{N} \Delta \mathbf{r}_i(t)^2. \tag{2.17}$$

The slope of this function yields the diffusion coefficient.

Shear viscosity reflects the resistance of a fluid to shear flows, where adjacent layers of the fluid move parallel to each other with different velocities. Each layer of the fluid will move with a different velocity, and friction between them will give rise to a force resisting their relative motion. If the flow is perpendicular to the axis y, then according to Newton's formula the tangential stress is proportional to the velocity gradient

$$\tau = \eta \frac{\partial u}{\partial y}, \tag{2.18}$$

where η, the proportionality constant, is the shear viscosity.

As for the diffusion, the expression connecting the viscosity with microscopic parameters can be obtained:

$$\eta = \lim_{t \to \infty} \frac{1}{2tk_BTV} \left\langle \left[\xi_{\alpha\beta}(t) - \xi_{\alpha\beta}(0) \right]^2 \right\rangle, \tag{2.19}$$

where k_B is the Boltzmann constant, T is the temperature, V is the volume and

$$\xi_{\alpha\beta} = \sum_{i=1}^{N} r_{i\alpha} p_{i\beta}, \tag{2.20}$$

where $\alpha, \beta \in \{x, y, z\}, \alpha \neq \beta$.

Using the Green-Kube relations [1, 6, 7] one can rewrite the expressions for diffusion and viscosity as integrals of an appropriate time correlation function. For the diffusion D it is the velocity correlation function

$$D = \frac{1}{3} \int \langle \mathbf{v}(t)\mathbf{v}(0) \rangle \, dt. \tag{2.21}$$

For the shear viscosity η such an expression can be written as

$$\eta = \frac{1}{k_BTV} \int \langle \sigma_{\alpha\beta}(t)\sigma_{\alpha\beta}(0) \rangle \, dt, \tag{2.22}$$

where $\sigma_{\alpha\beta}(t)$ are the off-diagonal elements of the microscopic stress tensor

$$\sigma_{\alpha\beta} = \sum_{i=1}^{N} \frac{p_{i\alpha} p_{i\beta}}{m} + \sum_{j>i}^{N} r_{ij\alpha} f_{ij\beta}. \tag{2.23}$$

The diffusion coefficient and viscosity for the LJ fluid were calculated numerically via correlation function (CF) approach and via mean-squared-displacement method (MSD) [67, 68]. In the CF approach, the transport coefficients are obtained from the Green-Kubo relation for the decay of correlations 2.21, 2.22. In the MSD approach, the transport coefficients are calculated from the appropriate Einstein relations 2.16, 2.19 that show how the squared displacement of the appropriate variables increases in time. All simulation runs were performed on NVT ensembles consisting of 616 LJ particles. The LJ potential was truncated at 2.5 σ. The runs were allowed to equilibrate for 100,000 time steps, after which the information was collected for the next 1,000,000 steps.

In order to improve the statistics, the multiple origin method was applied. It is especially important for the viscosity calculation. As it can be seen from the expression 2.21, 2.22, 2.16, and 2.19, the self-diffusion coefficient is a single-particle property and can be calculated separately for every particle. On the contrary, the viscosity is the system property and a sum over all particles is required to obtain a single value of $\sigma_{\alpha\beta}$ in the Eqs. 2.22 or ξ in the Eq. 2.19. Diffusion computations are inherently more accurate because they include N times more data. Implementation of multiple time origins yields considerable improvement of the statistics without significant increase of the computational time. This is done by overlapping the initiation of calculation, so that the statistics for the requirable values are collected in parallel way (Fig. 2.2). To gain maximal statistical advantage, these parallel calculations are separated by enough time steps in order to assure the independence of the consecutive time origins. Additional statistical accuracy is obtained by the averaging over the Cartesian coordinates. This gives the additional factor of three for D and the factor six for η.

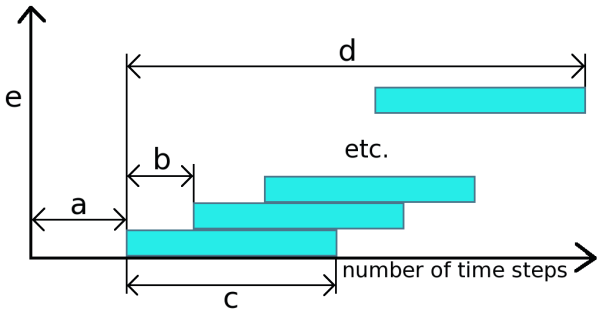

Figure 2.2.: *Scheme of data collection using a multiple origin method, including equilibration(a), separation of time origins (b), data accumulation (c), total simulation length (d), and number of time origins (e).*

2.3. Meso-Scale Simulation Methods

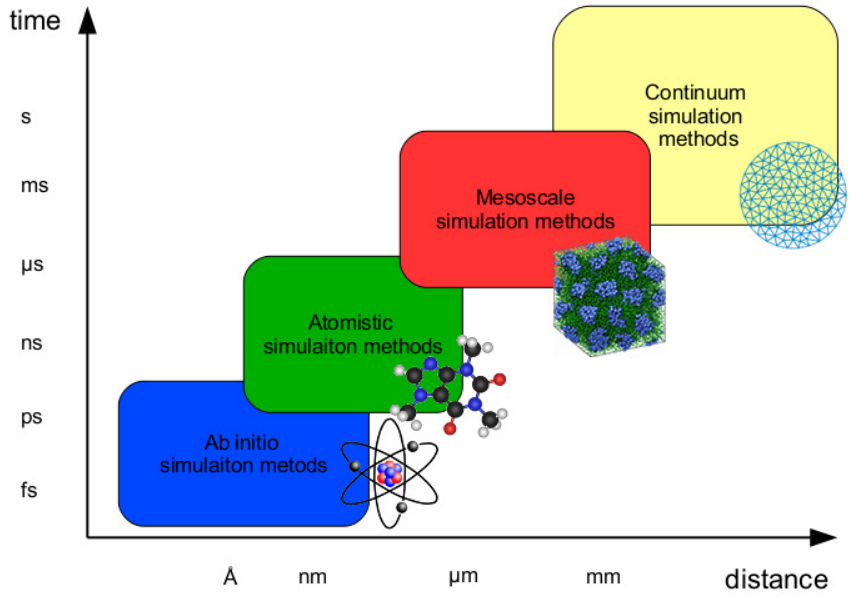

Figure 2.3.: *The length- and timescales of different simulation methods. The more detailed a simulation technique operates, the smaller is the accessibility of long times and large length scales.*

Various simulation algorithms are applied depending on the length and time scale if interest (Fig. 2.3). If we want to take into account quantum mechanical phenomena, we can use ab initio methods, but our simulation will be limited to Angstroms in space and femtoseconds in time. If quantum details are not important, we can use an atomistic model and then we will be able to reach micrometers and microseconds. With a continuum description we can simulate systems of centimeters size, but all molecular-level details will be lost. It is understandable that the more details of the system the description contains, the smaller system it allows to simulate in practice.

To cover the gap between atomistic and continuum simulation methods, a variety of mesoscale techniques have been developed. Such methods are necessary for the simulation of complex fluids, where molecular-level details are still important, but the interesting phenomena occur on much larger time and length scales. Examples of such fluids are colloidal suspensions, polymer solutions, amphiphilic mixtures, and all other fluids, where phenomena of interest cover the range from nano- to micrometers. For these systems, atomistic methods do not suit because they contain too many details and require too small time steps, and therefore can not reach the required times, but the

continuum description is also not applicable, because it ignores all microscopic details. The ideal algorithm for such fluids should contain essential features of the microscopic physics, be computationally efficient, easy to implement in complex geometries, easy to parallelize, and it could be use to predict fluid properties, test physical theories, and provide required information for experiments.

The most common mesoscale algorithms are Lattice Boltzman (LB) [15, 16], Dissipative Particle Dynamics (DPD) [19–21], Direct Simulation Monte Carlo (DSMC) [22], and Multi-Particle Collision Dynamics (MPC) [26, 27]. All of them mimic somehow the behavior of fluids on large length and long time scales. They average out irrelevant microscopic details, while keeping the essential features of the microscopic physics. Essentially all these algorithms are alternative ways to solve Navier-Stokes equation or its generalizations. This is because hydrodynamic equations are expressions for the local conservation laws of mass, momentum and energy, complemented by relations which reflect some microscopic aspects. Frisch et al. [13] demonstrated that discrete algorithms can be constructed which recover the Navier-Stokes equation in the continuum limit as long as these conservation laws are obeyed and space is discretized in a sufficiently symmetric manner.

The first model of this type was a cellular gas automaton, called the Lattice-Gas-Automaton (LGA) [13, 14]. The algorithm consist of particles which hop between cites of a regular lattice. The particles may experience collisions only on the lattice sites, collisions occur when more than one particle jump to the same cite. The collision process is controlled by a set of rules chosen in such a way that the number of particles and the local momentum of the system are conserved. The required macroscopic properties are obtained by averaging their microscopic equivalents on subregions of the lattice. The Lattice Boltzmann method (LB) [15,16], which follows the evolution of the single-particle probability distribution at each cite, is a natural generalization of this approach. LB solves the Boltzmann equation on a lattice with a small set of discrete velocities determined by the lattice structure. Disadvantages of both methods are the lack of Galilean invariance and anisotropy caused by the presence of the discreet lattice.

To avoid lattice artifacts, Hoogerbrugge and Koelman devised a new method, combining features of Molecular Dynamics simulations and Lattice Boltzmann, the so-called Dissipative Particle Dynamics [19]. It was subsequently reformulated and slightly modified by Espanol [20] to ensure the proper thermal equilibrium state. Like in MD, in the DPD method particles move in continuous space and discrete time steps. Particles represent whole molecules or fluid regions, rather than single atoms. Since atomistic details are not considered as relevant for the processes addressed, the particles internal degrees of freedom are integrated out and replaced by simplified pairwise dissipative and random forces, so as to conserve momentum locally and thus ensure correct hydrodynamic behavior.

The Direct Simulation Monte Carlo method uses probabilistic (Monte Carlo) approach to solve Boltzmann's equation for modeling rarefied gas flows [22–24]. Originally it was developed for dilute gas flow in engineering and in space science. The molecular motion and the collision process are uncoupled over the time interval Δt by the repeated application of the following procedure: first, all the molecules are moved a certain distances according to their velocities and Δt. Second, the simulation box is divided into cells of volume V_c, each with $N_c \approx 20 - 40$ particles. Third, within each cell, certain number M_c of pairs of particles are chosen to collide with a probability P_c, which depends on a some physical model.

Malevanets and Kapral introduced in 1999 [26, 27] a mesoscale simulation technique called Multi-Particle Collision Dynamics (MPC), which can be considered as a generalization of DSMC. The difference between the MPC and the DSMC algorithms is that in the former particles contained in cells experience one conjoint "collision". The way of performing this effective "collisions" can differ, the most common rule is to rotate relative velocities around a random axis. The MPC method will be discussed thoroughly in the next sections.

Except for conservation laws and symmetry requirements, there are relatively few constraints on the structure of mesoscale algorithms. However, the constitutive relations and the transport coefficients depend on the details of the algorithm, so that the temperature and density dependencies of the transport coefficients can be quite different from those of real gases or liquids. Yet this is not a problem as long as the functional forms of the resulting hydrodynamics equations are correct. The mapping to real system is achieved by tuning the relevant characteristic numbers, such as Reynolds and Peclet numbers, to those of a given experiment. Sometimes it can be quite difficult, because changing one parameter, for example the mean free path, usually affects all transport coefficients in different ways, and it may happen that a given mesoscale algorithm is not at all suited for a given application.

2.4. Multi - Particle Collision Dynamics

In this work Multi-Particle Collision Dynamics is used for the coarse-grained description of fluid. MPC is a mesoscale simulation method for fluid flow, which was introduced by Malevanets and Kapral in 1999 [26]. The solvent is modeled by a large number N of point-like particles of mass m which move in continuous space with continuous velocities. The algorithm consists of streaming and collision steps (Fig. 2.4). In the streaming step, the coordinates $\mathbf{r}_i(t)$ of all solvent particles at time t are updated according to

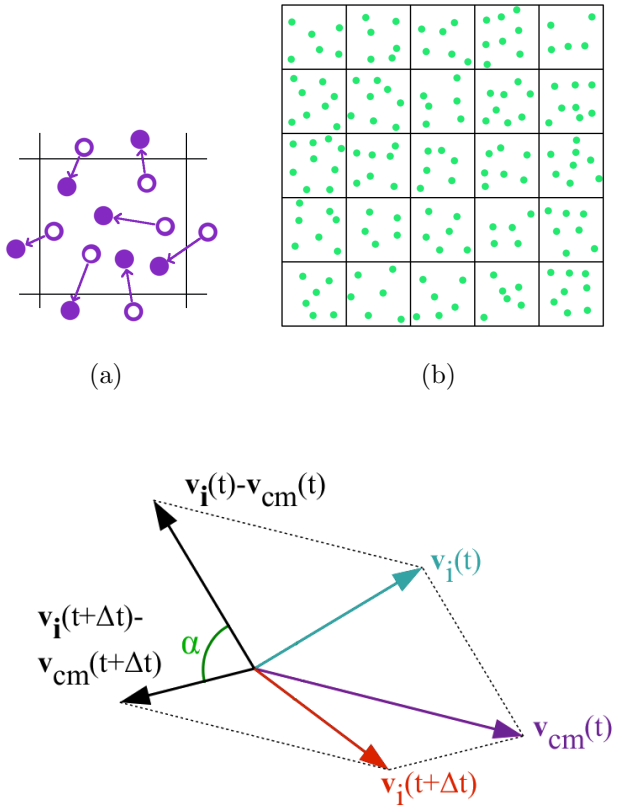

Figure 2.4.: *Diagram of the MPC dynamics: streaming step (a), particles are sorted into collision cells (b), and rotation of the particle velocity relative to the center-of-mass velocity.*

$$\mathbf{r}_i(t + \Delta t) = \mathbf{r}_i(t) + \mathbf{v}_i(t)\Delta t, \tag{2.24}$$

where Δt is the value of the discretized time step.

In order to define collisions, particles are sorted into cells, and they interact only with members of their own cell. Typically, the system is coarse-grained into cells of a regular, usually cubic, grid with lattice constant a. In practice, lengths are often measured in units of a, which corresponds to setting $a = 1$. The average number of particles per cell M is typically chosen to be between 3 and 20. The actual number of particles in a cell at a given time fluctuates. The collision step consists of a random rotation $\hat{R}$ of the relative velocities, with respect to the center-of-mass velocity of the cell, of all the particles in the collision cell:

$$\mathbf{v}_i(t+\Delta t) = \mathbf{v}_{cm}(t) + \hat{R}[\alpha; \mathbf{n}_\mu(t)]\{\mathbf{v}_i(t) - \mathbf{v}_{cm}\}, \tag{2.25}$$

where μ indicates the cell where the ith particle is located, $\hat{R}$ is the rotation matrix and $\mathbf{v}_{cm}(t)$ is the center-of-mass velocity of the N_c particles, which are located in the collision box μ at time t

$$\mathbf{v}_{cm}(t) = \frac{1}{N_c}\sum_{j\in\mu}\mathbf{v}_j(t). \tag{2.26}$$

All particles in the cell are subject to the same rotation, but the rotations in different cells and at different times are statistically independent. In three dimensions, various schemes for the random collisions are possible [26, 33, 43]. The one employed in this work consist in choosing a random axis $\mathbf{n}_\mu(t)$ for each box, around which the relative velocities are rotated by a fixed angle α. In this case the rotation matrix is

$$\hat{R}\big[\alpha; \mathbf{n}_\mu(t) = (n_x, n_y, n_z)\big] = \begin{pmatrix} n_x^2 + (1-n_x^2)c & n_x n_y(1-c) - n_z s & n_x n_z(1-c) + n_y s \\ n_x n_y(1-c) + n_z s & n_y^2 + (1-n_y^2)c & n_y n_z(1-c) - n_z s \\ n_x n_z(1-c) - n_y s & n_y n_z(1-c) + n_z s & n_z^2 + (1-n_z^2)c \end{pmatrix}, \tag{2.27}$$

where $c = \cos(\alpha)$, $s = \sin(\alpha)$, and the Cartesian coordinates of unit vector $\mathbf{n}_\mu$ are defined as

$$n_x = \sqrt{1-\theta^2}\,\cos\phi,\ n_y = \sqrt{1-\theta^2}\,\sin\phi,\ n_z = \theta, \tag{2.28}$$

where ϕ and θ are uncorrelated random numbers, which are taken from uniform distribution in the intervals $[0 : 2\pi]$ and $[-1, 1]$, respectively.

In its original form [26], the MPC algorithm was not Galilean invariant. This is most pronounced al low temperatures or small time steps, where the mean free path $\lambda = \Delta t\sqrt{k_B T/m}$ is smaller than the cell size a. If the particle travels a distance between collisions which is small compared to the cell size, essentially the same particles collide repeatedly before other particles enter the cell or some of the participating particles leave the cell. For small λ, a large number of particles remain correlated over several time steps. This leads to a breakdown of the molecular chaos assumption - i.e., particles become correlated and retain information of previous collisions.

Ihle and Kroll [28,30] showed that Galilean invariance can be restored by performing a random shift of the entire computational grid before every collision step. The grid shift constantly groups particles into new collision neighborhoods, the collision environment no longer depends on the magnitude of an imposed homogeneous flow field, and the resulting hydrodynamics equations are Galilean invariant for arbitrary temperatures. This

procedure is implemented by shifting the computational grid by the random vector with components uniformly distributed in the interval $[-a/2, a/2]$ before the collision step.

A feature of the MPC algorithm is that the dynamics depends on the time step Δt. In contrast to MD method, which approximates the continuous-time dynamics of a system, the time step does not need to be small. MPC defines a discrete-time dynamics which has been shown to yield the correct long-time hydrodynamics. One consequence of the discrete dynamics is that the transport coefficients depend explicitly on Δt.

The simplicity of the MPC algorithm allowed to derive analytic expressions for the transport coefficients which are valid for both large and small mean free paths [31,32,38, 42]. This is usually very difficult to achieve for other mesoscale particle-based algorithms: the difference between values measures in simulations and predicted theoretically can reach up to 50%. For MPC the agreement is usually about 1%.

2.5. Transport coefficients of MPC

2.5.1. Diffusion coefficient

The self-diffusion coefficient D of particle i is defined by

$$D = \lim_{t\to\infty} \frac{1}{2dt} \big\langle [\mathbf{r}_i(t) - \mathbf{r}_i(0)]^2 \big\rangle. \tag{2.29}$$

Using the discrete Green-Kubo relation [30,31,43] this expression can be rewritten as

$$D = \frac{\Delta t}{2d} \big\langle \mathbf{v}_i(0)^2 \big\rangle + \frac{\Delta t}{d} \sum_{k=1}^{\infty} \big\langle \mathbf{v}_i(k\Delta t)\mathbf{v}_i(0) \big\rangle, \tag{2.30}$$

where $t_k = k\Delta t$ denotes the discrete time of the kth collision. The average $\langle ... \rangle$ comprises both, averaging over the orientation of the rotation axis $\mathbf{n}_\mu$ and the distribution of velocities. The two are independent. To evaluate the expression, the velocity autocorrelation function is required [44]. An exact evaluation of the correlation function is difficult or even impossible, because it would imply that the full correlated dynamics of the particles can be calculated analytically. However, an approximate expression can be derived.

In a first step, the average over the random orientation of the rotation axis is performed. Since the orientation is isotropic in space, all odd moments of the cartesian components of $\hat{R}$ vanish and the second moments are given by $\langle \hat{R}_\beta \hat{R}_{\beta'} \rangle = \delta_{\beta\beta'}/d$. Thus,

$$\big\langle \hat{R}\{\Delta\mathbf{v}\} \big\rangle = \frac{1}{d}(1 + 2\cos\alpha)\Delta\mathbf{v}, \tag{2.31}$$

which yields

$$\big\langle \mathbf{v}_i(t+\Delta t)\mathbf{v}_i(t)\big\rangle = \big\langle \mathbf{v}_{cm}(t)\mathbf{v}_i(t)\big\rangle + \frac{1}{d}(1+2\cos\alpha)\big\langle \Delta\mathbf{v}_i(t)\mathbf{v}_i(t)\big\rangle. \tag{2.32}$$

To evaluate the correlation function with the center-of-mass velocity, we apply the molecular chaos assumption, which assumes that different particles are independent, i.e.

$$\big\langle \mathbf{v}_j(t)\mathbf{v}_i(t')\big\rangle = \delta_{ij}\big\langle \mathbf{v}_j(t)\mathbf{v}_i(t')\big\rangle \tag{2.33}$$

and

$$\big\langle \mathbf{v}_{cm}(t)\mathbf{v}_i(t)\big\rangle = \frac{1}{N_c}\sum_{k=1}^{N_c}\big\langle \mathbf{v}_k(t)\mathbf{v}_i(t)\big\rangle = \frac{1}{N_c}\big\langle \mathbf{v}_i(t)^2\big\rangle. \tag{2.34}$$

Hence,

$$\big\langle \mathbf{v}_i(t+\Delta t)\mathbf{v}_i(t)\big\rangle = \left[1-\frac{2}{d}(1-\cos\alpha)\left(1-\frac{1}{N_c}\right)\right]\big\langle \mathbf{v}_i(t)^2\big\rangle. \tag{2.35}$$

To account for particle number fluctuations, this expression has to be averaged applying the Poisson distribution $P(N_c) = e^{-M}M^{N_c}/N_c!$. Since we consider a particular particle on a cell, the probability distribution of finding $N_c - 1$ oder particles in that cell is $N_c P(N_c)/M$. Averaging over this distribution gives [32, 43]

$$\sum_{N_c=1}^{\infty} e^{-M}\frac{M^{N_c-1}}{(N_c-1)!}\left(1-\frac{1}{N_c}\right) = \frac{1}{M}\Big(e^{-M}+M-1\Big). \tag{2.36}$$

Thus,

$$\big\langle \mathbf{v}_i(t+\Delta t)\mathbf{v}_i(t)\big\rangle = (1-f)\big\langle \mathbf{v}_i(t)^2\big\rangle, \tag{2.37}$$

with

$$f = \frac{2(1-\cos\alpha)}{dM}\Big(e^{-M}+M-1\Big). \tag{2.38}$$

This expression reduces to (2.35) for $M \gg 1$. In fact, we can replace N_c by M already for $N_c > 5$.

More generally, iteration yields

$$\big\langle \mathbf{v}_i(k\Delta t)\mathbf{v}_i(0)\big\rangle = (1-f)^k\big\langle \mathbf{v}_i(0)^2\big\rangle. \tag{2.39}$$

Using this, the diffusion coefficient can be written as

$$D = \frac{\Delta t\big\langle \mathbf{v}_i(0)^2\big\rangle}{d}\left(\frac{1}{f}-\frac{1}{2}\right) = \frac{\Delta t k_B T}{m}\left(\frac{1}{f}-\frac{1}{2}\right) \tag{2.40}$$

or, substituting the expression for f,

$$D = \frac{k_B T \Delta t}{2m}\left(\frac{dM}{[1-\cos\alpha](M-1+e^{-M})} - 1\right). \tag{2.41}$$

As it was shown by M.Ripoll at al. [37], the simulation results for the velocity correlation function are in close agreement with the theoretical prediction for large mean-free paths λ, when particles are exposed to a nearly random collision environment at every step. For small collision times, the same particles collide several times with each other, which build up correlations, so the molecular chaos assumption doesn't work any more. Calculations of the diffusion coefficient reflect the same behavior. For $\lambda/a > 0.5$, the numerical results for D agree very well with the analytical expression, whereas for smaller λ values, a somewhat large D is obtained.

2.5.2. Shear viscosity of MPC: kinetic contribution

Two complementary approaches have been used to derive the transport coefficients of the MPC fluid. The first is an equilibrium approach which utilizes a discrete projection operator formalism to obtain Green-Kubo relations which express the transport coefficients as a sum over the corresponding autocorrelation functions. This approach was first utilized by Malevanets and Kapral [27], and later extended by Ihle, Kroll and Tützel [30, 31, 38] to include collisional contributions and arbitrary rotation angles.

The other approach uses kinetic theory to calculate the transport coefficients in a stationary non-equilibrium situation such as shear flow. The first application of this approach to MPC was presented in [28], where the collisional contribution to the shear viscosity for large numbers of paticle per cell M, where particle number fluctuations can be ignored, was calculated. This scheme was later extended by Kikuchi et al. [32] to include fluctuations of M, and then used to obtain expressions for the kinetic contributions to shear viscosity and thermal conductivity [36]. This non-equilibrium approach will be described in this section.

We consider a fluid with an imposed shear $\dot{\gamma} = \partial u_x(y)/\partial y$. On average, the velocity profile is given by $\mathbf{v} = (\dot{\gamma}y, 0, 0)$. The dynamic shear viscosity η is the proportionality constant between the velocity gradient $\dot{\gamma}$ and the frictional force acting on a plane perpendicular to y

$$\sigma_{xy} = \eta\dot{\gamma}, \tag{2.42}$$

where σ_{xy} is the off-diagonal element of the viscous stress tensor. This is the experimental definition of the viscosity [6]. For the MPC fluid, the stress tensor is composed of a kinetic and collisional contribution [27, 28, 32, 42, 43], which implies that the viscosity

$\eta = \eta_{kin} + \eta_{col}$ consist of a kinetic η_{kin} and collisional η_{col} part too. The kinetic contribution to the stress tensor comes from transverse momentum transport by the flow of fluid particles, i.e. $\sigma_{xy} = -$(flux of x-momentum crossing a plane of constant y).

During the streaming step Δt, particles will cross this plane only if $|v_y \Delta t|$ is greater than the distance to the plane. Therefore, the stress tensor can be written

$$\begin{aligned}\sigma_{xy} = &- \frac{\rho}{\Delta t}\int_{-\infty}^{\infty} dv_x \int_{-\infty}^{0} dy \int_{-y/\Delta t}^{\infty} dv_y v_x P(v_x - \dot{\gamma} y, v_y) \\ &+ \frac{\rho}{\Delta t}\int_{-\infty}^{\infty} dv_x \int_{0}^{\infty} dy \int_{-\infty}^{-y/\Delta t} dv_y v_x P(v_x - \dot{\gamma} y, v_y),\end{aligned} \tag{2.43}$$

where $P(v_x, v_y)$ is the velocity probability distribution of particles in the rest frame of fluid. By making the change of variable $v_x' = v_x - \dot{\gamma} y$, and changing the order of integration this reduces to [32]

$$\sigma_{xy} = \rho\left(\frac{\dot{\gamma}\Delta t}{2}\langle v_y^2\rangle - \langle v_x v_y\rangle\right), \tag{2.44}$$

It is important to note that it is not the Maxwell-Boltzmann distribution, since we are in a non-equilibrium steady state where the shear has induced correlations between v_x and v_y. As a consequence, $\langle v_x v_y\rangle$ is nonzero. To determine the behavior of $\langle v_x v_y\rangle$, the effect of streaming and collisions are calculated separately. During streaming, particles which arrive at y_0 with positive velocity v_y have started from $y_0 - v_y \Delta t$; these particles bring a velocity component v_x which is smaller than that of particle originally located at y_0. On the other hand, particles starting out at $y > y_0$ with negative v_y bring a larger v_x. The velocity distribution is therefore sheared by the streaming, so that $P^{after}(v_x, v_y) = P^{before}(v_x + \dot{\gamma} v_y \Delta t, v_y)$. Averaging $v_x v_y$ over this distribution gives [32]

$$\begin{aligned}\langle v_x v_y\rangle^{after} &= \int_{-\infty}^{\infty} dv_x \int_{-\infty}^{\infty} dv_y v_x v_y P(v_x + \dot{\gamma} v_y \Delta t, v_y) \\ &= \langle v_x v_y\rangle - \dot{\gamma}\Delta t \langle v_y^2\rangle,\end{aligned} \tag{2.45}$$

where the superscript denotes the quantity after streaming. The streaming step therefore reduces correlations by $-\dot{\gamma}\Delta t\langle v_y^2\rangle$, making v_x and v_y increasingly anti-correlated.

The collision step redistributes momentum between particles and tends to reduce correlations. Making the assumption of molecular chaos, i.e. that the velocities of different particles are uncorrelated, and averaging over the directions of the rotation axis, one finds [32, 42, 43]

$$\langle v_x v_y\rangle^{after} = f\langle v_x v_y\rangle^{before}, \tag{2.46}$$

where

$$f = \left\{ 1 + \frac{N_c - 1}{5N_c} \big[2\cos(2\alpha) - 2\cos\alpha - 4 \big] \right\}. \tag{2.47}$$

The number of particles in a cell, N_c is not a constant, and density fluctuations have to be included. As in the previous section, the probability to find N_c uncorrelated particles in a given cell is given by the Poisson distribution, $P(N_c) = exp(-M)M_c^N/N_c!$; the probability of a given particle being in a cell together with $N_c - 1$ others is $N_c P(N_c)/M$. Taking an average over this distribution gives

$$f = \left\{ 1 + \frac{M - 1 + \exp(-M)}{5M} \big[2\cos(2\alpha) - 2\cos\alpha - 4 \big] \right\}. \tag{2.48}$$

The difference between this result and just replacing N_c by M in 2.47 is small, and only important for $M \leq 4$. One sees that $\langle v_x v_y \rangle$ is first modified by streaming and then multiplied by a factor f in the subsequent collision step. In the steady state, it therefore oscillates between two values. Using 2.45, 2.47, and 2.48, we obtain the self-consistency condition

$$(\langle v_x v_y \rangle - \dot{\gamma}\Delta t \langle v_y^2 \rangle) f = \langle v_x v_y \rangle. \tag{2.49}$$

Solving for $\langle v_x v_y \rangle$, assuming equipartition of energy $\langle v_y^2 \rangle = k_B T/m$, and substituting into 2.44, we have

$$\sigma_{xy} = \frac{\dot{\gamma} M \Delta t k_B T}{m} \left(\frac{1}{2} + \frac{f}{1-f} \right). \tag{2.50}$$

Inserting the result into the definition of the viscosity 2.42 yields the expression for the kinetic contribution of the viscosity for the three-dimentional MPC fluid

$$\eta_{kin} = \frac{M k_B T \Delta t}{2a^3} \left\{ \frac{5M}{\big(M - 1 + \exp(-M)\big)\big[2 - \cos\alpha - \cos(2\alpha)\big]} - 1 \right\}. \tag{2.51}$$

2.5.3. Shear viscosity of MPC: collisional contribution

To calculate the collisional contribution to the shear viscosity, let us consider a collision cell of linear size a with a shear flow $u_x(y) = \dot{\gamma} y$. Since the collisions occur in a shifted grid, they cause a transfer of momentum between neighboring cells of the original unshifted reference frame [28,31,32]. The system is divided into two subcells by a plane at $y = h$, where $0 \leq h \leq a$. Consider now the momentum transfer due to collisions across the plane $y = h$. If we assume a homogeneous distribution of particles in the collision cell, the mean velocities in the upper ($y > h$) and the lower partitions are

$$\mathbf{u}_1 = \frac{1}{n_1}\sum_{i=1}^{n_1}\mathbf{v_i} \tag{2.52}$$

and

$$\mathbf{u}_2 = \frac{1}{n_2}\sum_{i=n_1+1}^{n}\mathbf{v_i}, \tag{2.53}$$

where $n_1 = n(a-h)/a$ and $n_2 = nh/a$, and n is the number of particles in the cell. As the average distance between the subcell centers is $\Delta y = a/2$ the shear rate is

$$\dot{\gamma} = \frac{\partial u_x}{\partial y} = \frac{u_{1x} - u_{2x}}{\partial y} = \frac{2n}{a(n-n1)}(u_{1x} - v_{cmx}), \tag{2.54}$$

where v_{cmx} denotes the x-component of the center-of-mass velocity of the cell.

The momentum transfer between the two subcells reads

$$\sigma_{xy} = -\frac{\sum_i^{n_1} p_{ix}(t+\Delta t) - \sum_i^{n_1} p_{ix}(t)}{a^2\Delta t}. \tag{2.55}$$

Averaging over an isotropic distribution of the rotation axis gives [32]

$$\sigma_{xy} = \frac{m}{a^2\Delta t}\left(\frac{2}{3}n_1(1-\cos\alpha)(u_{1x} - v_{cmx})\right). \tag{2.56}$$

Using Eqs. 2.54, 2.55, and the definition of the viscosity 2.42 we obtain

$$\eta_{col} = \frac{mn_1(n-n1)}{3a^2n\Delta t}(1-\cos\alpha). \tag{2.57}$$

As number of the particles in the cell is generally small we must fluctuations in the particle density. The numbers of the particles in the subcells n_1 and n_2 are binomially distributed. Averaging over them yields [32]

$$\eta_{col} = \frac{m(1-\cos\alpha)}{3a^2\Delta t}(n-1)\left(\frac{h}{a}\right)\left(1-\frac{h}{a}\right). \tag{2.58}$$

Using the Poisson distribution to average over n gives [32]

$$\eta_{col} = \frac{m(1-\cos\alpha)}{3a^2\Delta t}(M-1+\exp(-M))\left(\frac{h}{a}\right)\left(1-\frac{h}{a}\right). \tag{2.59}$$

Finally, averaging over all planes $0 \le h \le a$ yields

$$\eta_{col} = \frac{m(M-1+\exp(-M))}{18a\Delta t}\big[\cos(\alpha)-1\big]. \tag{2.60}$$

Various numerical experiments show very good agreement between the viscosities determined by analytical expressions 2.51 and 2.60 and calculated using simulation results. For small mean free paths λ, the viscosity is determined by the collisional contribution, whereas for $\lambda \gg 1$, the kinetic contribution dominates. Since the analytical expression for η_{kin} has been derived with an assumption of molecular chaos, which is not true for small λ, there are small deviations between simulation and theoretical results for $\lambda \ll 1$.

3. Hybrid MD/MPC model

In this chapter the way to couple two different particle-based descriptions of fluids, Molecular Dynamics (MD) and Multi-Particle Collision dynamics (MPC), will be presented. The basic idea is to connect these two methods via a transition region, where particles change slowly their identity. Since the coupled method is supposed to model complex fluids, for which microscopic details including thermal fluctuations play a crucial role, it is very important to assure the free exchange of particles over the borderline.

The particle moving from one representation to another should not only feel no borders while moving to the transition zone, but it also should be in equilibrium with its actual surrounding. A necessary condition is equilibrium between the different regimes, i.e. theidentity of certain thermodynamic quantities, such as chemical potential, pressure, and temperature. However, due to fundamental differences of the methods, this can not be assured just by matching parameters for the different simulation schemes. That means the coupling method should maintain two different representations with different chemical potentials and pressure in thermodynamical equilibrium. All these aspects will be discussed in the following chapter.

3.1. Hybrid simulation methods

A wide variety of scientific and engineering problems include multiple scales. Traditional approaches which cover only one scale in space and time have proven to be insufficient, even with the largest supercomputers, because of the range of scales and the large number of variables involved. Hence, there is a growing need to develop systematic modeling and simulation approaches for multiscale problems. Although multiscale modeling is quite recent area of investigation, there are already many schemes [53–60, 64], covering a broad range of various scales, using diverse approaches, and applied for very different kinds of systems.

There are two ways of combining different scales for one system: sequential and simultaneous. In a sequential approach separate simulations at the different levels are performed; then the information obtained from the simulation is passed on to the next lever of the resolution in the form of external parameters. But there are a wide variety of problems where the physical phenomena on the various scales are strongly coupled

and therefore can not be separated into a series of independent calculations. Simulations of such systems require concurrent coupling of length scales, where two (or more) levels of descriptions are combined in one system, providing the information exchange "on the fly" during the simulation run. Such schemes are often called "hybrid", and over last ten years there has been much effort to develope such methods [53–60, 64].

One of the most widely used multiscale algorithms is the Quantum-Mechanical / Molecular-Mechanical method (QM/MM) [53, 54]. It has become a popular approach for modeling local electronic events in large systems with thousands of atoms. QM methods are used to describe the active site where chemical reactions or electronic excitations occur, and MM methods are employed to capture the effect of environment on the active site. The QM/MM concept was introduced in 1976 by Warshel and Levitt [53] who presented the first semi-empirical QM/MM model and applied it to an enzymatic reaction. This approach found wide acceptance only much later, in the 1990s. By now it is established as a valuable tool for modeling large biomolecular systems, but it is also often applied to study processes in explicit solvent and to investigate large inorganic/organometallic and solid-state systems [54].

To overcome the limits imposed by MD methods, the coupling between MD and continuum models was developed. The pioneering simulations in this area were performed by Kohlhoff [55], where classical atomistic and continuum elastic models were coupled to successfully model the directional cleavage anisotropy of a BCC crystal. The key problem with coupling atomistic and continuum models of matter is finding way to connect these conceptually very different descriptions. Atomic positions need to be mapped onto a continuous displacement field, and energy calculations from interatomic potentials in the atomistic region and constitutive laws in the continuum region need to be harmonized. Such methods have been applied to many systems, for example to study the interaction of dislocations with grain boundaries [56] and the effect of grain orientation on fracture [57].

A particle-continuum hybrid method with another particle model was developed by A.L.Garcia et al. [58, 59]. The particle algorithm is Direct Simulation Monte Carlo (DSMC), a molecular-level scheme based on the Boltzmann equation. The continuum algorithm is based on the Landau-Lifshitz Navier-Stokes (LLNS) equations, which incorporate thermal fluctuations into macroscopic hydrodynamics by using stochastic fluxes. To achieve bi- directional dynamic coupling between the particle and continuum regions, the continuum solver provides state-based boundary conditions to the particle subdomain, while the particle solver provides flux-based boundary conditions for the continuum subdomain. This scheme simulates the dynamics of a compressible fluid with thermal fluctuations.

An example of the coupling of more than two levels of description simultaneously is the method presented in [60] to simulate light-induced phenomena in soft matter. The absorption of light by soft (bio-)materials initially causes photophysical or photochemical molecular processes which are highly local in space and time. These fast quantum-mechanical events often trigger much slower, macroscopically observable phenomena. The connection between the quantum level and the mesoscopic one was made by bringing together non-adiabatic ab initio Molecular Dynamics, classical Molecular Dynamics, and coarse grained simulation technique. This method was applied to model light-induced phase transition on a liquid crystal containing the azobenzene photo-switch.

Another very interesting way is to couple different level of resolution within a unified Molecular Dynamics simulation scheme. The advantage is the possibility to achieve large time and length scale while retaining the full chemical details only in the region of interest. Such a multiscale technique is the adaptive resolution molecular dynamic scheme (AdResS) [61, 64]. In AdResS, a high resolution all-atom region is coupled to a coarse-grained particle reservoir. This method is particular well suited to situations where the full chemical details are only important within a few nanometers from the solvated macromolecule. The remaining solvent molecules, that are present to maintain equilibrium with the bulk solution, can be represented by single coarse-grained beads. The coupling leads to the correct concentration fluctuations within the small full-atom region, making the all-atom region an "effective" open boundary system. This approach was used to calculate solvation free energies of aqueous mixtures.

All these different methods have some common issues:

- *handshaking*. The two models need to interact at the border that separates two regions. How do each of the models react to having an artificial surface where we switch to using the other model?
- *validation*. Given any particular hybrid scheme it has to be validated against the scheme with higher resolution.
- *selection*. How do we select which regions are to be treated by which model?

In the present work we will investigate the coupling between molecular dynamics simulation and the Multi-Particle Collision dynamics.

3.2. Energy-based and force-based hybrid schemes

The basic idea for going from one model to another utilized in the present work is to introduce a transition region between two representations, where the particles slowly change their "identity" (Fig. 3.1). When the particle is in the one of two "pure" regions,

it is equilibrated with its surroundings. When the particle moves through the buffer zone, it also should be in equilibrium with its actual surroundings, adapting itself to the change of the representation. The natural way to construct such a coupling is the energy-based approach, where a smooth space dependent function interpolates between the two Hamiltonians corresponding to the two force fields. The idea of a hybrid scheme formulated in terms of a global Hamiltonian was introduced in [65] in 2013.

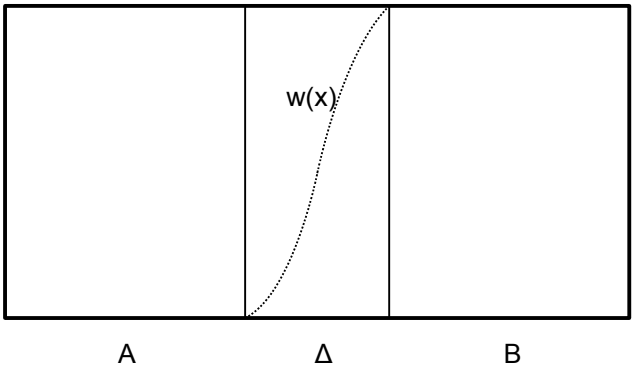

Figure 3.1.: *Schematic picture of the partitioning of space in regions with different representations* **A** *and* **B**, *and transition region* Δ. *The smooth transition from one representation to another is allowed by the switching function* $w(x)$.

3.2.1. Energy-based hybrid scheme

Let us consider a hybrid scheme of two methods, A and B, each describing interactions between atoms via pairwise potentials U^A and U^B, respectively. The Hamiltonian of the "pure" system A consisting of N_A particles can be written as

$$H^A = \sum_{i=1}^{N_A} \frac{\mathbf{p}_i^2}{2m_i} + \sum_{i=1}^{N_A} U_i^A, \tag{3.1}$$

where potential of the ith particle is defined as

$$U_i^A \equiv \frac{1}{2} \sum_{j \neq i}^{N_A} U^A\big(|\mathbf{r}_i - \mathbf{r}_j|\big). \tag{3.2}$$

Analogously, the Hamiltonian of the "pure" system B is

$$H^B = \sum_{i=1}^{N_B} \frac{\mathbf{p}_i^2}{2m_i} + \sum_{i=1}^{N_B} U_i^B, \tag{3.3}$$

where

$$U_i^B \equiv \frac{1}{2}\sum_{j\neq i}^{N_B} U^B\big(|\mathbf{r}_i - \mathbf{r}_j|\big). \tag{3.4}$$

The "mixed resolution" Hamiltonian H is defined as

$$H = \sum_i \frac{\mathbf{p}_i^2}{2m_i} + \sum_i \Big\{ w_i U_i^A + (1-w_i) U_i^B \Big\}, \tag{3.5}$$

where the coupling parameter $w_i = w(\mathbf{r}_i)$ is introduced, which depends on the position of the particle. The coupling parameter $w(\mathbf{r})$ varies between 1 (system with potential U^A) and 0 (system with potential U^B), intermediate values define a hybrid region.

Using the "mixed" Hamiltonian one can derive the force acting on the ith particle

$$\mathbf{F}_i = \sum_{j\neq i} \left\{ \frac{w_i + w_j}{2}\mathbf{F}_{ij}^A + \Big(1 - \frac{w_i + w_j}{2}\Big)\mathbf{F}_{ij}^B \right\} - \big[U_i^A - U_i^B\big]\nabla_i w_i. \tag{3.6}$$

The first term of the Eq.(3.6) contains weighted sum of pairwise forces and is antisymmetric with respect to an exchange of the particle indices, satisfying therefore Newton's third law. The second term, $\mathbf{F}_i^{dr} \equiv -\big[U_i^A - U_i^B\big]\nabla w(\mathbf{r}_i)$, introduces a drift force in the buffer region which violates Newton's third law and momentum conservation. The presence of this force causes pressure and density inhomogeneities. At the equilibrium, the drift force is balanced by the pressure gradient across the buffer zone given by $\nabla P = \rho\langle \mathbf{F}^{dr}(\mathbf{r})\rangle$, where ρ is the density.

In order to compensate this drift force, the "mixed" Hamiltonian has to be modified:

$$\hat{H} = H - \sum_i \Delta H(w(\mathbf{r}_i)). \tag{3.7}$$

The compensation term changes the drift force to

$$\hat{\mathbf{F}}_i^{dr} \equiv -\left[U_i^A - U_i^B - \frac{d\Delta H(w)}{dw}\bigg|_{w=w(\mathbf{r}_i)} \right]\nabla w(\mathbf{r}_i). \tag{3.8}$$

If we wish to compensate a pressure gradient across the buffer region, we need to assure that $\nabla P = \rho\langle \hat{\mathbf{F}}^{dr}\rangle \equiv 0$ or

$$\frac{d\Delta H(w)}{dw}\bigg|_{w=w(\mathbf{r}_i)} \equiv \big\langle [U_i^A - U_i^B] \big\rangle_{\mathbf{r}_i}. \tag{3.9}$$

If one wishes to correct density inhomogeneities, a different compensation term has to be taken:

$$\Delta H(w(\mathbf{r}_i)) \equiv \Delta\mu(w(\mathbf{r}_i)), \tag{3.10}$$

where $\Delta\mu$ is the difference in the chemical potential across the hybrid region.

3.2.2. Force-based hybrid scheme

The other way to construct a coupling is the force-based approach [61–64]. Again, the hybrid system again consists of two regions, each filled by particles interacting via pair potentials U^A and U^B (Fig. 3.1). In the "pure" systems A and B, force acting between two particles i and j can be written as gradient of the corresponding potential

$$\mathbf{F}_{ij}^A = -\nabla U_{ij}^A, \quad \mathbf{F}_{ij}^B = -\nabla U_{ij}^B. \tag{3.11}$$

For the hybrid system, the "mixed" force becomes

$$\mathbf{F}_{ij} = w(\mathbf{r}_i)w(\mathbf{r}_j)\mathbf{F}_{ij}^A + \big(1 - w(\mathbf{r}_i)w(\mathbf{r}_j)\big)\mathbf{F}_{ij}^B. \tag{3.12}$$

Since $\mathbf{F}_{ij}^A = -\mathbf{F}_{ji}^A$ and $\mathbf{F}_{ij}^B = -\mathbf{F}_{ji}^B$, the mixed force $\mathbf{F}_{ij}$ is also antisymmetric with respect to an exchange of particles indicies, and Newton's third law is fulfilled.

It should be mentioned that the force given in the Eq.(3.12) cannot be expressed as a derivative of a Hamiltonian. Which means that for particles from the transition region, the energy is not only not conserved, but even not defined. However, in such a scheme the strict definition of a potential is not required. The change of resolution can be interpreted in terms of similarity with a geometrically induced first order phase transition with an associated latent heat, and the has have to be removed by a local thermostat.

Considering the different representations as different phases, the question of equilibrium between different regimes can be formulated in terms of the differences of the chemical potentials and pressure characterizing each resolution. In general, the values of chemical potentials and pressures in the "pure" systems A and B are not the same and the phase equilibrium conditions

$$T^A = T^B,\ \mu^A = \mu^B,\ P^A = P^B, \tag{3.13}$$

which demand the equality of the temperatures, chemical potentials and pressures in the co-existing phases, are not satisfied. The violation of these conditions causes a flux of particles between regions with different representation and the whole system is inhomogeneous. To prevent such a behavior, an external force can be introduced to compensate for the drift of the particles, which is derived either from the gradient of the pressure

$$\mathbf{F}^{ext}(\mathbf{r}) = \frac{1}{\rho}\nabla P(\mathbf{r}) \tag{3.14}$$

or from a gradient of the chemical potential

$$\mathbf{F}^{ext}(\mathbf{r}) = -\nabla\mu(\mathbf{r}). \tag{3.15}$$

Added to the "mixed" forces defined in Eq.(3.12), it should compensate for any drift caused by the different resolutions, making the density profile uniform throughout the whole hybrid system.

Since for the MPC system the Hamiltonian is not defined, the hybrid MD/MPC scheme in the present work uses the force-based approach to construct a coupling.

3.3. Matching the systems

In the present work we construct a hybrid MD/MPC algorithm. In the region with a detailed representation (MD) particles interact via pairwise Lennard-Jones potential, in the rest of the system a mesoscale MPC approach is used. But before we couple two different methods to a one hybrid algorithm, we have to be sure that they describe the same fluid. Often, if the MPC approach is used to model the solvent, it is only dynamically similar to the physical system, i.e. the relevant dimensionless numbers (e.g. Peclet, Reynolds, Schmidt, Knutsen numbers, etc.) are kept equivalent [66]. Since in our case the hydrodynamics is of crucial importance, the transport coefficients, i.e. viscosity and diffusion coefficient are also needed to be matched.

There are five independent parameters to be specified in MPC simulations: the cell size a, the time step Δt, the particles mass m_{MPC}, the average number of the particles in a cell M and the rotation angle α. There is a certain freedom in choosing these parameters. For example, for matching the mass densities of the MPC system and the reference one, the masses of the particles itself don't have to be the same: the point-like MPC particle doesn't represent a real particle, doesn't have a specific volume, and thus can represent any microscopic amount of fluid. Assigning the MPC particle mass equal to several masses of a "real" particle, one requires less particles to represent the same volume of fluid and therefore gains simulation time.

However in our case it is more convenient to set $m_{MPC} = m_{MD}$. In our coupling algorithm the particle leaving the region with one representation changes its "identity", so if one MPC particle would represent n MD particles, an algorithm for converting an MPC region to n MD particles and otherwise should be introduced. In the AdResS hybrid scheme [61, 64], a particle leaving the cross-grained representation also slowly

switch to many particles, but this "set" of particles still remains an entity due to bounds between its constituents. In our case, as MPC particles are divided into several MD ones, they are free to move separately. That is why we set $m_{MPC} = m_{MD} = m$. Since the mass densities of the MD and MPC systems need also to be matched, the cell size a and the average number of particles in a cell M are not independent any more, but related

$$M = \frac{\rho}{m} a^3. \tag{3.16}$$

As mentioned above, the most important characteristics to be matched in our hybrid scheme are the transport coefficients. The definition of the transport coefficients of mass (diffusion) and momentum (viscosity) was discussed in the section 2.2. In MD simulations these values can be obtained by direct calculation according to Eqs.(2.21) and (2.22).

We carried out Molecular Dynamics simulations for 616 particles at the temperature $T = 1.5\epsilon/k_B$. The parameters of the MD system are $\sigma = 0.3405\,nm$, $\epsilon/k_B = 119.8\,K$, $\rho\sigma^3 = 0.8$, mass of the particle $m = 39.95\,a.u.$, resembling the argon fluid. The values of diffusion coefficient and viscosity are $D = 5.58\times10^{-3}\,nm^2/ps$ and $\eta = 1.74\times10^{-4} Pa{\cdot}s$.

The analytical formulae for the MPC transport coefficients are discussed in the section 2.5. The theoretical expressions for the diffusion coefficient (2.41) and viscosity (2.51) and (2.60) are generally in a very good agreement with results obtained from simulations. For the viscosity η the deviation from the predicted value is about 1%. For the diffusion coefficient D the relative difference between the value obtained from the simulation and the analytical expression can reach 30 % [34,37] for very small mean free pathes λ due to hydrodynamic interactions. The transport coefficients calculated from MD simulations are the desired values of η_{MPC} and D_{MPC}.

There are still three independent MPC parameters (a, α, and Δt). That means that we can match the transport properties of our two fluids by solving the system of equations with the parameters for the MPC-method as variables:

$$\begin{cases} D_{MD} &= D_{MPC}(a, \Delta t, \alpha) \\ \eta_{MD} &= \eta_{MPC}(a, \Delta t, \alpha). \end{cases} \tag{3.17}$$

Expressing the time step Δt by the first equation and substituting it in the second one, we obtain the set of parameters α and a as an implicit function $a(\alpha)$ given by $\eta_{MD} = \eta(a, \alpha)$. For the transport values obtained from our Molecular Dynamics simulation the possible values of α and a are shown on the Fig. 3.2. The parameters for the MPC system were chosen as follows: rotation angle $\alpha = 1.8\,rad$ and cell size $a = 0.78\,nm$. Substituting these values in the first equation of the system (3.17), one obtains the MPC time step $\Delta t = 0.262\,ps$.

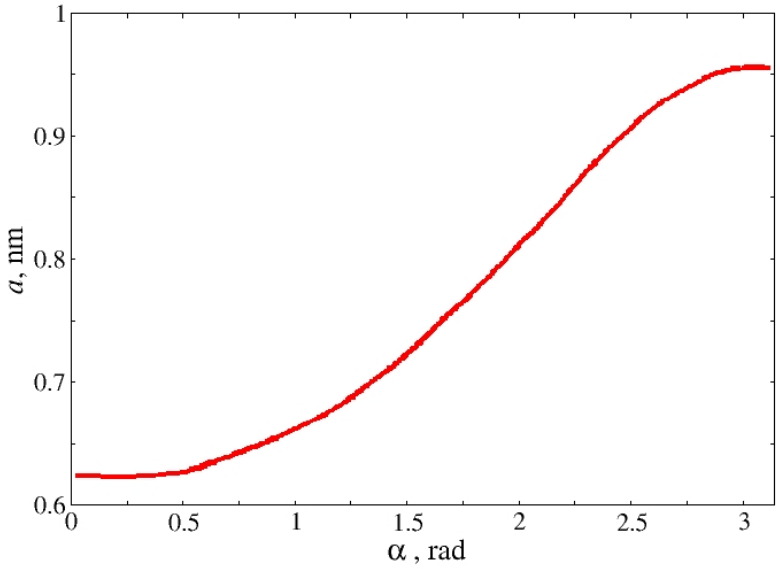

Figure 3.2.: *Possible values for the rotational angle α and cell size a, which allow to obtain the desirable diffusion coefficient D and viscosity η for the MPC system*

Since it is extremely unusual to use SI units in MPC simulations, all parameters have to be rescaled to the MPC units. Thus the values really used in the program are $\alpha = 1.8\,rad$, $a = 0.78\,nm = 1[MPC\,unit]$, particle mass $m = 39.95\,a.u. = 1[MPC\,unit]$, the average number of particles in cell $M = \rho a^3/m = 9.625$, time step $\Delta t = 0.262\,ps = 1[MPC\,unit]$. To characterize the time scale of MPC simulations one usually uses the mean free path λ. Since at equilibrium the MPC particles have a Maxwellian velocity distribution, the mean free path can be determined as $\lambda = \Delta t\sqrt{k_B T/m}$. In our simulations $\lambda = 0.0665$.

Unfortunately, it is not possible to match all fluid characteristics. Since the MPC system is essentially an ideal gas, the speed of sound and the Mach number (the ratio of the speed of an object moving through a fluid and the local speed of sound) differ from that of the MD system. This is an indication that the MPC fluid cannot represent the thermodynamics of the MD solvent, and means that the MPC fluid always has an artificial high compressibility compared to that of the MD fluid. Besides, because MPC particles are ideal, the pure MPC solvent has zero bulk viscosity, zero chemical potential, and a zero virial term in the pressure. It doesn't cause a lot of troubles if one wish to replace an MD solvent with the MPC one, but in our case, where the two fluids have to coexist side by side and be in equilibrium, this implies some problems to be solved, which will be discussed in the following section.

3.4. Hybrid model

Let us introduce the hybrid particle-based atomistic/coarse-grained model. Consider a box of particles divided into two parts with a handshaking layer between them: one part is occupied by particles interacting via a Lennard-Jones potential, the other part is filled up with the corresponding coarse-grained MPC particles. The buffer zone between them is introduced in order to achieve a smooth transition between the two different descriptions smooth. Fig. 3.3 shows a schematic representation of the coupling.

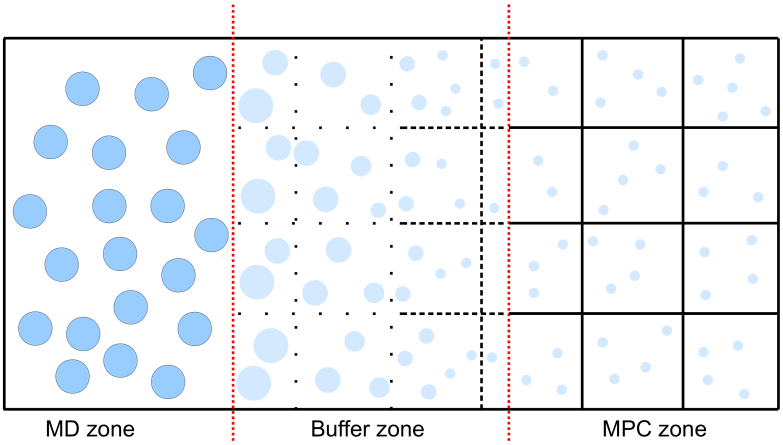

Figure 3.3.: *The general coupling scheme: in the left part of the system particles interact via a Lennard-Jones potential; the right part is filled with MPC fluid. There is a buffer region between them, where particles assume a mixed identity.*

The central task is to keep the liquid homogeneous and equilibrated across the box as it were in a homogeneous system. From the "particle's point of view", the artificial boundary must be essentially invisible, i.e. the particles cross the border without experiencing any "barrier". The MD and MPC domains exchange particles which adapt their identity accordingly: in the MD zone it is a MD particle, interacting via Lennard-Jones potential with its neighbor particles, in the MPC zone it is a MPC particle, experiencing a multi-particle collision within a corresponding cell, and while propagating through the buffer layer, the particle has a mixed identity and therefore interacts with its surroundings in some mixed way.

3.4.1. Mixed identity

In order to describe the changing of "identity" for a given particle we have to specify the weighting function $w(x)$. This function $w \in [0, 1]$ is defined in such a way that values

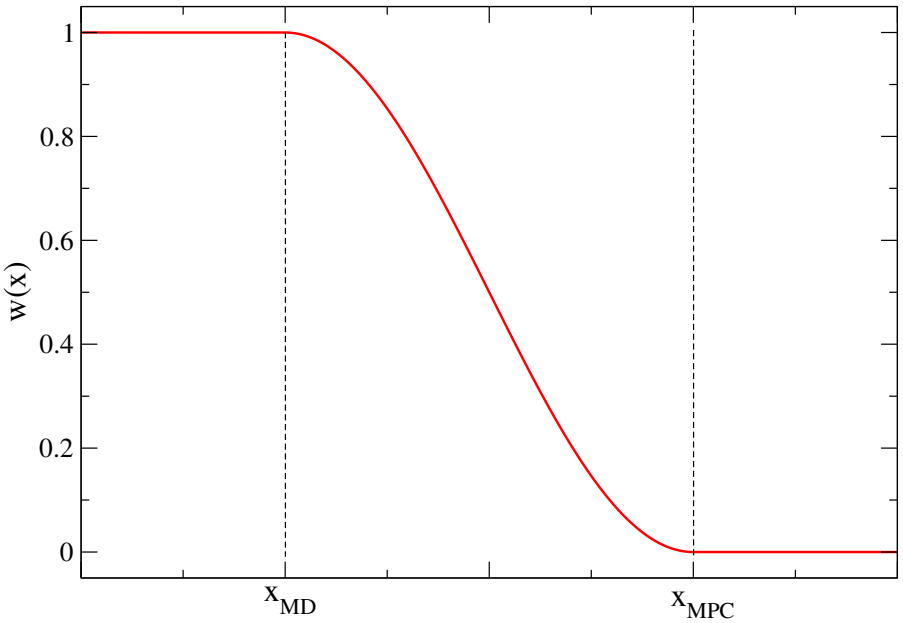

Figure 3.4.: *The weighting function function $w \in [0,1]$ defined by Eq.(3.18). The values $w = 1$ and $w = 0$ correspond to the atomistic and coarse-grained regions of the coupled atomistic/mesoscopic system, respectively, while the values $0 < w < 1$ correspond to the interface layer. The vertical lines indicate the boundaries of the interface.*

$0 < w < 1$ correspond to a "hybrid identity" with the limiting cases $w = 1$ for the MD system and $w = 0$ for MPC:

$$w(x) = \begin{cases} 1 & , \quad x < x_{MD} \\ \frac{1}{2}[\cos(\pi \frac{x - x_{MD}}{l_{buf}}) + 1] & , \quad x_{MD} \leq x \leq x_{MPC} \\ 0 & , \quad x > x_{MPC} \end{cases} \tag{3.18}$$

where x_{MD} is the coordinate of the MD region border, x_{MPC} is the coordinate of the cross-grained-region border and $l_{buf} = x_{MPC} - x_{MD}$ is the width of the buffer zone. Eq.(3.18) is a convenient way to define $w(x)$ because it ensures an interpolation between $w = 0$ and $w = 1$ that is monotonous, continuous, differentiable, and has a zero slope at the boundaries with the atomistic and coarse-grained regions (Fig. 3.4). The precise functional form of the $w(x)$ is not important, it could be any other function which satisfies these requirements.

To understand better what is the "hybrid identity" of the particle, one can use the analogy with the quantum-mechanical mixed-state description and consider a hybrid particle in the interface layer as a normalized linear combination of a Lennard-Jones particle and a coarse-grained MPC particle. As a given particle moves from the MPC boundary of the interface layer to the Molecular Dynamics boundary, w is gradually

changed from 0 to 1, and the particles "identity" changes accordingly. The continuos identity transition is required since the MPC particles have no excluded volume and can be located within any distance from each other, or even at the same place, while for two LJ particles experience a repulsion force. Thus it can happen that when a particle changes its identity from MPC to LJ, it is located closely to neighboring particles and the repulsion force is inadequately large. The presence of the buffer layer avoids this by allowing the particles to adapt their mutual location via a slow increase of the LJ forces between them.

3.4.2. Mixed interaction

If a particle gradually changes its identity while propagating through the buffer zone, the way how particles interact changes accordingly. SInce the "identity" of the particle located in the buffer region is mixed, the way it interacts with its surroundings has also to be mixed: the force acting on the particle i should consist of both MD and MPC contributions, weighted accordingly to the position of the particle

$$\mathbf{F}_i = \xi_1(w_i)\mathbf{F}_i^{MD} + \xi_2(w_i)\mathbf{F}^{MPC}. \tag{3.19}$$

The functions $\xi_1(w)$ and $\xi_2(w)$ weight the interactions in such a way, that if the particle is located in the buffer zone close to the MD boundary, than the contribution of the MD interaction is prevailing, if the particle is located in the buffer zone close to the MPC boundary, than the MPC part of the interaction is dominating.

Following the ideas of coupling full atomistic to coarse-grained Molecular Dynamics simulations in the AdResS scheme [61, 64], we define the weighted Lennard-Jones interaction as

$$\mathbf{F}_{ij}^{LJ,w} = w(\mathbf{r}_i)w(\mathbf{r}_j)\mathbf{F}_{ij}^{LJ}, \tag{3.20}$$

where $\mathbf{F}_{ij}^{LJ}$ is the Lennard-Jones force between ith and jth particles with coordinates $\mathbf{r}_i$ and $\mathbf{r}_j$. Taking into account that the weighting function for any pure MPC particle is zero, it is clear that as soon as one of the two interacting particles is a pure MPC one, $w(\mathbf{r}_i)w(\mathbf{r}_j) = 0$ and $\mathbf{F}_{ij} = 0$. After summation over all surrounding particles the wighted Lennard-Jones force acting on ith particle is

$$\mathbf{F}_i^{LJ,w} = \sum_{j\neq i} \mathbf{F}_{ij}^{LJ,w} = w(\mathbf{r}_i) \sum_{j\neq i} w(\mathbf{r}_j)\mathbf{F}_{ij}^{LJ}. \tag{3.21}$$

Since the force between every ith and jth particle is weighted symmetrically, the sum of the forces over all particles remains zero and Newton's third law is satisfied.

By using the force-based coupling scheme it is not possible to define a potential in the switching region [63, 64]. However, in our coupling scheme such a definition is not

necessary. In a similar manner as the transition from a less to a more coarse-grained description in the AdResS scheme, the change of resolution in our coupling system can be interpreted in terms of a "geometry-induced first-order phase transition": two parts of the system, liquid-like and gas-like, have to be in a equilibrium.

There is no pairwise interaction in the MPC scheme, but we have to "weight" the MPC algorithm contribution in changing the velocity of the particle. A particle with mixed identity experiences the mixed force consisting of both MD and MPC forces contributions. Since the cross-grained analogue of intermolecular forces responsible for momenta change is the multi-particle collision, we have to change some how the collision rule. For example, we could diminish gradually a rotation angle, modeling the decreasing contribution of MPC "forces" for particle moving toward the MD zone. Or a collision in a cell occurs not every step, but with a probability $P = 1 - w(\mathbf{r}_{c.m.})$, where $\mathbf{r}_{c.m.}$ is a center of mass for a given cell. In this work the latter variant is used. By applying this probability rule, the average momentum change of the particle i after one step becomes

$$\langle \Delta \mathbf{p}_i^{MPC,w} \rangle = \big(1 - w(\mathbf{r}_{c.m.})\big) \langle \Delta \mathbf{p}_i^{MPC} \rangle, \tag{3.22}$$

therefore the average weighted MPC "force", acting on the particle i is

$$\langle \mathbf{F}_i^{MPC,w} \rangle = \frac{\langle \Delta \mathbf{p}_i^{MPC,w} \rangle}{\Delta t} = \big(1 - w(\mathbf{r}_{c.m.})\big) \frac{\langle \Delta \mathbf{p}_i^{MPC} \rangle}{\Delta t} = \big(1 - w(\mathbf{r}_{c.m.})\big) \langle \mathbf{F}_i^{MPC} \rangle. \tag{3.23}$$

3.5. Equilibration

As mentioned above, the coexistence of two different levels of resolution in one system resembles a two-phase system. The more detailed region can be depictured as a subsystem at a given temperature T in a fixed volume V with an average number of particles N and pressure P. This has to be coupled to a more coarse-grained surroundings in a way that the structural and dynamical properties within the detailed region are not altered at all. This also requires that there is no kinetic barrier introduced by the transition region between the two representations. Viewing the different regimes as different phases, the question of equilibrium between them can be formulated in terms of the differences in the temperature, pressure and chemical potential characterizing each resolution, hence:

$$\mu_{MD} = \mu_{MPC},\ P_{MD} = P_{MPC},\ T_{MD} = T_{MPC} \tag{3.24}$$

must be satisfied. These conditions assure that there is no net flux of particles between MD and MPC regions and the liquid is homogeneous across the simulation box.

In a homogeneous fluid, pressure is the momentum transfer per unit area per unit time across an imaginary flat fixed surface. There are both kinetic and virial contributions

to the pressure. The first arises from the momenta transported across the surface by particles that cross the surface in the unit time interval; it yields the ideal-gas contribution $P_{id} = Nk_BT/V$ to the pressure. Since MD particles interact via pair-additive, central forces, the intermolecular "potential" contribution leads to the virial equation of state [6]:

$$P_{MD} = \rho k_B T + \frac{1}{3V}\left\langle \sum_{i=1}^{N} \mathbf{r}_i \cdot \mathbf{F}_i \right\rangle. \tag{3.25}$$

The pressure of MPC fluid has no virial part:

$$P_{MPC} = \rho k_B T. \tag{3.26}$$

The reason is that the stochastic rotations, which define the collisions, transport on average no net momentum across a fixed dividing surface. That means that if temperatures for MD and MPC fluids are equal, the pressure in the MD region P_{MD} will be larger than pressure in the MPC region P_{MPC}. Hence, the MD particles will move readily from the MD-zone to the MPC-zone, so that densities and concentrations in these regions won't be equal any more.

The similar problem occurs for the chemical potential. The calculation of the chemical potential μ for a MD system is not so straightforward as the pressure calculation. A direct approach is to run a simulation of a grand canonical ensemble (μ, V, T), where μ is specified, but there are some technical difficulties associated with grand canonical simulations [6]. The most widely applied method for calculating μ is the so called "test particle insertion" method. In this method the test particle is inserted in a random place within the system and the potential energy change U_{test} which would result from the addition is calculated. The chemical potential estimation is based on the relation

$$\exp(-\mu/k_BT) = Q_{N+1}/Q_N, \tag{3.27}$$

which is valid at large N for both NVT and NPT ensembles (Q is the partition function). From this equation we can obtain the expression for the excess chemical potential

$$\mu^{ex} = -k_BT \ln\left\langle \exp(-U_{test}/k_BT)\right\rangle. \tag{3.28}$$

The test particle is not "really" inserted, it is "ghost", i.e. the other N real particles are not affected by its presence.

For a MPC fluid, since there is no gain or loss of energy by inserting a particle in the system, the chemical potential is zero. Thus, the conditions (3.24) are satisfied only for the temperature, and the inequality of chemical potentials and pressures will cause a flux of particles from the MD to the MPC region. In order to prevent such a behavior

either we have to make MPC-fluid not ideal by introducing some repulsion forces (and increasing therefore the values of P and μ), or we have to introduce a restraining force in the buffer-zone to stop particles from leaving the MD-region.

3.5.1. Non-ideal MPC fluid

Since the symmetrical inter-cellar repulsion forces would not affect the local momentum conservation, the way of adjusting the values of chemical potential and pressure for an MPC fluid to the non-ideal ones would be more "natural". The original MPC algorithm models a fluid with an ideal-gas equation of state, which causes a high compressibility. There is a more general MPC algorithm, which takes into account excluded volume effects and therefore reduces compressibility effects, which provides an additional contribution to the equation of state [45–47].

The generalization of the two-dimensional algorithm, presented by T.Ihle et al. in [45] into three dimensions consists of the following. As in the original MPC algorithm, the solvent is modeled by a large number of point-like particles of mass m which move in continuous space with a continuous distribution of velocities. The system is coarse-grained into cells of a cubic lattice with cell size a. The algorithm consists of individual streaming and collision steps.The free-steaming step is exactly the same as that in the original MPC method. In order to define the collision, a second grid with sides of length 2a is introduced which groups the adjacent eight cells into one supercell. A random shift of the lattice before the collision step is required to ensure Galilean invariance. To initiate a collision, pairs of cells in every supercell are randomly selected. The possible directions of the inter-cellar collisions are shown in Fig. 3.5. The directions ζ_1, ζ_2 and ζ_3 are parallel to the Cartesian axes x, y, and z, three pairs of directions ζ_4 and ζ_7, ζ_5 and ζ_8, and ζ_6 and ζ_9 are diagonal parallel to the xy, xz and yz planes. Diagonal collisions are essential to equilibrate the kinetic energies in the x-, y- and z-directions. To initiate the collision, pairs of cells in every supercell are randomly selected.

In every cell we calculate the center-of-mass velocities $\mathbf{u}_n$ according to the 2.26 (n is the cell index). The projection of the difference of the center-of-mass velocities of the selected cell pairs on ζ_j, $\Delta\mathbf{u} = \zeta_j(\mathbf{u}_1 - \mathbf{u}_2)$, is then used to determine the probability of collision. If $\Delta\mathbf{u} < 0$, no collision will be performed. For positive $\Delta\mathbf{u}$, a collision will occur with an acceptance probability p_A which depends on $\Delta\mathbf{u}$ and the numbers of particle in the two cells, $N_{c,1}$ and $N_{c,2}$. This mimics a hard-sphere collision on a coarse-grained level: for $\Delta\mathbf{u}$ clouds of particle collide and exchange momenta. While there is a considerable freedom in choosing p_A, the requirement of the thermodynamic consistency imposes certain restrictions [45–47]. One possible choice is

$$p_A(N_{c,1}, N_{c,2}, \Delta\mathbf{u}) = \Theta(\Delta\mathbf{u}) \tanh(\Lambda), \tag{3.29}$$

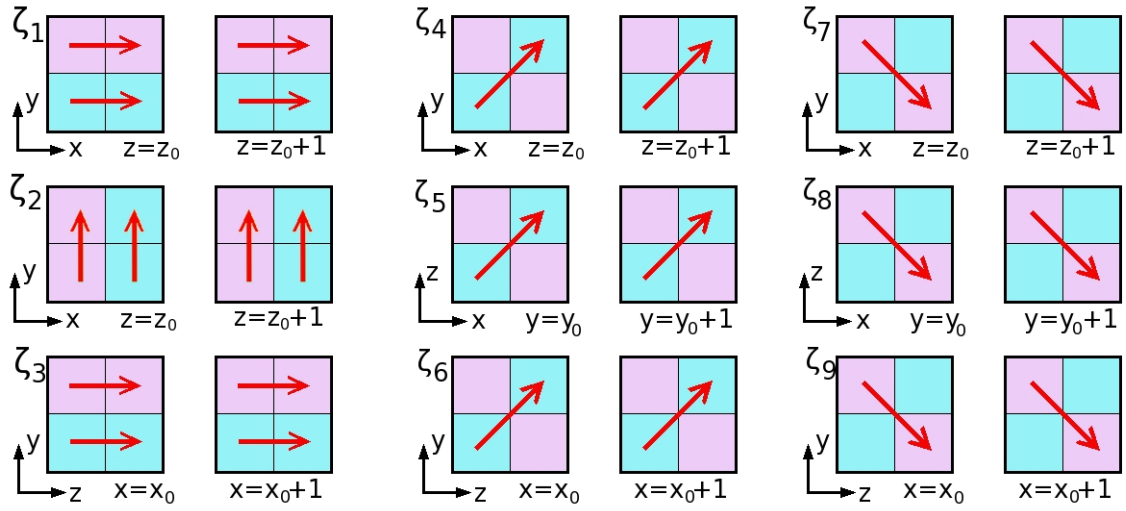

(a) (b)

Figure 3.5.: *Schematic of collision rules for an non-ideal MPC fluid. Momentum is exchanged parallel to different directions ζ: parallel to the Cartesian coordinates (a) and diagonal (b). Diagonal collisions are essential to equilibrate the kinetic energies in the x-, y- and z-directions. The collisions in directions ζ_1, ζ_2 and ζ_3 occur with the probability $p_\zeta = 1/9$. The collisions in diagonal directions ζ_4 and ζ_7, ζ_5 and ζ_8, and ζ_6 and ζ_9 occur with the probability $p_{\zeta,d}$=2/9.*

where Θ is the unit step function, $\Lambda = A\Delta\mathbf{u}N_{c,1}N_{c,2}$ and A is a parameter which allows us to tune the equation of state. The choice $\Lambda \sim N_{c,1}N_{c,2}$ leads to a non-ideal contribution to the pressure which is quadratic in the particle density.

Once it is decided to perform a collision, an explicit form for the momentum transfer between the two cells is needed. The collision should conserve the total momentum and kinetic energy of the cell pairs participating in the collision, and in analogy to the hard-sphere liquid, the collision should primarily transfer the component of the momentum which is parallel to the connecting vector ζ_j. There are many possibilities which fulfill these conditions. Since our aim was to reduce the compressibility, a collision rule was selected which leads to the maximum transfer of the parallel component of the momentum and does not change the transverse momentum. The rule is following: the component of the mean velocities of the two cells, parallel to the chosen direction ζ are exchanged, which is equivalent to a reflection of the relative velocities

$$v_i^{\parallel}(t+\Delta t) - u^{\parallel} = -(v_i^{\parallel} - u^{\parallel}), \tag{3.30}$$

where $u^{\parallel}$ is the parallel component of the mean velocity of the particles of both cells.

The perpendicular component remains unchanged

$$v_i^{\perp}(t + \Delta t) = v_i^{\perp}. \tag{3.31}$$

The collision rules defined specifically for all directions ζ_j can be found in the A.1. It is easy to verify that these rules conserve momentum and energy in the cell pairs.

Because of $x - y - z$ symmetry, the probabilities for choosing cell pairs in the x-, y-, and z-directions (with unit vectors ζ_1, ζ_2 and ζ_3) are equal and will be denoted by p_ζ. The probability for choosing diagonal pairs (ζ_4 and ζ_7, ζ_5 and ζ_8, or ζ_6 and ζ_9) are also equal and are given by $p_{\zeta,d} = 1 - 3p_\zeta$. Both p_ζ and $p_{\zeta,d}$ must be chosen so that the hydrodynamic equations are isotropic and do not depend on the orientation of the underlying grid. An equivalent criterion is to guarantee that the relaxation of the velocity distribution is isotropic [45]. These conditions require $p_\zeta = 1/9$ and $p_{\zeta,d} = 2/9$.

These modifications yield the non-ideal component to the equation of state, allowing for a more realistic modeling of dense gases and liquids. Unfortunately, this extended MPC method was nevertheless not capable to assure the dynamical equilibrium between the two regions in the coupled system: the MPC system still doesn't resist the insertion of a new particle, this means that there is no hindrance preventing an MD particle to move to the MPC zone, and the density profile is not homogeneous across the box. To solve this problem we tried to model non-ideal MPC fluid with inter-cellar repulsion forces directly depending on number of the particles in the cells, but all tries led to the unexplained clustering of the system.

3.5.2. External buffer-force

While moving through the buffer region, a particle slowly changes its representation, and the weighted part of explicit potential force (Lennard-Jones in our case) is changing accordingly, causing a decrease of the chemical potential and the virial part of the pressure. Taking into account that the space-dependent weighting function $w(\mathbf{r})$ is continuos and differentiable, it can be assumed that in the buffer zone the chemical potential and the pressure are also space-dependent continuos functions $\mu(\mathbf{r})$ and $P(\mathbf{r})$, correspondingly. The reason of the spatial change of both $\mu(\mathbf{r})$ and $P(\mathbf{r})$ is the change of the "intensity" of interaction between particles. There is no well-defined potential energy for the particles in the buffer zone, but since $\mu(\mathbf{r})$ and the virial part of $P(\mathbf{r})$ are non-zero due to interactions between particles, the gradients of these functions can be interpreted as "thermodynamic" forces $F_\mu^{TD} = -\nabla\mu$ and $F_P^{TD} = V\nabla P$. Subtracted from the weighted force (3.21), they should compensate any drift originating from the different resolution, making the density profile uniform throughout the whole simulation box.

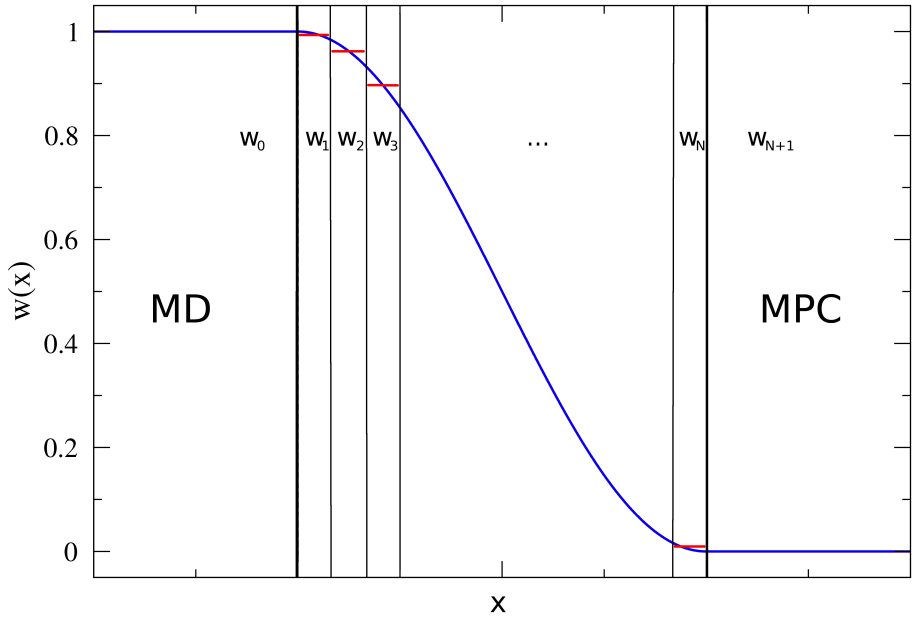

Figure 3.6.: *Schematic representation of the simulation box and different levels of resolution. The region on the left (MD) is the Molecular Dynamics region, the region on the right (MPC) is the Multi-Particles Collision dynamics region. The central part is the transition region, where the switching function (curve in rosa) is defined. In order to calculate the chemical potential and pressure of each intermediate resolution, the transition zone is divided into N slices which corresponds to discretized values of the switching function w_i.*

In principle, the derivation of the external "thermodynamic" force causing the flux of the fluid from the chemical potential and the pressure is equivalent. We will employ and compare both approaches. The idea of the chemical potential (and the virial part of the pressure) calculation is illustrated on Fig. 3.6. The simulation box is divided into three regions: the region with a usual pair-potential force (MD), the region without collision forces (MPC), and the transition zone in between. The MD region is characterized by the value of the switching function $w_0 = 1$. The MPC region is characterized by the value of the switching function $w_{N+1} = 0$. In real simulations the value of w in the buffer zone varies continuously, but we approximate it by discretizing w into N steps $w_1, w_2, ..., w_{N-1}, w_N$. If the system consists of the particles with the fixed values of w, the energy of the system is well defined and it is possible to calculate the chemical potential (and pressure) for such a system. Then we take the value of a chemical potential of the

particles in a bulk system of the specific representation as a local value of the chemical potential in the buffer region: $\mu(x_i) = \mu_{w_i}$. This implies the assumption that each of the slices in Fig. 3.6 can be taken as a bulk system statistically independent of others. The same for the pressure: $P(x_i) = P_{w_i}$. Repeating this procedure with all values of w_i we obtain space-dependent profiles for the chemical potential $\mu(x)$ and pressure $P(x)$.

Knowing the chemical potential function $\mu(x)$ we can derive an external restraining force. Due to this force, particles from the buffer zone effectively should not "see" the difference of the chemical potential. In Fig. 3.7 (a) simulation results, spline fits for the chemical potential profile $\mu(x)$, and the restraining external force are presented. As it can be seen from the density profile (Fig. 3.8), this restraining force is able to prevent particles from leaving the MD region, but the density profile in the buffer zone is still far from the desired one. The fact that in the buffer zone the density value it much smaller than the expected mean value shows that the applied external force does not fully compensate the "thermodynamic" force by the representation difference.

Carrying out the similar procedure for the pressure-based approach, we obtain the similar results: the particles in the MD zone are prevented from leaving, but the density profile still has prominent deviations (Figs. 3.7 (b), 3.8). Besides, the force obtained from the pressure profile is not the same as that obtained from the chemical potential profile. The explanation of this is that our assumption of statistical independence of "slices" in the buffer region is not correct, and profiles $\mu(\mathbf{r})$ and $P(\mathbf{r})$ obtained from separate bulk simulations differ from the "real" ones in the coupling system. When we consider the particle i from the system which consists of the particles with mixed but the same for all of them identity, all its interaction partners j have the same weighting function value w. Considering a particle located in a "slice" in the buffer zone, it can be seen that w possesses quite different values within the cut-off radius, which determines the interaction partners for a given particles. Besides, $w(x)$ can lnoy be approximated as linear in the middle of the buffer zone, so there can be a noticeable difference between values calculated for the particles from "slices" located near the borders with MD and MPC regions and the corresponding bulk systems.

Having the buffer force obtained from the pressure or chemical potential profile, even that imperfect, it is possible to adjust it to the required form by some iteration process: using the calculated density profile at the previous iteration step one can obtain a correction for a used external force. Then the simulation is performed with the new external force, the new density profile is calculated and the procedure is repeated.

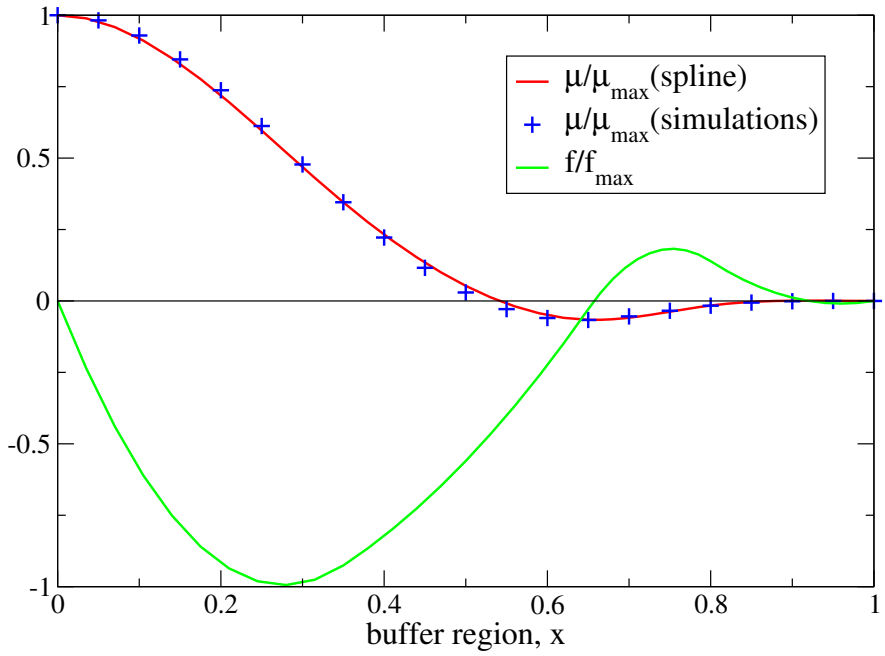

(a)

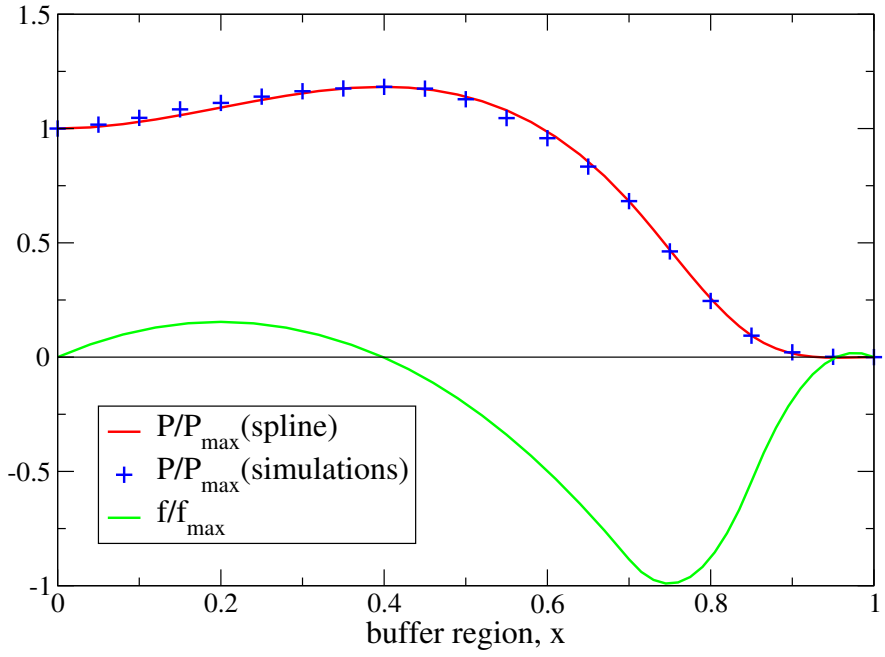

(b)

Figure 3.7.: *Chemical potential (a) and pressure (b) as function of the position in the buffer zone: values calculated from simulations (+) and spline interpolations of these values (red line). The external restraining force derived from the interpolated function is represented by a green line.*

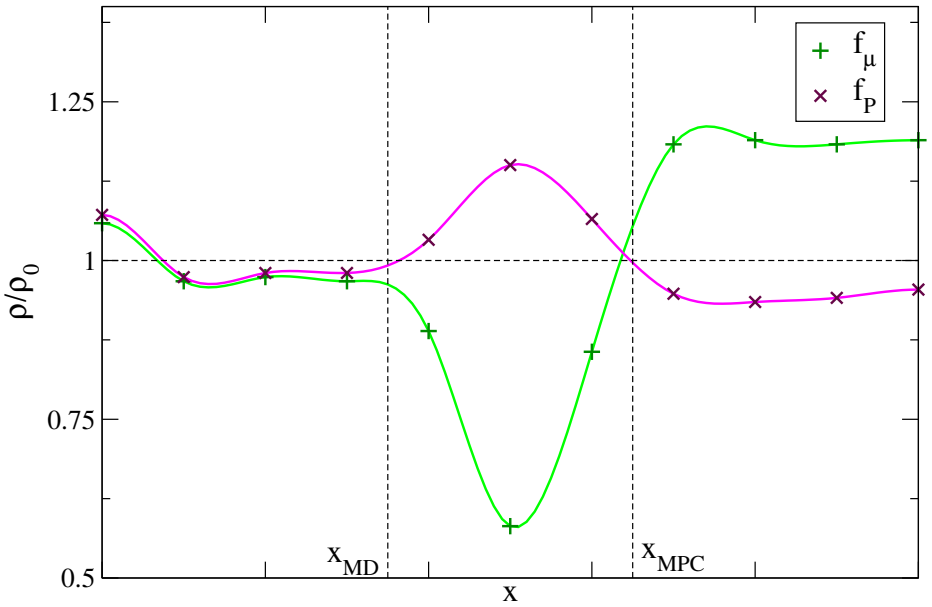

Figure 3.8.: *Density profile of the coupled system after introducing a restraining force, derived from the chemical potential function (green) or pressure function (violet), respectively. Although both restraining forces are able to prevent the particles from leaving the MD region, they cannot provide an uniform density profile along the buffer zone.*

3.5.3. Buffer-force obtained by iteration

The procedure of finding the external force profile which fully compensates the "thermodynamic" force acting on the particles in the buffer zone follows the ideas of the control theory for feedback systems (Fig. 3.9), where the sensor measures whether the system output is equal to the reference signal, and if not, the system input has to be tuned. The change of the system input depends on the measured error.

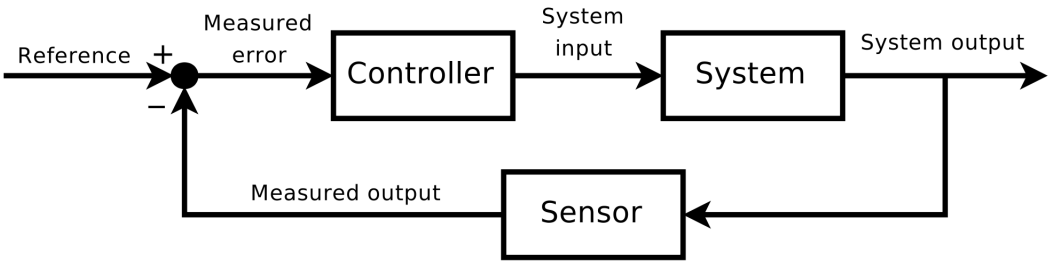

Figure 3.9.: *The concept of the feedback loop to control the dynamic behavior of the system.*

In our case, the system output is the density profile $\rho(x)$ with the reference uniform distribution, and the system input is the external force $F^{ext}(x)$. The correction rule is

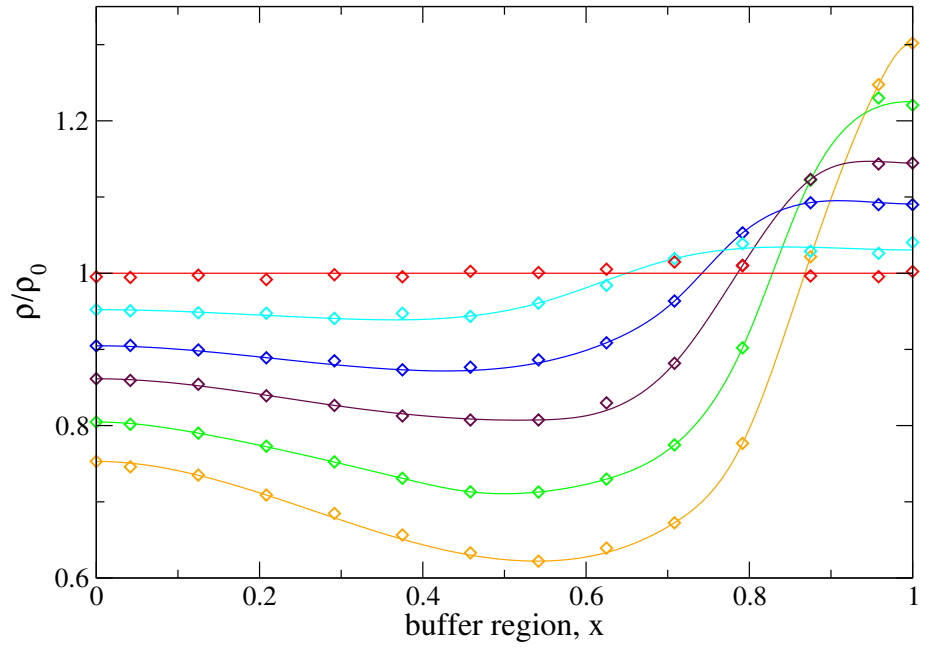

(a)

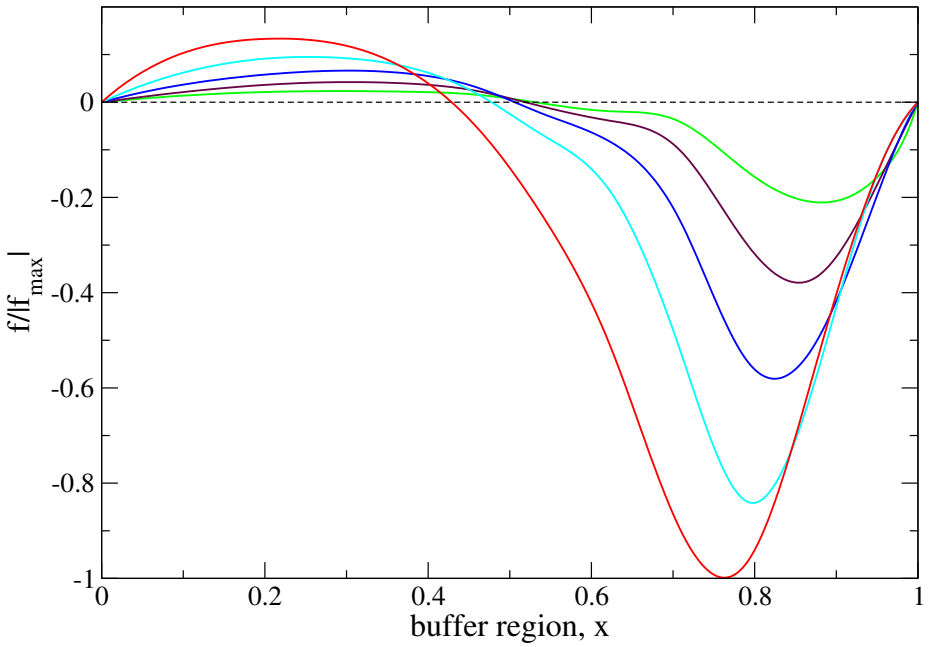

(b)

Figure 3.10.: *Density and external profiles alteration of the coupled system during the iteration process. The obtained final force (b, solid red line) provide a uniform density profile in the buffer zone (a, red symbols).*

as follows: for every iteration loop step i, if for any coordinate x_0 from the buffer zone the density function $\rho_i(x)$ is not a constant, the local external force $F_i^{ext}(x_0)$ has to be corrected by a term proportional to the gradient of the density function $\rho_i(x)$

$$\begin{aligned} F_{i+1}^{ext}(x) &= F_i^{ext}(x) + dF_i(x), \\ dF_i(x) &= C\frac{d\rho_i(x)}{dx}, \end{aligned} \tag{3.32}$$

where i and $i+1$ denote the current and next step. Using this iteration procedure one can adjust restraining forces obtained from the chemical potential or pressure profiles. But it is also possible to use any other function with values from an appropriate range. The results shown on the Figs. 3.10 are obtained from the simulations with initial external force profile $F_0^{ext}(x) = 0$. As it can be seen, the final restraining force provides a uniform (within deviations caused by fluctuations) profile.

3.6. Thermostatting

Since the applying of the external restraining force in the buffer region causes the heating of the system, the thermostatting of the system is required even in equilibrium simulations. Furthermore, if the hybrid system is under the flow, then the thermostatting is required to compensate the viscous heating. A basic requirements for any thermostat is that it does not violate local momentum conservation, smear out local flow profiles, or distort the velocity distribution too much. When there is homogeneous heating, the simplest way to maintain a constant temperature T_0 is to scale velocities with a factor S

$$v_\alpha^{new} = Sv_\alpha, \tag{3.33}$$

where

$$S = \sqrt{\frac{T_0}{T}}, \quad T = \frac{\sum_i^N m\mathbf{v}^2}{3k_B}. \tag{3.34}$$

This can be done with a single global scale factor, or a local factor which is different in every cell. If the system is under flow, it is important not to distort the macroscopic velocity profile. For a known flow profile $\mathbf{u_{flow}}$, the relative velocities $\mathbf{v} - \mathbf{u_{flow}}$ can be scaled.

The Berendsen thermostat [48] is similar to the velocity rescaling approach, but assigns a time scale for the updating of the velocities, rather then assuming they are completely scaled to the constant temperature value after every time step. The underlying idea of this thermostat is that the system is coupled to a heat bath with the time scale of heating transfer τ

$$S^2 = 1 + \frac{dt}{\tau}(\frac{T_0}{T} - 1), \tag{3.35}$$

where dt is the time step.

The Andersen thermostat [49] couples the system to a heat bath via stochastic forces that modify the kinetic energy of the atoms or molecules. Each molecule undergoes "collisions" with a heat bath at random intervals, and the collision frequency defines the strength of the thermostat. During the "collision" the new momentum of the molecule is chosen at random from a Maxwell-Boltzmann distribution at the desired temperature. This kind of thermostat can be applied in the MPC simulations [40, 50]. In this case, instead of performing the rotation of the relative velocities in the collision step, new relative velocities are generated. Due to the stochastic nature of this thermostat it can only be used in simulations where the exact dynamic of the system is not of interest.

The thermostat, often applied for MPC systems is the cell-level thermostat [43]. The thermostat consist of the following procedure which is performed independently in every collision cell:

- Randomly select a real number $\psi \in [1, 1 + c]$, where c is a small number between 0.05 and 0.3 which determines the strength of the thermostat.
- Accept this number as a scaling factor $S = \psi$ with probability 1/2; otherwise, take $S = 1/\psi$.
- Create another random number $\xi \in [0, 1]$. If ξ is smaller than the acceptance probability $p_A = min(1, A)$, where

$$A = S^{3(N_c-1)} \exp\Big[- \frac{m}{2k_B T_0} \sum_{i_1}^{N_c} (\mathbf{v}_i - \mathbf{u_{cm}})^2 (S^2 - 1)\Big], \tag{3.36}$$

  rescale the velocities.
- If the attempt is accepted, scale the velocities according to $v_\alpha^{new} = S v_\alpha$.

This thermostat reproduces the Maxwell velocity distribution and does not change the viscosity of the fluid.

4. Structure and dynamics of the hybrid fluid

To find out how our coupling method works, we have to test how physical properties are affected while particles cross the buffer zone. To arrive at an understanding of the buffer zone, we first studied a set of systems exclusively composed of hybrid particles with a fixed "identity" $0 \leq w = w(x) = const \leq 1$ (the same for all particles in a given system).

4.1. Pair distribution function

The pair distribution function

$$g(r) = \frac{1}{n^2} \sum_{i \neq j} < \delta(\mathbf{r} - \mathbf{r_i})\delta(\mathbf{r_j}) >, \tag{4.1}$$

where $n = N/V$, describes the average distribution of particle separations in fluids. The red curve in the Fig. 4.1 shows $g(r)$ for a "pure" LJ system. It has a usual shape for a monatomic liquid [2, 4]. Low r correspond to the excluded volume region. Although the potential used in our simulations is not infinity for $r = 0$, it nevertheless is high enough to prevent particles from overlapping. Hence, at low r the pair distribution function vanishes.

At a distance roughly equal to the atomic diameter, there is a pronounced peak in $g(r)$, which denotes a sphere of nearest neighbors. At higher values of r there are oscillations representing more distant neighbors. These oscillations decrease in amplitude with increasing r and eventually $g(r)$ approaches the mean density of the system.

For MPC particles there is no excluded volume and there is no restrictions on overlapping, thus the distribution of particle separations is uniform (the brown curve in Fig. 4.1). The oscillations seen at low r are numerical effects and have no physical significance. For particles with mixed identities and therefore mixed interactions the $g(r)$ keep characteristic peaks, but their amplitudes are lower and the maxima are shifted to smaller distances.

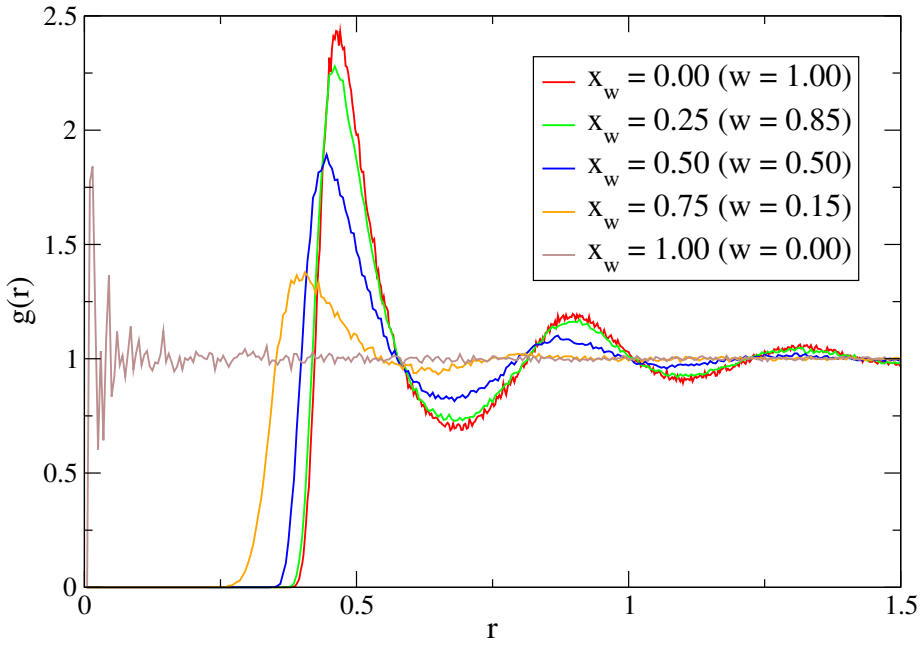

Figure 4.1.: *Pair distribution function for systems consisted of particles with different identity: Lennard-Jones particles ($w = 1.0$), MPC particles ($w = 0.0$) and particles with a mixed identity ($w = 0.85; 0.50; 0.15$). The first peak denotes a sphere of nearest neighbors.*

4.2. Velocity autocorrelation function

The velocity autocorrelation function (VACF)

$$c_{vv}(t) = \frac{1}{3} \langle v_\alpha(t) v_\alpha(0) \rangle \tag{4.2}$$

provides insight into the fluid dynamics. The short time behavior of the VACF for the pure MD system is very sensitive to the details of the interactions between particles [4]. At low densities $c_{vv}(t)$ decays monotonically, a behavior implying the absence of many-body correlation effects. For high densities (as in our system) a tagged molecule is confined in a cage formed by its immediate neighbors, that is why $c_{vv}(t)$ takes on negative values (Fig. 4.2). Dotted lines for VACFs of MPC and mixed systems are plotted only for better representation: in contrast to MD simulations, the MPC time step can not be chosen arbitrarily small without changing the transport characteristics.

The long-time behavior of the VACF is not expected to depend on molecular aspects of self-diffusion. Instead it should reflect the collective correlations in the fluids. The fact that velocity autocorrelation function does not decay exponentially at long times is one of the most significant discoveries made by means of computer simulations [1, 4, 7]. At the time, the non-exponential decay in the velocity correlation function was in contradic-

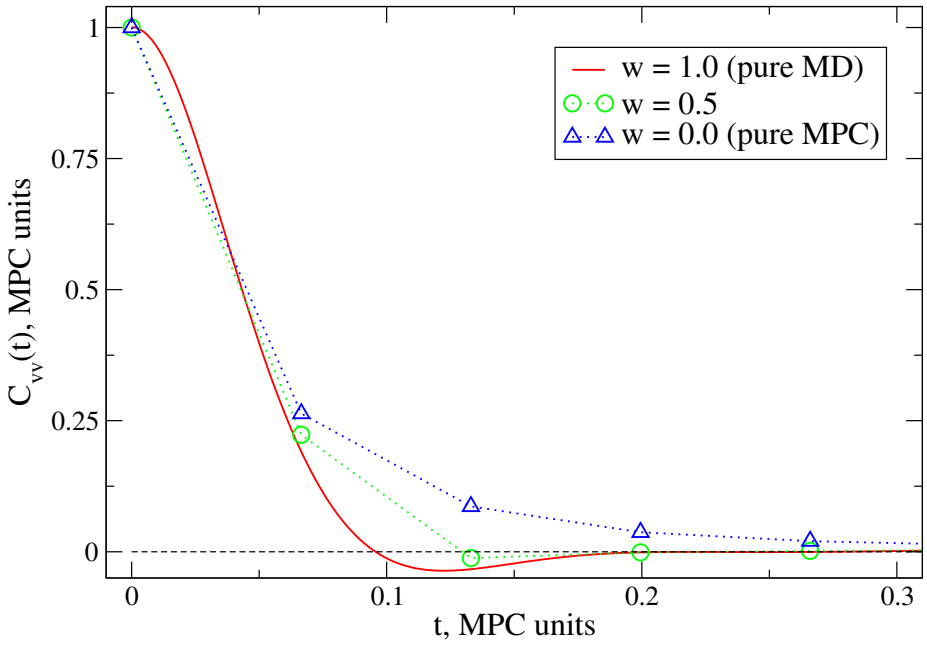

Figure 4.2.: *Velocity autocorrelation functions for systems consisted of particles with different identity: Lennard-Jones particles ($w = 1.0$), MPC particles ($w = 0.0$) and particles with a mixed identity ($w = 0.50$). The difference of the VACFs related to the different "identites" is caused by the difference of the structure of the MD and MPC fluids.*

tion to the results obtained from the Boltzmann-Enskog kinetic theory and the Langevin equation [3,7]. These theories predicted that on time scales much longer than the molecular scale, particles are uncorrelated and therefore execute a random walk leading to an exponential decay for the VAF. In the pioneering work of Alder and Wainwright, which dealt with Molecular Dynamics simulations of dense hard-sphere fluids [69], it was found that a particle's velocity was correlated with its initial velocity even after a time period corresponding to approximately 20 collisions. After this seminal work various theoretical, experimental and computational studies have been undertaken [4, 70–72, 74–77] in order to understand the aspects of the long-time behavior of the VAF in a homogenous fluid.

Using the conservation equations of classical hydrodynamics under the local equilibrium hypothesis, it can be shown that [3, 7, 70–72, 74]

$$c_{vv}(t) = \langle v_\alpha(t) v_\alpha(0) \rangle \rightarrow \frac{2k_B T}{3\rho} (4\pi(D+\nu)t)^{-3/2}, \tag{4.3}$$

where D is the self-diffusion coefficient and ν is the kinematic viscosity. The hydrodynamic explanation for this non-exponential decay of $c_{vv}(t)$ is as follows. For a compress-

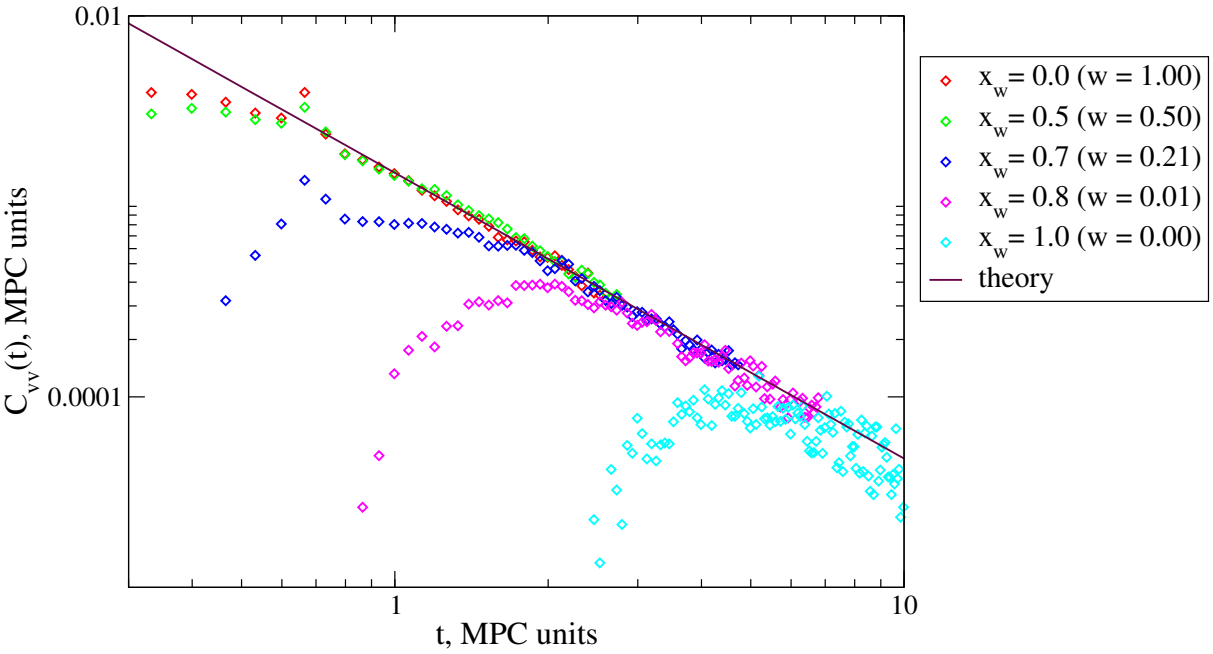

Figure 4.3.: *Long-time tail of the velocity autocorrelation function for systems consisted of particles with different identity: Lennard-Jones particles ($w = 1.0$), MPC particles ($w = 0.0$) and particles with a mixed identity. The solid line indicates the asymptotic behavior with $C_{vv} \sim t^{-3/2}$, which shows that the transport properties are the same for systems with hybrid identity.*

ible fluid, particle momentum dissipates via two pathways: longitudinal hydrodynamic modes (sound waves) and transverse hydrodynamic modes (vortex). Longitudinal sound waves, which are fast processes associated with fluctuations in density and temperature. They propagate at the speed of sound c_s in the medium. These modes decay exponentially and limit the maximum correlation time obtainable by the MD method using periodic boundary conditions because these modes are expected to influence the velocity field after a time $t_{max} = l/c_s$, where l is the length of the simulation box in a given direction.

Transverse shear modes, which propagate via a slow diffusive process with a velocity proportional to $(\eta/\rho)^{1/2}$ and dominate at long times. They are responsible for the vortex formation in the velocity field. The vortices, created by the moving particle couple them back and push it further in the already chosen direction. This gives rise to the $t^{-3/2}$ decay in $c_{vv}(t)$.

The velocity correlation function in MPC simulations also shows a nonexponential decay [37, 38]. Since a long-time tail is the universal feature of the fluids in thermal equilibrium and can be observed in both MD and MPC fluids, the same decay can

be expected in systems with mixed identity. The characteristic time values, at which nonexponential decay becomes observable are different for MD and MPC systems. The corresponding values for the mixed systems lie between them. The calculated autocorrelation functions $c_{vv}(t)$ for systems with different identities, as well as the asymptotic theory curve are shown at Fig. 4.3.

4.3. Dynamic structure factor

The analysis of correlation function of the particle density $n(\mathbf{r}, t)$ provides insight into the transport properties of the fluid. The dynamic structure factor is easily accessible by scattering techniques and, thus, is widely used to determine dynamic and transport coefficients of fluids [4].

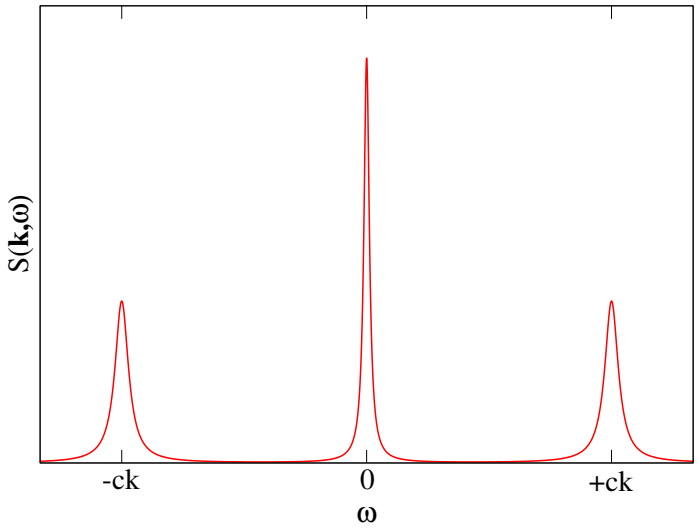

Figure 4.4.: *Usual form of the dynamic structure factor for the adiabatic systems. The central peak corresnponds to the thermal diffusivity mode, the two others are related to the acoustic modes. Their spectral positions are determined by the velocity of the sound c.*

The dynamic structure factor is the Fourier transform of the density-density correlation function. It is defined as [4, 7]

$$S(\mathbf{k}, \omega) = \int \langle n(\mathbf{k}, t) n(-\mathbf{k}, 0) \rangle e^{-i\omega t} dt, \tag{4.4}$$

where

$$n(\mathbf{k},t) = \frac{1}{\sqrt{N}} \sum_{j=1}^{N} e^{i\mathbf{k}\mathbf{r}_j(t)} \tag{4.5}$$

is the density of point-like particles in Fourier space. In adiabatic systems, the dynamic structure factor exhibits three peaks. The usual form of the $S(\mathbf{k},\omega)$ spectrum is shown in the Fig. 4.4. The central (or Rayleigh) peak caused by fluctuations at constant pressure and corresponds to the thermal diffusivity mode. The two other spectral lines, which are shifted in frequency by $-ck$ and $+ck$, are the Stokes and anti-Stokes components of the Brillouin-Mandelstam doublet; they correspond to the acoustic modes. Their spectral positions are determined by the velocity of the sound, c. The width of the central peak is determined by the thermal diffusivity, while that of the two Brilllouin peaks is related to the sound attenuation coefficient.

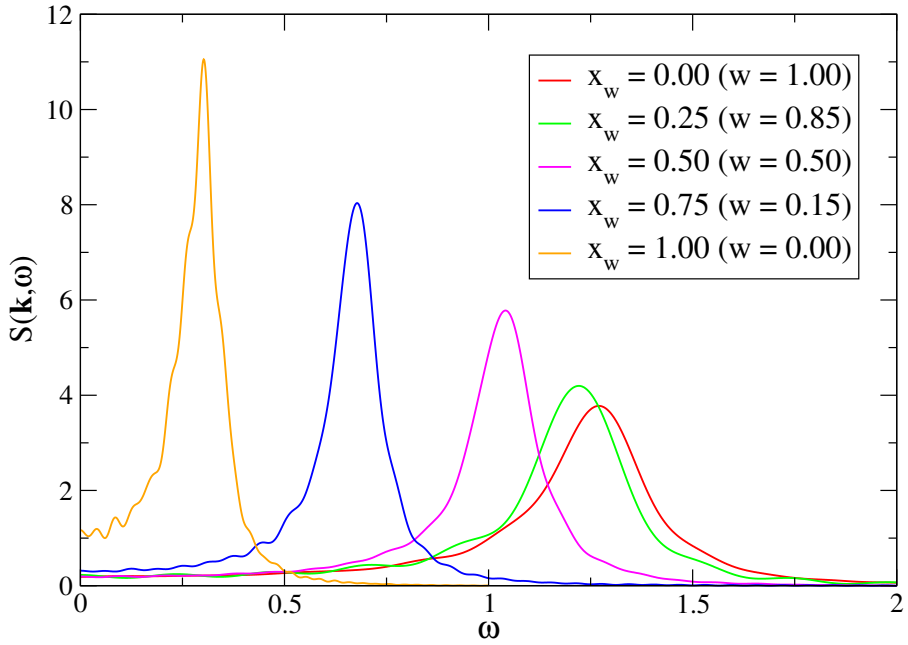

Figure 4.5.: *Dynamic structure factor for systems consisted of particles with different identity: Lennard-Jones particles ($w = 1.0$), MPC particles ($w = 0.0$) and particles with a mixed identity ($w = 0.85; 0.50; 0.15$), $\mathbf{k} = 2\pi/L(1,0,0)^T$. The sound velocities for the systems with hybrid identity are different, which causes the shift of spectral positions of the peaks.*

If the system is thermalized with a local thermostat, the dynamic structure factor undergoes significant changes [82]. The central peak completely vanishes and the Brillouin peaks are shifted to frequencies of smaller magnitude. This happens because the local thermostat suppresses the diffusive energy transport. The thermostat controls the temperature on the small length scale, that means the velocities of all particles within this

area obey the correct energy distribution function. The frequency $\omega_B(k)$ of the Brillouin peak is connected with the generalized sound velocity by the dispersion relation

$$\omega_B(k) = c_T(k)k. \tag{4.6}$$

Hence, the spectral positions of Brillouin peaks are now related to the isothermal velocity.

Our simulations for the systems with a mixed identity were performed with a local thermostat. The results for the dynamic structure factor are shown in the Fig. 4.5. For each curve one of two symmetrical Brillouin peaks is represented. It can be seen that thermal sound velocity is different for particles of systems with different identities.

4.4. Longitudinal current correlation functions

In this section we will discuss the longitudinal current correlation function. The current in the Fourier space is defined as

$$j_\alpha(\mathbf{k}, t) = \frac{1}{\sqrt{N}} \sum_l v_{l\alpha}(t) e^{i\mathbf{k}\mathbf{R}_l(t)}. \tag{4.7}$$

The current correlation function can be written as

$$J_{\alpha\beta}(\mathbf{k}, t) = \langle j^*_\alpha(\mathbf{k}, 0) j_\beta(\mathbf{k}, t) \rangle \tag{4.8}$$

From (4.8) one can extract the longitudinal J_l and transverse J_t current correlation functions by writing

$$J_{\alpha\beta}(\mathbf{k}, t) = \frac{k_\alpha k_\beta}{k^2} J_l(\mathbf{k}, t) + \left(\delta_{\alpha\beta} - \frac{k_\alpha k_\beta}{k^2} \right) J_t(\mathbf{k}, t), \tag{4.9}$$

where $\delta_{\alpha\beta}$ is the Kroneker delta function. In the Fig. 4.6 the longitudinal current correlation functions for systems of particles of different identities are represented.

The longitudinal current correlation function in frequency and wavenumber space $J_l(\mathbf{k}, \omega)$ can be obtained from $J_l(\mathbf{k}, t)$ via Fourier transform:

$$J_l(\mathbf{k}, \omega) = \int_{-\infty}^{\infty} dt e^{-i\omega t} J_l(\mathbf{k}, t) \tag{4.10}$$

It can be shown [4] that there is a relation between the density correlation function $S(k, \omega)$ and the longitudinal current correlation function $J_l(k, \omega)$:

$$J_l(\mathbf{k}, \omega) = \frac{\omega^2}{k^2} S(\mathbf{k}, \omega) \tag{4.11}$$

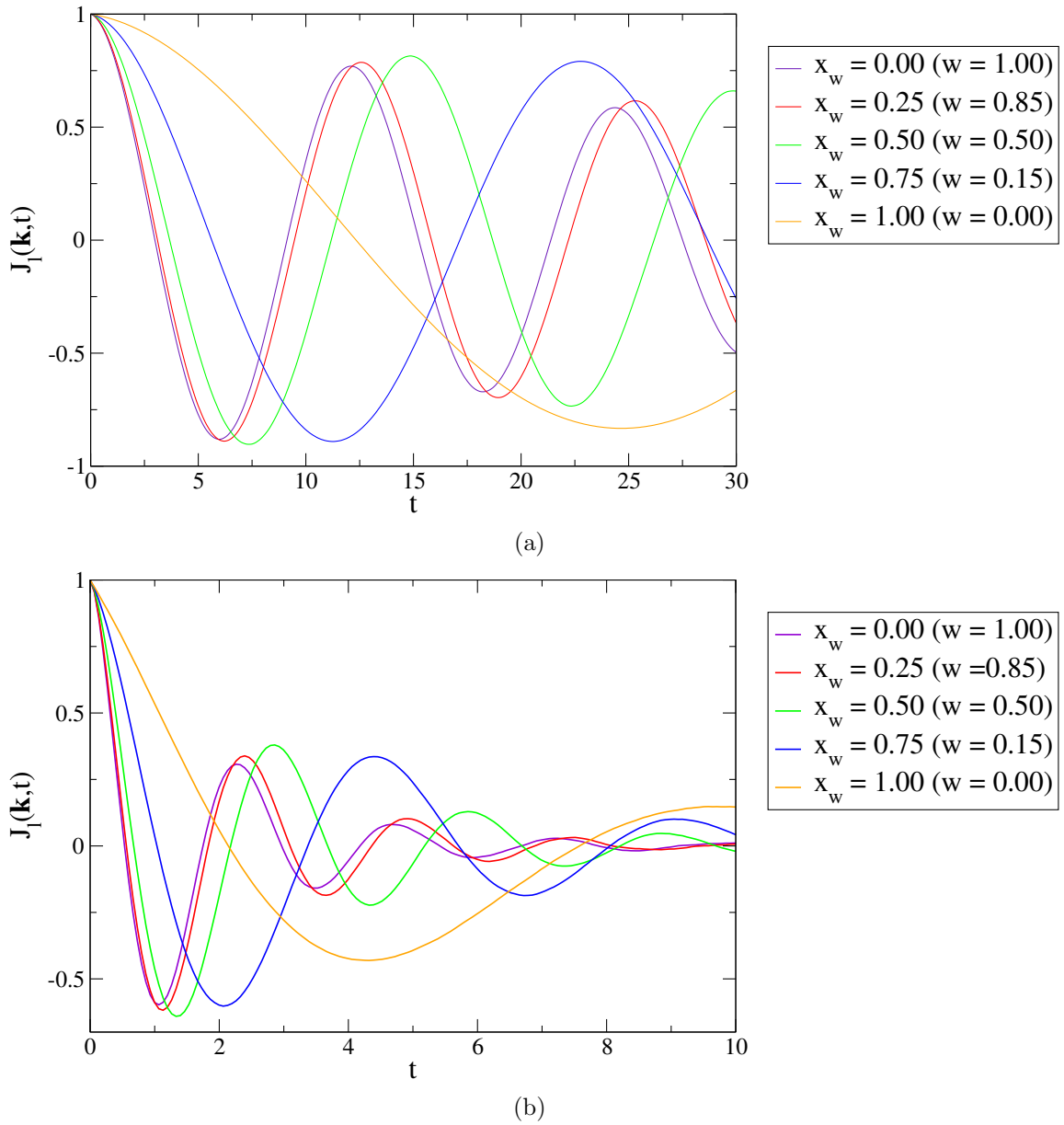

Figure 4.6.: *Longitudinal current correlation functions for systems composed of particles with different identity: Lennard-Jones particles (identity switching function $w = 1.0$), MPC particles ($w = 0.0$) and particles with a mixed identity ($w = 0.85; 0.50; 0.15$), for $\mathbf{k} = 2\pi/L(1,0,0)^T$ (a) and $\mathbf{k} = 2\pi/L(5,0,0)^T$ (b).*

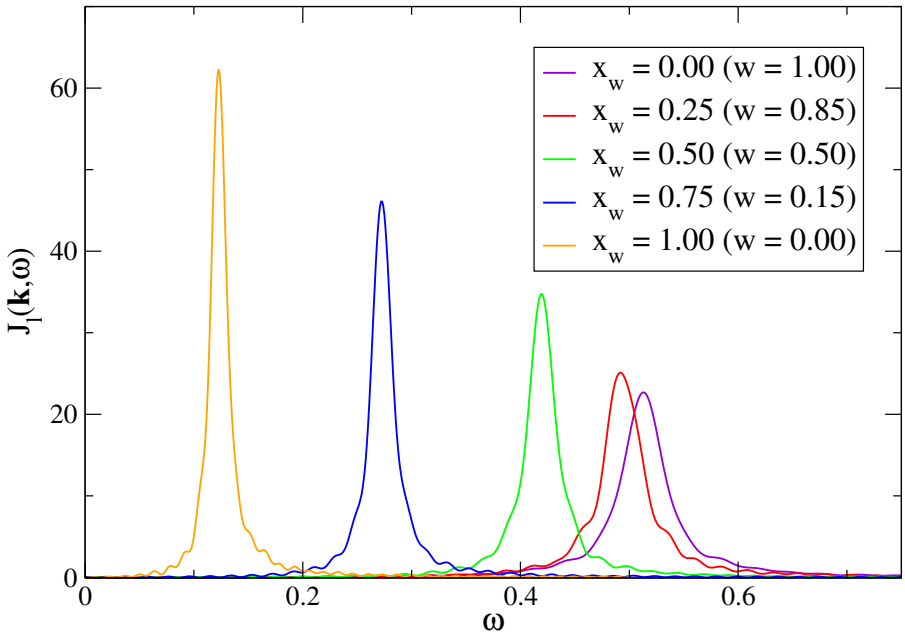

Figure 4.7.: *Spectra of longitudinal current correlation functions for systems consisting of particles with different identity: Lennard-Jones particles ($w = 1.0$), MPC particles ($w = 0.0$) and particles with a mixed identity ($w = 0.85; 0.50; 0.15$),* $\mathbf{k} = 2\pi/L(1,0,0)^T$.

Since this relation is just a consequence of the continuity equation, it is rigorous if the particles in a system are not being created or absorbed. The ω^2 factor in (4.11) means that the central Rayleigh component in $S(\mathbf{k},\omega)$ is effectively suppressed and will not show up in $J(\mathbf{k},\omega)$. If the sound peak in S is sharp, it will appear also as a sharp peak in J_l at essentially the same frequency. But if the sound peak in S is broad, it can appear considerably distorted in J_l and the peak position can be substantially higher. The calculated spectra for longitudinal correlation functions are shown on the Fig. 4.7.

From the spectra of the longitudinal correlation function $J_l(\mathbf{k},\omega)$ one can get the speed at which collective modes propagate in the fluid. The sound speed is defined [4] as

$$c_l(k) = \frac{\omega_m(k)}{k}, \tag{4.12}$$

where $\omega_m(k)$ is the frequency where $J_l(\mathbf{k},\omega)$ assumes its maximum value. Since $J_l(\mathbf{k},\omega)$ has a peak at any k, $\omega_m(k)$ is well defined and (4.12) may be regarded as the k-dependent sound speed. Calculated values for $c_l(k)$ are shown in the Fig. 4.8.

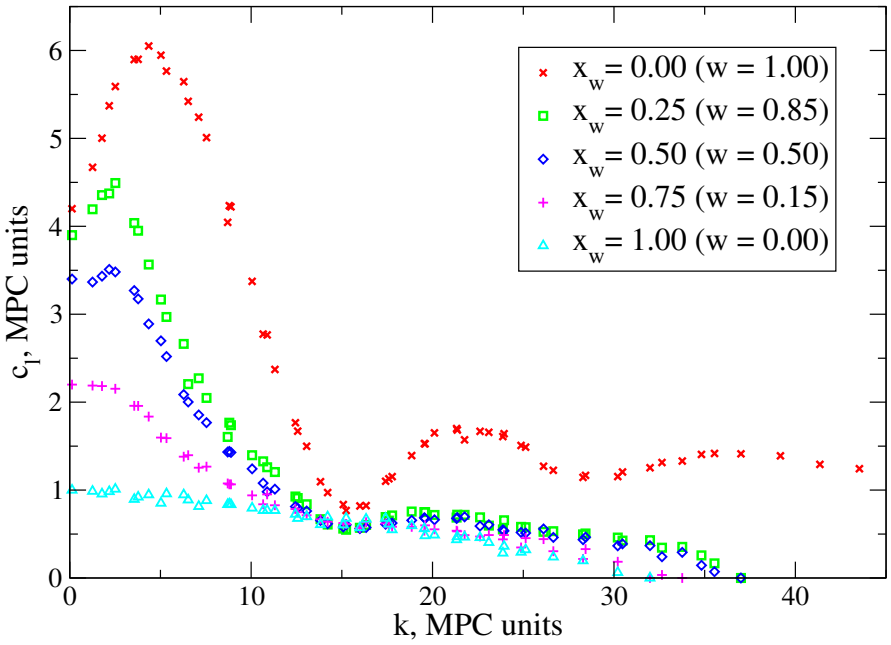

Figure 4.8.: *Velocity dispersion for systems consisting of particles with different identity: Lennard-Jones particles ($w = 1.0$), MPC particles ($w = 0.0$) and particles with a mixed identity ($w = 0.85; 0.50; 0.15$).*

4.5. Transverse current correlation functions

In the hydrodynamic regime the transverse current correlation function $J_t(\mathbf{k}, t)$ satisfies the transverse part of the linearized Navier-Stokes equation, which yields [4]

$$\frac{\partial}{\partial t} J_t(\mathbf{k}, t) = -\nu k^2 J_t(\mathbf{k}, t). \tag{4.13}$$

From this equation we get the theoretical formula for the transverse current correlation function:

$$J_t(\mathbf{k}, t) = e^{-k^2 \nu t}. \tag{4.14}$$

Since we chose the parameters for both MD and MPC systems in such a way that the viscosity η (or consequently the kinematic viscosity $\nu = \eta/\rho$) is the same, it can be expected that $J_t(\mathbf{k}, t)$ would be the same for systems with particles of different identities, depending only on wave vector $\mathbf{k}$. In the Fig. 4.9 the simulation results for several $\mathbf{k}$ values are shown. It can be seen that for every $\mathbf{k}$ the transverse current correlation function $J_t(\mathbf{k}, t)$ is in a very good agreement with a theory for all MD, MPC and mixed systems.

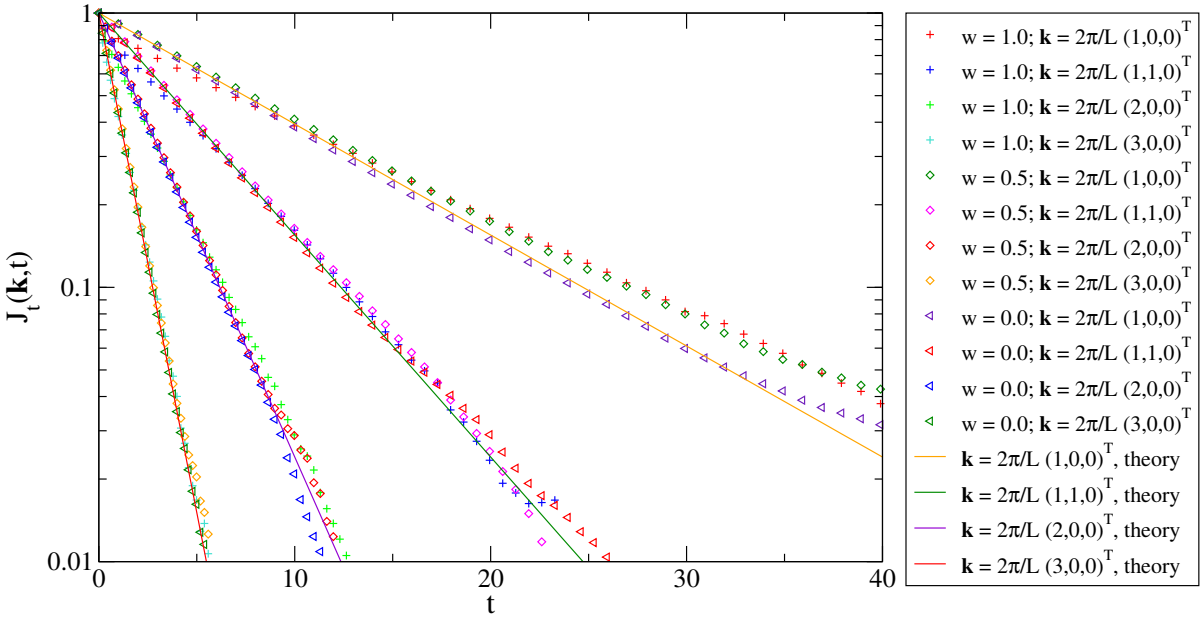

Figure 4.9.: *Transverse current correlation functions for systems consisting of particles with different identity: Lennard-Jones particles ($w = 1.0$), MPC particles ($w = 0.0$) and particles with a mixed identity ($w = 0.5$) for different* $\mathbf{k}$ *values. The agreement of the simulation results with the theoretical predictions shows that the viscosity remains the same for all hybrid identities.*

5. Implementation

The implementation of the hybrid scheme was made on the basis of the program MP2C (Massively Parallel Multi-Particle Collision dynamics) [78]. This program models complex fluids consisting of a solvent and embedded mesoscale particles, such as polymers or membranes. Since the program MP2C already includes MD and MPC models, it is convenient to modify this program to describe the desired coupling. This requires the implementation of a buffer zone. After the short description of the MP2C program, the modified implementation will be discussed in this chapter.

5.1. MP2C program

The MP2C program allows to simulate hydrodynamics of complex fluids. The solvent is described by MPC model, which takes into account thermal fluctuations and makes it possible to simulate flow phenomena on a mesoscale level. The embedded particles are simulated via MD method. A coupling between Molecular Dynamics and Multi-Particle Collision dynamics is realized as follows. The solvent is allowed to penetrate the solute and the stochastic rotation part is carried out for both the solvent and solute particles together. This method is appropriate for solvated complex molecules consisting of monomers, where angular momentum of the monomers does not play an important role. For single large particles, which carry linear and angular momentum, which both are important for the dynamical properties, this coupling is not appropriate. For such particles, the solvent should not be allowed to penetrate the solute and the momentum should be transferred by surface collision. The coupling between MD and MPC fluids allows to take into account hydrodynamic interactions between solvated particles, relevant for structural and dynamical effects. Different boundary conditions allow various experimental settings, like shear boundary conditions or channel flow. The program is implemented in module-oriented Fortran 90. The parallel algorithm is based on a three-dimensional domain-decomposition approach, and for homogeneous systems, excellent scaling behavior is obtained on the massively parallel architectures.

5.2. Hybrid MD/MPC program

5.2.1. Basic quantities

The schematic representation of the hybrid system modeled in simulations is shown in the Fig. 5.1. The basic quantities are

- Number of particles N. The number of particles in the whole system remains constant.
- Number of particles in the MD and adjacent buffer zones N_{MD}.
- Number of particles in the MPC zone N_{MPC}. Both N_{MD} and N_{MPC} can fluctuate, but the sum of them $N_{MD} + N_{MPC} = N$ remains constant.
- Box lengths L_x, L_y and L_z.
- MD zone length L_x^{MD}.
- Buffer zone length L_x^{buff}.

The information about particles, such as mass `m`, coordinates `x`, velocities `v` and relative velocities `v_rel`, are stored in two arrays: `slt` (solute) for MD and mixed particles, `slv` (solvent) for MPC particles (the structure of the derived types can be seen in A.2). Before every MPC step is performed, all particles are checked, whether or not they will stay in the MPC region. If the particle is going to cross the border between MPC and buffer zones during the next MPC time step, it is moved from the `slv` array to the `slt` array. For the particle i located in the MPC region, both the Lennard-Jones force and the external restraining force are zero, so while moving from the `slv` to the `slt` array, the value of `slt(i)%f` is set zero. The relocation of the particle from the `slv` to the `slt` array before the MPC time step is done for a smooth transition of MPC particles to the buffer region. The time step for MPC particles Δt_{MPC} is considerably larger then the MD time step Δt_{MD}. In our simulations $\Delta t_{MPC} = 20\Delta t_{MD}$. If such a particle had propagated as a MPC one, it would appear suddenly at some place in the buffer zone, quite far from the boundary. Since the simulated fluid is quite dense, this could cause an inconsistent increase of force for surrounding particles and the emerged particles itself. While propagating as MD particle, it will slowly approach the buffer zone with a predefined velocity, experiencing a smooth force increase after crossing the buffer zone boundary. The absolute index `i` remains the same for particle during the simulation run and can be used to track the particle.

The Lennard-Jones potential used in simulations is usually slightly modified. First, it is convenient to use a force-shifted potential to ensure that both potential U^{fs} and force $\vec{F}^{fs}$ are not only equal zero for particles with distances larger than the cut-off radius r_c,

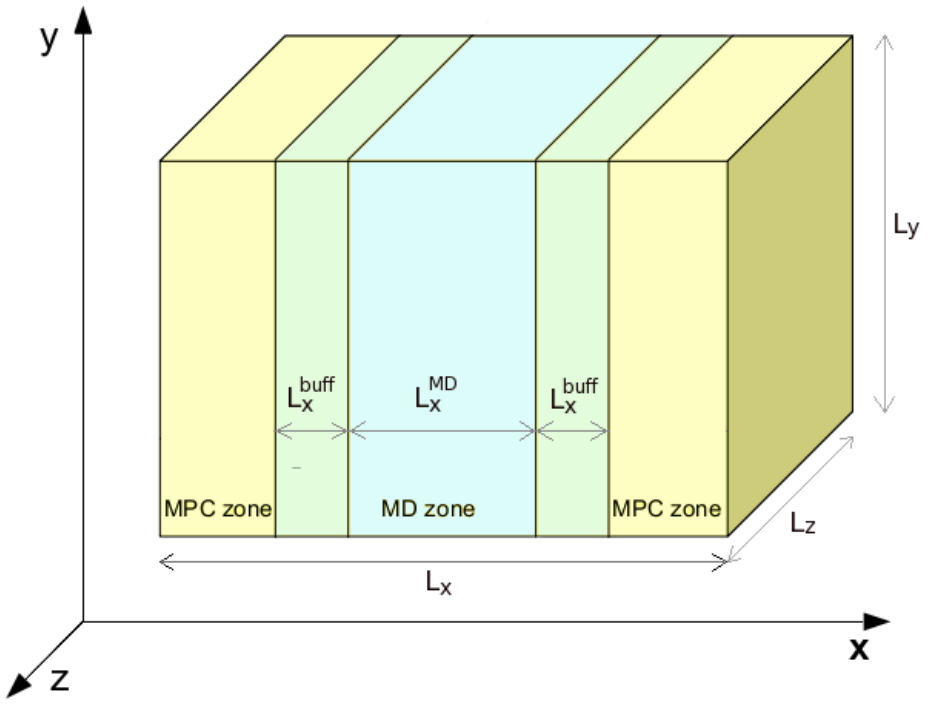

Figure 5.1.: *Scheme of the hybrid system used in simulations. L_x, L_y and L_z are simulation box length, L_x^{MD} is the length of the MD region, L_x^{buff} is the length of the buffer region.*

but that the force $\vec{F}^{fs}$ is a continuous function of r. Second, particles located near the MPC region can happen to be located very close to each other, and even though the LJ-interaction for such particles is quite strongly weighted with $w \simeq 0$ the singularity for $r = 0$ has to be avoided. The force-shifted potential and the corresponding force applied in our simulations can be seen in A.3.

5.2.2. Program structure

The structure of the modified program is as follows (Fig. 5.2):

MPC part I

- *mpc to md identity change*: before the propagation step for MPC particles will be performed, those `slv` particles which are going to leave the MPC zone are to be moved to the array `slt`.

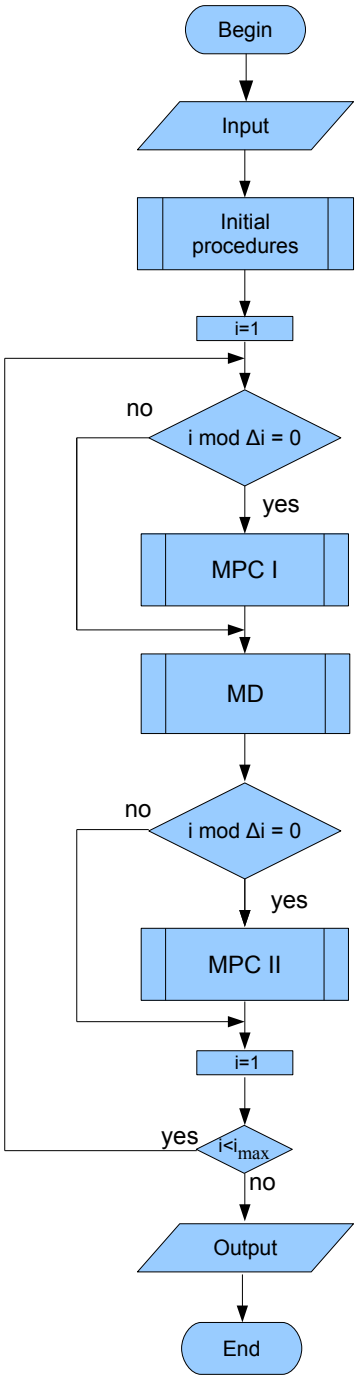

Figure 5.2.: *Flowchart of the program. Every MPC time step corresponds to Δi MD time steps, i_{max} is the number of MD time steps.*

- *streaming step*: new coordinates for the rest of solvent (MPC) particles are calculated

- *boundary conditions*: if particle's new coordinates are outside the simulation box, they have to be recalculated. Which coordinates are assigned depends on boundary condition rules

- *particle exchange*: if particle's new coordinates are outside the computational domain, it have to be transferred to the corresponding processor

MD part, repeated $\Delta t_{MPC}/\Delta t_{MD}$ times

- *integration 1*: this procedure consists of two the first steps of velocity Verlet algorithm (Eqs.(2.10), (2.11))

- *boundary conditions*: if particle's new coordinates are outside the simulation box, they have to be recalculated. Which coordinates are assigned depends on boundary condition rules

- *particle exchange*: if particle's new coordinates are outside the computational domain, it have to be transferred to the corresponding processor

- *interaction*: forces for new particles' position are calculated

- *force exchange*: for interacting particles located on the different processors, the information should be exchanged

- *extra buffer force*: for particles located in the buffer zone, an external restraining force has to be implied

- *integration step 2*: the last part of velocity Verlet algorithm

MPC part

- *md to mpc identity change*: MD particles propagated to the MPC region, are moved from the `slt` to the `slv` array

- *cell filling step*: mixed and MPC particles are sorted to the collision cells

- *exchange cell information*: if the collision cell lies on several processors, the information between them have to be exchanged

- *rotation step*: rotation of relative velocities of particles located in the buffer and MPC zones

5.3. Parallel implementation

The program MP2C is written in module-oriented Fortran 90. Message passing between processors is realized with the MPI standard [9]. The parallelization is based on a three-dimensional domain-decomposition approach, where particles are sorted onto processors according to their spatial coordinates. Boundaries of spatial domains are not altered during a simulation, so when a particle leaves a domain, it is transferred to the appropriate adjacent processor. For both the MD and the MPC part a minimum communication scheme is followed, i.e. particles are transferred in 2 x d communication steps, where d is the physical dimension.

5.3.1. Multi-Particle Collision dynamics

The underlying algorithm for Multi-Particle Collision dynamics is local in space, i.e., all operations are considered only in collision cells. Therefore, only information on the collision-cell level has to be exchanged between processors.

For the random shift, at each MPC time step a random vector $\boldsymbol{\xi}, \xi_\alpha \in [-a/2, a/2]$, is determined on a selected processor and broadcasted to all other processors. Since domain boundaries between processors are fixed, the collision grid overlaps in general with processor boundaries, so that collision cell are sheared between several processors, i.e., in two dimensions a collision cell may belong to 1, 2, or 4 processors, while in three dimensions they may belong to 1, 2,4 , or 8 different processors, depending on which domain boundary is cut by a collision cell.

In the collision step the center-of-mass velocity of a cell is required, therefore, data have to be exchanged between processor domains in order to determine the center-of-mass velocity uniquely for each overlapping cell. Besides, every cell needs a set of random numbers which determine the orientation of the random axis n_μ, which is required for the rotation of relative velocities. One possibility is to replicate particle coordinates and velocities in overlapping collision cells of neighbors' processors and to calculate the center-of-mass velocity on every processor in the same way. This method requires a data transfer in all directions.

A more efficient way of data exchange can be achieved by a forward data transfer in positive direction $(+x, +y, +z)$ and a backward data transfer in negative direction $(-x, -y, -z)$ only. Besides, instead of copying all the particle's information from one processor to another, only partial center of mass velocities can be sent, i.e.

$$\mathbf{v}_{cm}^{(\mu,\alpha)} = \frac{1}{m_{slv}^{(\mu,\alpha)}} \sum_{i=1}^{N_{slv}^{(\mu,\alpha)}} m_i, \mathbf{v}_i, \tag{5.1}$$

where $N_{slv}^{(\mu,\alpha)}$ is the number of solvent particles in a subvolume α in cell (μ). The sub-volume is the part of the cell, which is located within the geometrical domain of the local processor.

5.3.2. Molecular Dynamics

The most time-consuming part of the MD algorithm is force calculation. In the most direct implementation one would run a double loop over all particles in the system: for every particle i and every particle $j > i$ the distance between them is calculated, and if this distance is greater than the cutoff radius, the program skips to the end of the inner loop, avoiding expensive calculations. In such a method, in every time step $N(N-1)/2$ terms have to be computed, most of which turn out to be zero. To avoid unnecessary calculations, following scheme was proposed by L.Verlet in 1967 [79]. Every n-th step, all the $N(N-1)/2$ distances are computed and, for every particle i a list is established of all the particles which are within a distance r_L of that particle. Then, for the next $n-1$ steps in time, one takes into account only particles from this list. This method is exact as long as r_L is sufficiently larger than the cutoff radius r_c, so that no particle outside the list can penetrate the "skin" of depth $r_L - r_c$ in $n-1$ time steps. Verlet performed MD simulation of 864 particles, and the reported speed-up of the algorithm reached more the 10 times.

However, as the size of the system increases over 1000 particles, the conventional neighbor list becomes too large to store easily, and the testing of every particle on the system is inefficient. An alternative method of keeping track of neighbors for large systems is the linked-cell algorithm. The simulation box is divided into a regular lattice of M cubic cells. The side length of the cell is larger than the cutoff radius. Then for a given particle i, the possible interacting partners can be found only in adjacent cells. Using just two arrays, HEAD of size M containing the identification number of a particle in a cell and LIST of size N containing the linked list of the other particles in a cell, it is possible to limit the search of the possible interacting particles to there located in adjacent cells [6].

A similar linked-cell algorithm can be used in parallel implementation, but one should take into account that for some cells adjacent ones will be found on the other processors [81]. As for MPC parallel implementation, the data transfer between processors in all directions should be avoided. Hence, first data are exported to the $(-x, -y, -z)$-directions. Using Newton's principle of action/counter-action, in the force calculation

for every particle in a given cell within the domain, only 13 neighbor cells have to be considered. Calculation the forces on a processor within a given geometrical domain also includes the calculation between resident and imported particles. The latter forces are transferred back to the processors from where particles were imported before. This back-transfer of forces takes place in the same sequence as the import of particles before, i.e. the indices, associated with forces are stored in the same way as for the particles before. This guarantees that the lists, which were created in the export-step, may be used to sum up forces of exported particles correctly. Since the organization of cells is static in the present version of the program and the domain boundaries as well as size of the import regions remain constant during a simulation, lists are created in the beginning of a simulation, which contain the relevant neighbors of the cells for which interactions are calculated.

When particles move across processor domain boundaries, they have to be transferred to the processor associated with the geometrical region of their new positions. In this communication step, particles are exported/imported together with their coordinates, velocities, masses and absolute indices. Communication is realized via asynchronous MPI operations where a receive operation is posted, waiting for data to be received. After the communication step, the particle arrays on every processor have voids at those indices corresponding to exported particles. The import buffer of particles is therefore sorted into the existing array in such a way that first the voids are filled and the remaining imported particles are put at the end of the array. If there are less particles imported than exported, particle entries from the end of the array are taken to fill voids. This type of sorting of particles mixes indices in long simulation runs completely. It is the absolute index of the particles, which is carried across domain boundaries and which guarantees a unique mapping of particles to molecules and particle properties.

6. Validation of the method

In this chapter some test simulations with the hybrid system will be presented. The aim of these simulations is to check whether hydrodynamic interactions between regions with different representations are altered by coupling. To do that, the following flow simulations were performed: poiseuille flow, shear flow and couette flow. Also the transverse correlation function for the whole hybrid system was calculated. The coupled system in all these simulations has following dimensions (Fig. 6.1): 70 MPC cells in x-direction, containing the MD-zone in the middle separated with two buffer-zones from the MPC region. The size of the MD-zone is 20 MPC cells, the size of each buffer zone is 10 MPC cells. The size of the system in the y- and z- directions is 50 and 30 MPC units respectively. The system contains 1010625 particles. For most simulations it is confined between two planar walls parallel to the yz-plane, in the other two directions periodic boundary conditions are applied. The results obtained for the coupled system will be compared with theory and analogous simulations with systems consisting only of MPC or MD particles. These "pure" systems have the same size (70x50x30 cells), the same number of particles and the same boundary conditions as the coupled one.

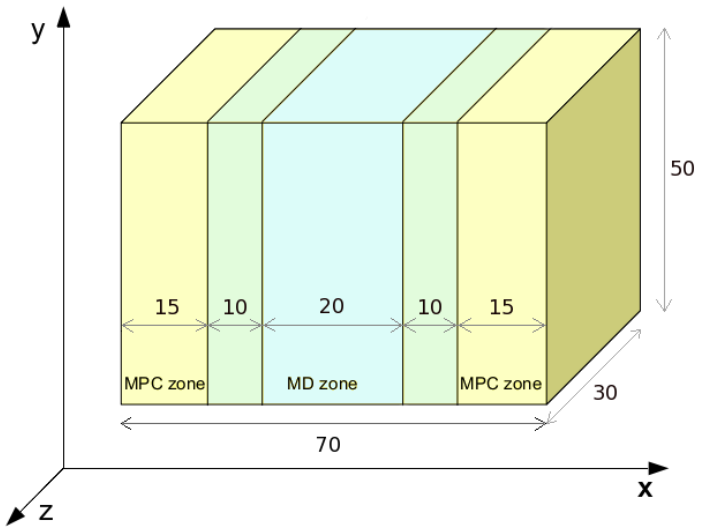

Figure 6.1.: *Scheme with measurements of the coupled system used in simulations with the dimensions of the various domains.*

6.1. Transverse current correlations for the hybrid system

In chapter 4 various correlation functions characterizing different hydrodynamic properties of the fluid were calculated for the systems consisted of particles with "mixed" identity, including the transverse correlation function $J_t(k,t)$. We also calculated $J_t(k,t)$ for the whole coupled system. This case is a bit different from that discussed above, because the coupled system fluid is not isotropic. When we write in the legend of the Fig. 4.9 $\mathbf{k} = 2\pi/L(1,0,0)^T$ (the first curve), it is actually an average curve for $\mathbf{k}_1 = 2\pi/L(1,0,0)^T$, $\mathbf{k}_1 = 2\pi/L(0,1,0)^T$ and $\mathbf{k}_1 = 2\pi/L(0,0,1)^T$. But since for the fluid in the cubic box consisting of identical particles there is no preferred direction, all curves are the same and can be averaged.

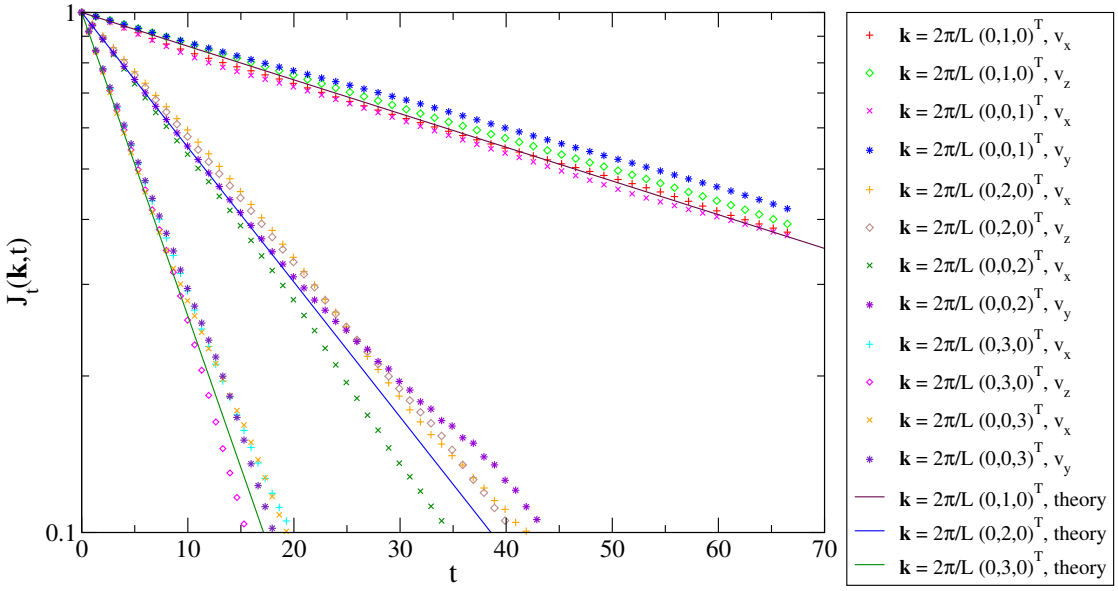

Figure 6.2.: *Transverse current correlation functions for the coupled system for different* $\mathbf{k}$ *values. There is a good agreement with the theory for the current in all directions.*

The situation with a hybrid system is different. There is a distinguished direction in the system: the direction perpendicular to the buffer zone. This is the direction in which particles change their identity and in which the external restraining force is applied. That is why it would be interesting to check, whether the anisotropy of the system disturbs the transverse current correlation function. For that purpose we calculated two separate transverse correlation functions $J_t(k,t)$ for every k vectors: one parallel to the particular direction x and the other perpendicular to it. As it can be seen on the Fig. 6.2, both transversal components for every direction of the wave vector $\mathbf{k}$ show a good agreement with theory.

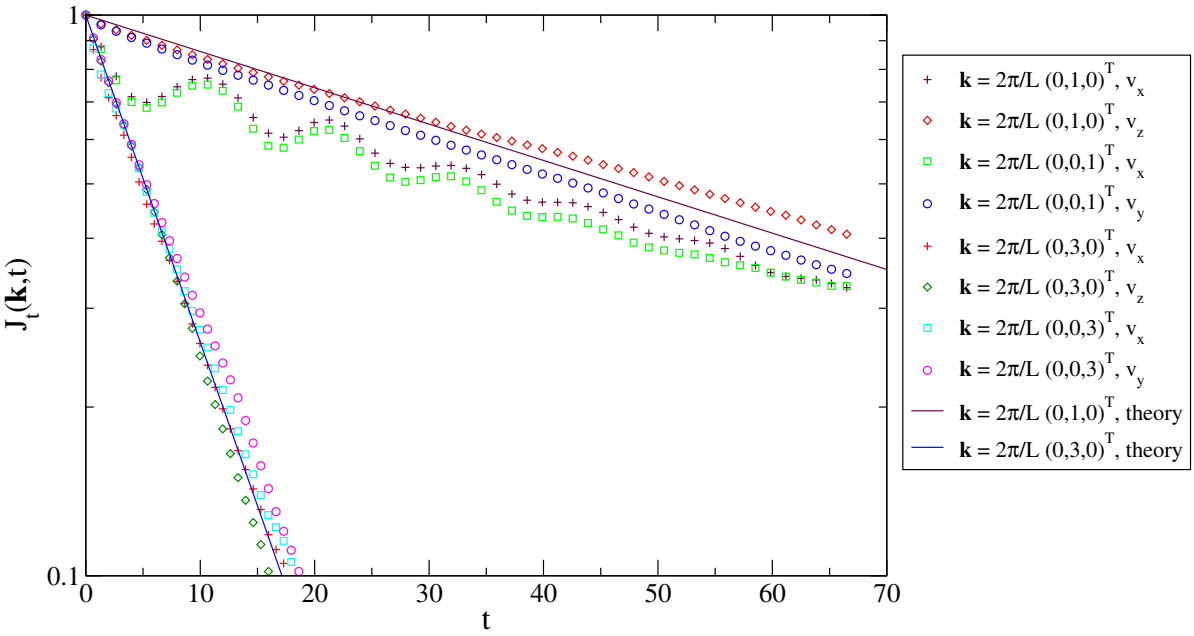

Figure 6.3.: *Transverse current correlation functions for the particles of the MD-zone of the coupled system for different* $\mathbf{k}$ *values. For the wave vector* $|k| = 2\pi/L$*, the component in* x*-direction (the distinguished direction of our system) shows damped oscillations.*

When the current of the whole system is calculated, the contributions from all particles are summed up. That means at every time step we obtain the current value averaged between MD, MPC and buffer zones. It could also be interesting to look at parts of system only, to obtain the information on the current of the individual regions.

Since we calculate the current for a part of the system only, the number of particles in the summation is not a constant any more and the expressions for current and its correlation function have to be rewritten:

$$j_\alpha^{part}(\mathbf{k},t) = \sum_l^{N_{part}(t)} v_{l\alpha}(t) e^{i\mathbf{k}r_l(t)}. \tag{6.1}$$

$$J_{\alpha\beta}^{part}(k,t) = \frac{1}{\langle N_{part}(t)\rangle} \langle j_\alpha^{part*}(\mathbf{k},0) j_\beta^{part}(\mathbf{k},t)\rangle \tag{6.2}$$

In our simulations the direction perpendicular to the buffer zone is the x-direction. So if we calculate the current for particles from the given region of the system, this "subsystem" will have periodic boundary conditions only in y- and z- directions. To reveal the properties of currents from the various regions for a given wave vector $\mathbf{k}$,

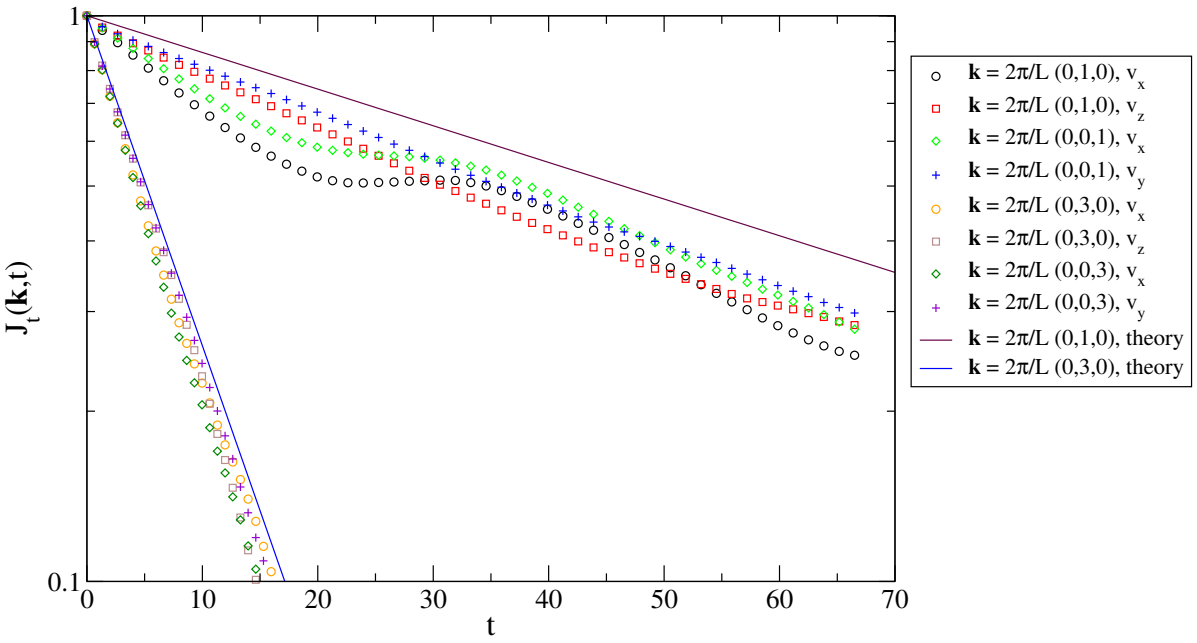

Figure 6.4.: *Transverse current correlation functions for the particles of the MPC-zone of the coupled system for different* **k** *values. For the wave vector* $|k| = 2\pi/L$*, the component in* x*-direction (the distinguished direction of our system) shows damped oscillations.*

we performed series of simulations for **k** parallel to the y-direction and calculated two transverse current correlation functions: one in z-direction and other in x-direction. The obtained simulation results (Figs. 6.3, 6.4, 6.5) are somewhat confusing at first glance. For the smallest wave vector $|\mathbf{k}| = 2\pi/L$ the component in x-direction (the distinguished direction of our system) shows damped oscillations. The corresponding component in z-direction has no oscillations, but the agreement with theory is not extremely good. For larger $|\mathbf{k}|$ values there is a good agreement with the theoretical predictions. Thus the question arises: what causes the oscillations? Is it the coupling disturbing the proper propagation of transverse modes, or is it a consequence of calculating $J_t(k,t)$ only for part of the particles?

In order to answer this question the following simulations were performed. The simulation box of the same size is considered, but consisted exclusively of MD particles, interacting via Lennard-Jones potential. Then the transverse current correlation function is calculated, but only for particles from the region corresponding to the MD region in the coupled system. The results shown that for the smallest value of wave number $\mathbf{k} = 2\pi/L(0,1,0)^T$, both transverse current correlation functions J_t^z and J_t^x present the same behavior as for the coupled system: the function J_t^x parallel to x-direction shows oscillations, the function J_t^z perpendicular to the x-direction deviates from the theoreti-

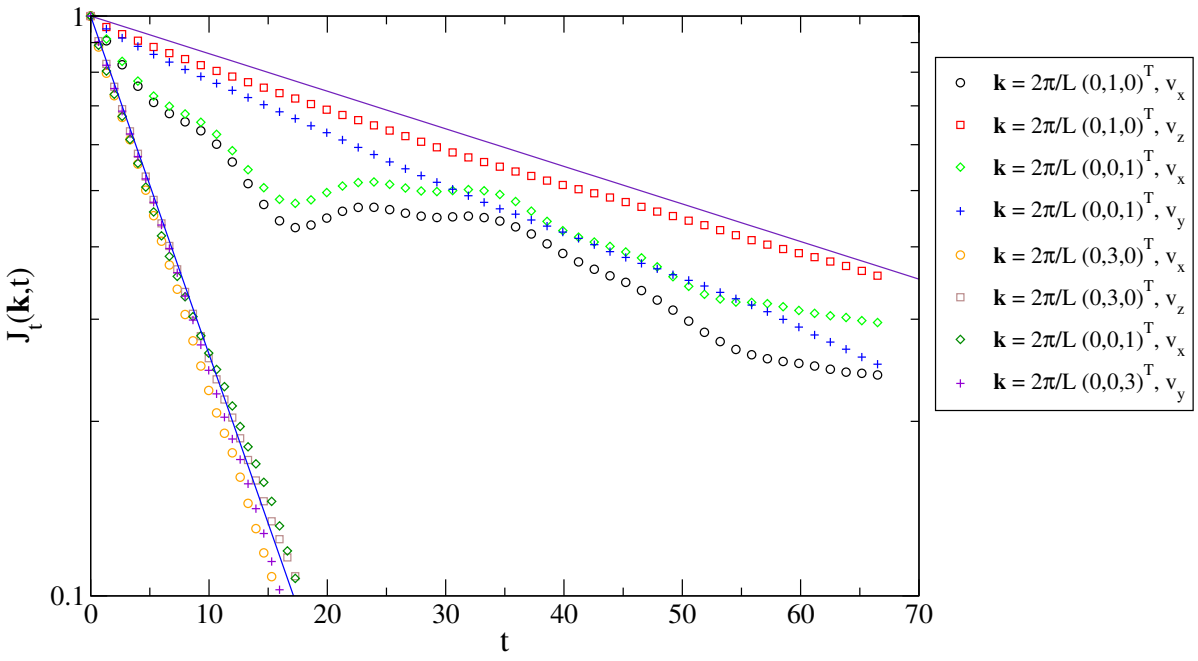

Figure 6.5.: *Transverse current correlation functions for the particles of the buffer zone of the coupled system for different* $\mathbf{k}$ *values. For the wave vector* $|k| = 2\pi/L$*, the component in x-direction (the distinguished direction of our system) shows damped oscillations.*

cal value (Fig. 6.6), although the transverse current correlation function $J_t^{wh.sys.}(k,t)$ for the whole system agrees with theory very well.

The explanation for this is that the $J_t^{wh.sys.}(k,t)$ is not only the sum of transverse current correlation functions for the composing subsystems, but there are also some "cross-terms" (A.4):

$$\begin{aligned} J_t^{wh.sys.}(k,t) &= \frac{1}{N}\left\langle \sum_l^N v_{l,t}(0)e^{-i\mathbf{k}\mathbf{R}_l}(0) \sum_l^N v_{l,t}(t)e^{i\mathbf{k}\mathbf{R}_l}(t)\right\rangle \\ &= \frac{\langle N_1\rangle}{N} J_t^{part1}(k,t) + \frac{\langle N_2\rangle}{N} J_t^{part2}(k,t) \\ &\quad + \frac{1}{N} J_t^{cross12}(k,t) + \frac{1}{N} J_t^{cross21}(k,t), \end{aligned} \tag{6.3}$$

where

$$\begin{aligned} J_t^{cross12}(k,t) &= j_t^{part1*}(k,0) j_t^{part2}(k,t) \\ J_t^{cross21}(k,t) &= j_t^{part2*}(k,0) j_t^{part1}(k,t). \end{aligned} \tag{6.4}$$

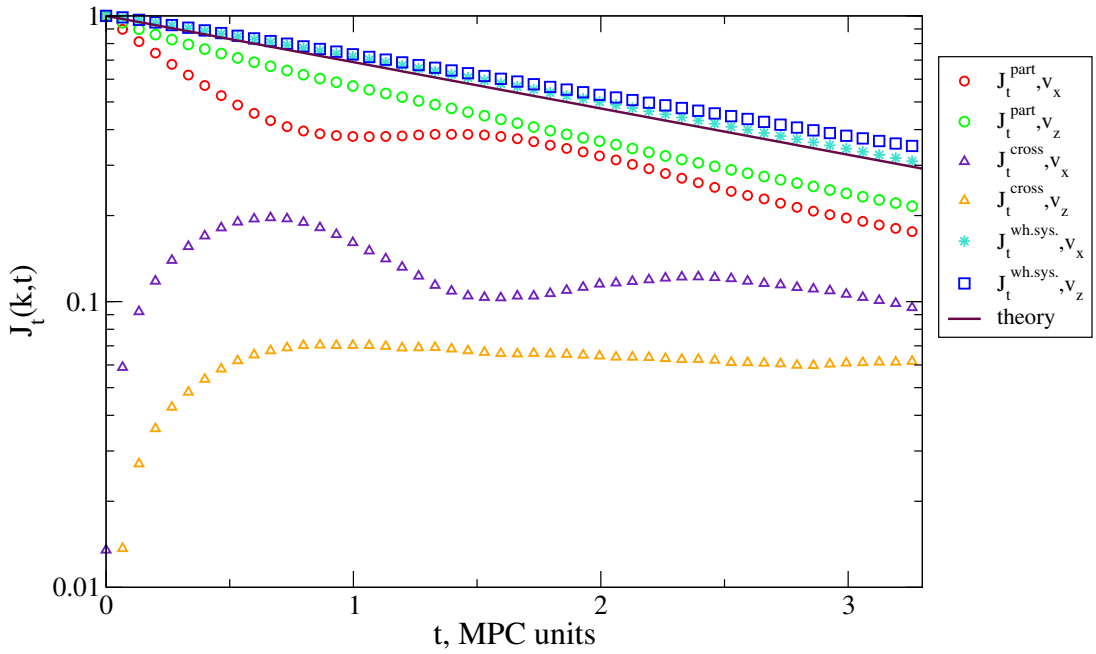

Figure 6.6.: *Transverse current correlation functions for the whole MD system and a part of it. The component in x-direction shows damped oscillations, which is it a consequence of calculating $J_t(k,t)$ only for part of the particles.*

The purple and orange curves on the Fig. 6.6 indicate the cross-terms in x- and z-directions.

6.2. Poiseuille flow

In Poiseuille flow simulations, the fluid is confined between two planar walls parallel to the yz-plane of the coupled system. A gravitational field acting on every fluid particle induces a flow along the y-axis corresponding to a pressure-driven flow. Hence, the propagation step along the flow direction is now given by

$$\hat{v}_{iy}(t + \Delta t) = v_{iy} + g\Delta t, \tag{6.5}$$

$$r_{iy}(t + \Delta t) = r_{iy}(t) + v_{iy}(t)\Delta t + \frac{1}{2}g\Delta t^2. \tag{6.6}$$

If there is no slip between fluid and walls, the profile of velocity in y-direction in the stationary state is parabolic:

$$v_y(x) = \frac{v_{max}(H - x)x}{H^2}, \tag{6.7}$$

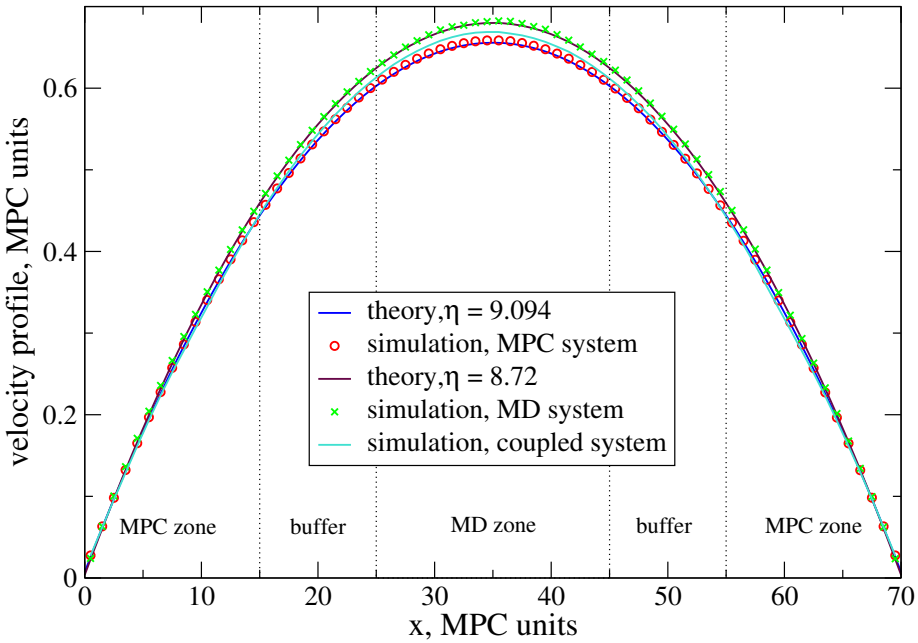

Figure 6.7.: *Velocity profiles of the fluid under Poiseuille flow for various systems. Simulation results are compared with theoretical calculations. The red circles represent the velocity profile obtained from simulations with a pure MPC system. It shows very good agreement with theoretical predictions (solid blue). Numerical data for the velocity profile of the pure MD system is represented by green symbols. It is fitted by a theoretical curve with viscosity $\eta_{MD} = 8.72$, somewhat different from the expected one. The solid light-blue line shows velocity profile for the coupled system obtained from simulations.*

where H is the distance between the two walls and v_{max} is the maximum flow velocity. The velocity v_{max} depends on the strength of the applied field g, the surface separation H, and the kinematic viscosity ν of the fluid

$$v_{max} = \frac{gH^2}{8\nu}. \tag{6.8}$$

In MPC no-slip boundary conditions are conveniently simulated by employing a bounce-back rule, i.e. the velocities of particles which hit the wall are inverted after collision. But it was shown [29] that a simple bounce-back rule only works if walls coincide with the boundaries of the collision cell. However in most situations of interest, the walls don't coincide with the cell boundaries, and even are not parallel to them. Moreover, if the mean-free path is small, then a shift of the cell lattice is required to guarantee Galilean invariance, so partially occupied boundary cells are unavoidable even for the simplest flow geometries. To avoid the slip of the fluid, Lamura et al. proposed the following generalization of the bounce-back rule for partially filled cells [29]. For all cells which are cut by walls and therefore have a number of particles N_c smaller then the

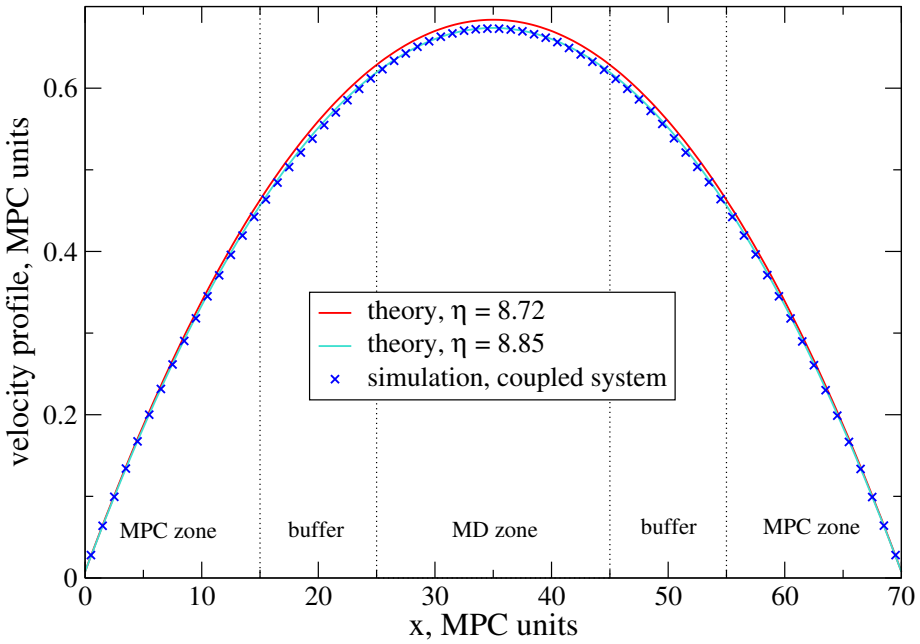

Figure 6.8.: *Velocity profiles of the fluid under Poiseuille flow. Coupled system with tuned MPC parameters. Numerical results are represented by blue symbols. The solid red line shows the expected profile and the solid light-blue line the fitted one. The difference between the obtained profile and the theoretical one lies within 2%.*

average number M of bulk cells, we fill the "wall" part of the cell with virtual particles in order to make the effective density of real plus virtual particles equal the average density. The velocities of the wall particles are drawn from a Maxwell-Boltzmann distribution of zero average velocity and the same temperature T as the fluid. The collision step is performed with the average velocity of all particles in the cell.

In Fig. 6.7 velocity profiles of the fluid under Poiseuille flow for various systems are shown. The profile obtained from simulations with a hybrid system (light-blue line) is compared with the results of the simulations performed with the pure MD (green symbols) and MPC (red circles) systems. The remarkable agreement with theory for the MPC system can easily be seen (blue line). The theoretical velocity profile for the viscosity value $\eta_{MPC} = 9.094$ calculated from Eqs.(2.51) and (2.60) fit perfectly to the velocity profile obtained from simulation. Although there is still a slip between the fluid and the wall (0.2 MPC units), but such a small value is almost unnoticeable.

While matching parameters of the LJ and MPC fluids (section 3.3), the viscosity η_{MD} calculated via the Green-Kubo relation (2.22) was used, which is not accurate enough. Indeed, the error was about 10%, so a small deviation between η_{MD} and η_{MPC} values can be expected. The theoretical fit for the velocity profile of the pure MD fluid under

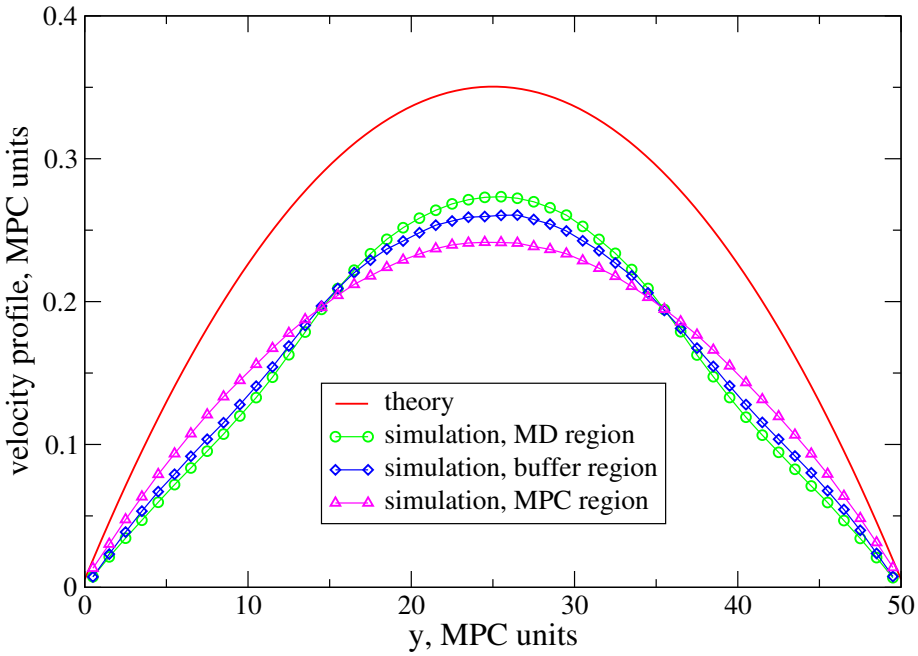

Figure 6.9.: *Velocity profiles of the fluid under Poiseuille flow perpendicular to the buffer layer. The velocity profiles show noticeable deviations from the expected theoretical values.*

Poiseuille flow gives $\eta_{MD} = 8.72$. The deviation from η_{MPC} is about 4%. The velocity profile for the coupled system lies between the MD- and MPC- profiles, which corresponds to a average viscosity value.

It is possible to tune the MPC parameters in such a way that viscosity will be $\eta_{MPC} = 8.72$. One could expect that in this case the viscosity of the coupled system will be also $\eta_{coupl.sys.} = \eta_{MPC} = \eta_{MD} = 8.72$, but there is still small deviation (1%) from this value (Fig. 6.7). The curve obtained from simulations corresponds to the value of viscosity $\eta_{coupl.sys.} = 8.85$. The explanation is that although the viscosities of MD and MPC fluids are perfectly matched, there can be some region within a buffer zone, where combined influence of the two fluids cannot ensure the exact value of viscosity.

We also performed Poiseuille flow simulations with the same system but in x-direction. That means, the system was confined between two walls parallel to xz-plane and the external force acted in the x-direction. For such an orientation, the external driving force acts perpendicular to the buffer zone. In the Fig. 6.9 one can see that in this case the velocity profile is very far from the desirable analytical one. The velocity profile of particles from the MPC zone shows that the effective viscosity is several times larger than the normal one, and for particles from the MD and buffer zones the profile is not even parabolic any more.

6.3. Shear flow

The study of shear flow is interesting because this kind of flow occurs whenever a fluid flows past a surface. In continuum fluid mechanics, the simplest shear flow model is when only one component of the velocity vector assumes a non-zero value: $v_y = v_y(x), v_x = v_z = 0$. The quantitative characteristics of the shear flow is the shear rate, the rate of change of velocity at which one layer of fluid passes over an adjacent layer

$$\dot{\gamma} = \frac{dv_y(x)}{dx}. \tag{6.9}$$

The existence of the shear flow is possible due to the presence of viscosity in the fluid: a moving fluid layer drags the adjacent layers with it. The shear stress τ between two adjacent layers is proportional to the shear rate and viscosity:

$$\tau = \eta \frac{dv_y(x)}{dx}. \tag{6.10}$$

If the fluid is homogeneous, the velocity gradient dv_y/dx is constant and perpendicular to the velocity itself.

To simulate a steady shear flow, one confines a fluid between two walls, which are moving with constant velocities in opposite directions. It is important to implement no slip between the walls and the fluid because otherwise the walls' velocity won't be conveyed properly to the adjacent fluid layers. In our simulation the walls parallel to the yz-plane are moving in opposite directions along the y-axis (Fig.6.1). The absolute values of walls' velocities are equal.

As mentioned above, for a homogeneous fluid, the velocity gradient is constant. So the expected velocity profile is just a stright line between the boundary values at the walls. All velocity profiles obtained from simulations, both for the coupled and for pure systems are in very good agreement with the theory. The deviations from the expected behavior are for all cases very small and almost not observable that is why in the Fig. 6.10 not the velocity profiles themselves are presented, but their deviations from the ideal theory curve.

The red and green curves in the Fig. 6.10 show velocity profiles obtained from simulations of the pure systems, MD and MPC respectively. Both lines are the straight but non-zero lines, which shows that in both systems there is a small slip between the fluid and the wall. The other three curves represent the coupled system. As expected, for all of them the slip length is the same as for pure MPC system. The blue-square curve shows simulation results for a system with initial MPC parameters, providing $\eta_{MPC} = 9.094$. Taking into account the location of different representation regions, it can easily be seen that η_{MPC} is larger than η_{MD}, which is consistent with the results of

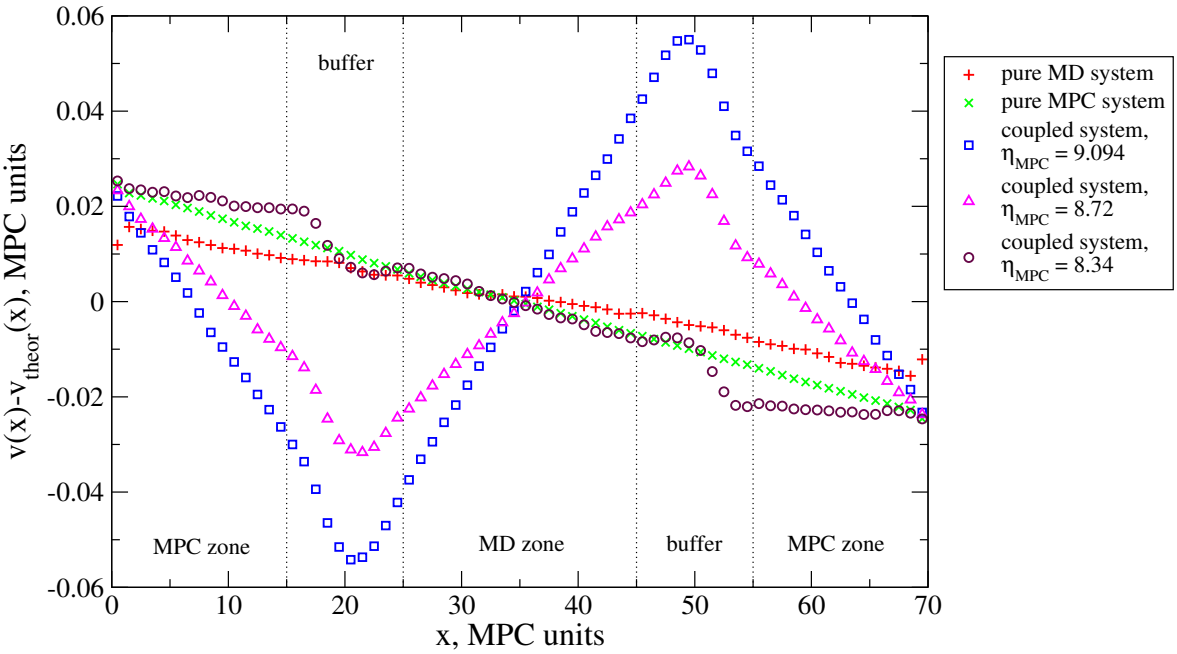

Figure 6.10.: *Deviations of the velocity profiles from the theoretical one for a fluid under the shear flow for different systems, pure and coupled with slightly different MPC parameters. All deviations from the theoretical values lie within 2%.*

the previous section. Essentially, we have two fluids with different viscosities separated by the buffer zone. The moving walls force adjacent fluid layers to move with them, these layers force to move the next ones. Since the viscosity in the middle part of the coupled system (in the MD region) is smaller, the particles from this zone move more easily, so the velocity profile slope in this zone is larger then the theoretical one.

The purple-triangle curve presents results for the coupled system with tuned MPC parameters, where $\eta_{MPC} = \eta_{MD}$. In this case the deviations are smaller, but still exist and in the particular form of the profile in the buffer zone become more visible. The violet-circle curve shows that even with further tuning of MPC parameters there are still deviations of the velocity profile in the buffer zone. As in the previous section, it shows that the combined influence of the two fluids cannot ensure the exact value of viscosity along the whole length of the buffer zone.

6.4. Oscillatory Couette flow

To simulate an oscillatory Couette flow, the right wall (Fig. 6.1) velocity was varied in the y-direction with the frequency ω and amplitude U, while the left wall always remained stationary. This problem was investigated analytically by Mattews and Hill [83]. Below

we review the problem and its solution for our flow geometry. A velocity profile of the form $v_y = v_y(x,t), v_x = v_z = 0$ is assumed, thus the y-component of the momentum equation (parallel to the walls) yields

$$\rho \frac{\partial u_y}{\partial t} = -\frac{\partial p}{\partial y} + \eta \frac{\partial^2 u_y}{\partial x^2}. \tag{6.11}$$

The x- and z-components of the momentum equation imply $\partial p/\partial x = \partial p/\partial z = 0$, and since $v_y = v_y(x,t)$, this means $p = 0$. Hence, the equation to solve is

$$\rho \frac{\partial u_y}{\partial t} = \eta \frac{\partial^2 u_y}{\partial x^2}. \tag{6.12}$$

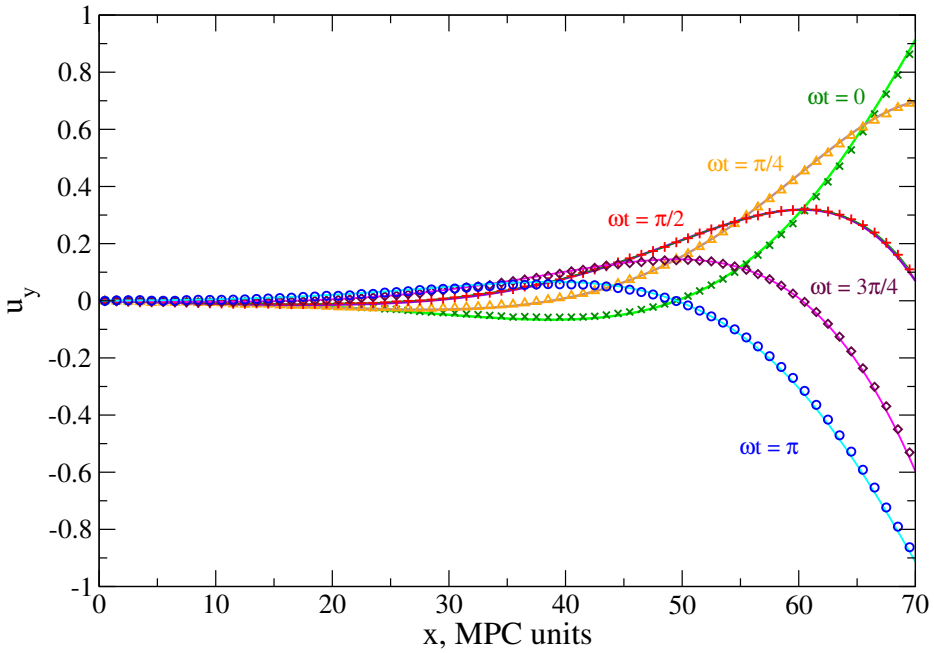

Figure 6.11.: *Average velocity profiles for a MPC fluid in Couette flow at times* $\omega t = 0, \pi/4, \pi/2, 3\pi/4,$ *and* π. *The symbols indicate simulation results, the solid lines are theoretical predictions.*

The boundary conditions at the left and the right walls are specified as follows:

$$\begin{aligned} u_y\Big|_{x=x_{left}} &= l_1 \frac{\partial u_y}{\partial x}\Big|_{x=x_{left}}, \\ u_y\Big|_{x=x_{right}} &= U cos(\omega t) - l_2 \frac{\partial u_y}{\partial x}\Big|_{x=x_{right}}. \end{aligned} \tag{6.13}$$

The slip lengths at the left and right walls $l_1 \neq l_2$ are assumed to be different but constant. Assuming a solution of the form

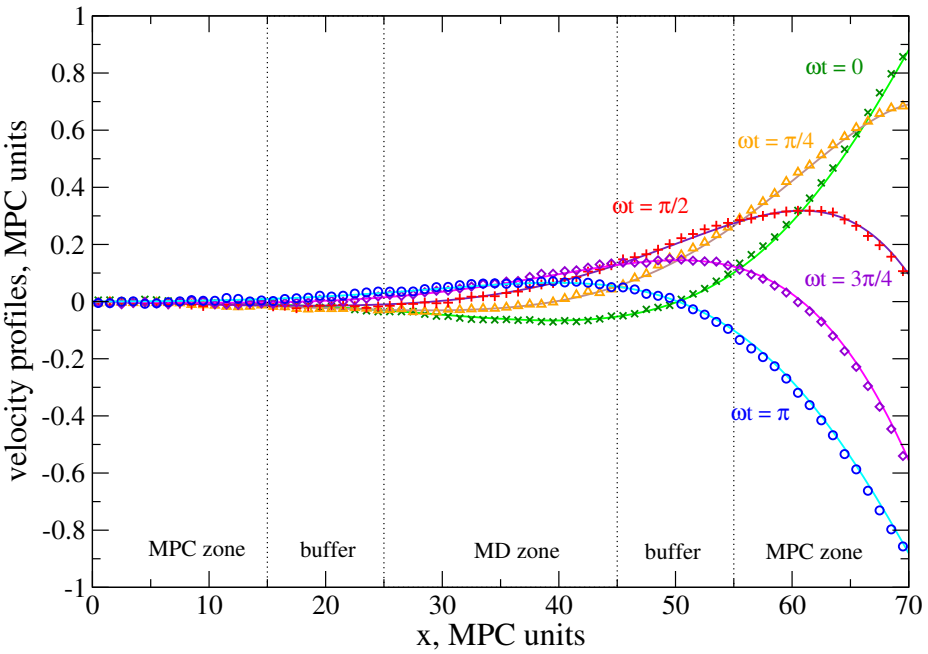

Figure 6.12.: *Average velocity profiles for a hybrid fluid in Couette flow at times* $\omega t = 0, \pi/4, \pi/2, 3\pi/4,$ *and* π. *The symbols indicate simulation results, the solid lines are theoretical predictions.*

$$v_y(x,t) = Re\big[\exp(i\omega t) f(x)\big], \tag{6.14}$$

where $Re[f]$ denotes the real part of f, the boundary condition at $x = x_{right}$ can be written as

$$x = x_{right} : u_y = U Re\big[\exp(i\omega t)\big] - l_2 \frac{\partial u_y}{\partial x}. \tag{6.15}$$

Substituting the assumed form of the velocity profile into Eq.(6.12) yields

$$i\rho\omega f = \eta \frac{d^2 f}{dx^2}, \tag{6.16}$$

which must be solved subject to

$$\begin{aligned} x = x_{left} \quad &: \quad f = l_1 \frac{df}{dx}, \\ x = x_{right} \quad &: \quad f = U - l_2 \frac{df}{dx}. \end{aligned} \tag{6.17}$$

The general solution of the Eq.(6.16) satisfying the boundary conditions (6.17) is

$$\begin{aligned} f(x) &= C_1 \exp\left(-\sqrt{\frac{i\omega\rho}{\eta}}x \right) + C_2 \exp\left(\sqrt{\frac{i\omega\rho}{\eta}}x \right) \\ &= C_1 \exp\big[-(1+i)kx \big] + C_2 \exp\big[(1+i)kx \big], \end{aligned} \tag{6.18}$$

where we have used the result $i = (1+i)^2/2$, $k = \sqrt{\omega\rho/2\eta}$ and C_1 and C_2 are integration constants, which are found to be

$$\begin{aligned} C_1 = U\big[1 - l_1 k(1+i)\big] \times \\ \Big\{ \big[1 - l_1 k(1+i)\big]\big[1 - l_2 k(1+i)\big] \exp\big[-(1+i)kH \big] \\ - \big[1 + l_1 k(1+i)\big]\big[1 + l_2 k(1+i)\big] \exp\big[(1+i)kH \big] \Big\}^{-1}, \end{aligned} \tag{6.19}$$

$$\begin{aligned} C_2 = U\big[1 + l_1 k(1+i)\big] \times \\ \Big\{ \big[l_1 k(1+i) + 1\big]\big[l_2 k(1+i) + 1\big] \exp\big[(1+i)kH \big] \\ - \big[1 - l_1 k(1+i)\big]\big[1 - l_2 k(1+i)\big] \exp\big[-(1+i)kH \big] \Big\}^{-1}, \end{aligned} \tag{6.20}$$

where H is the distance between the left and the right wall. Writing $a = a^+ - a^-$ and $b = b^+ + b^-$, which are defined as follows:

$$\begin{aligned} a^{\pm} = \exp(\pm kH) \Big\{ \big[1 \pm (l_1 + l_2)k\big] \cos(kH) \\ - \big[(l_1 + l_2)k \pm 2 l_1 l_2 k^2\big] \sin(kH) \Big\}, \end{aligned} \tag{6.21}$$

$$\begin{aligned} b^{\pm} = \exp(\pm kH) \Big\{ \big[1 \pm (l_1 + l_2)k\big] \sin(kH) \\ + \big[(l_1 + l_2)k \pm 2 l_1 l_2 k^2\big] \cos(kH) \Big\}, \end{aligned} \tag{6.22}$$

the integration constants may be written as

$$C_1 = \frac{U\Big\{ l_1 k(a+b) - a + i\big[l_1 k(a-b) + b \big] \Big\}}{a^2 + b^2}, \tag{6.23}$$

$$C_2 = \frac{U\Big\{ l_1 k(a+b) + a + i\big[l_1 k(a-b) - b \big] \Big\}}{a^2 + b^2}. \tag{6.24}$$

The velocity profile is then given by

$$\begin{aligned} u_y(x,t) = \frac{U}{a^2+b^2}\Big\{ & \exp(kx) \times \Big[\big[l_1 k(a+b)+a\big]\cos(\omega t + kx) \\ & - \big[l_1 k(a-b)-b\big]\sin(\omega t + kx)\Big] \\ & + \exp(-kx) \times \Big[\big[l_1 k(a+b)-a\big]\cos(\omega t - kx) \\ & - \big[l_1 k(a-b)+b\big]\sin(\omega t - kx)\Big]\Big\}. \end{aligned} \tag{6.25}$$

To obtain the velocity profile for a given phase value ωt, the statistics was gathered "stroboscopically": the measurements of the velocity profile are performed at discrete times $\omega t_n = n\pi/4 + 2\pi m$, where $n = 0, 1, ...$ and m is integer. Each point of the profile is the averaged value within vertical slab of thickness $\Delta x = 1a$ during the time interval $T/100$, where $T = 2\pi/\omega$ is the oscillation period.

At first simulations of a pure MPC system are performed. Assuming the slip length at the left wall $l_1 = 0$ and knowing the analytical value of viscosity for a MPC fluid, we find a value of the slip length at the right wall l_2 such that the velocity profiles obtained by simulations will be well fitted by the theoretical solution (6.25) of the Eq. (6.12) (Fig. 6.11). The solid lines of the figure are theoretical calculations and the discrete data are simulation results. The presented curves cover half of the oscillations period.

Since the coupled system embodies an MPC layers near the boundary walls, the value $l_2 = 1.35$ can be used as a parameter for solution for the coupled system too. In the Fig. 6.12 one can see that the agreement for the coupled system with the theory is also very good, and there are no disturbances of the velocity profile at the boundaries between regions with different representations.

6.5. Two particles in optical traps

Hydrodynamic interactions play a crucial role in many physically interesting systems, such as colloidal suspensions, polymers in solution and the microscopic dynamics of proteins. Unfortunately, it can often be difficult to separate the effects caused by hydrodynamics from other ones: in experiments, measurements are usually made on bulk systems with indirect methods; in simulations one has to combine different scales in space and time.

In [84], Meiners and Quake reported a direct measurements of the hydrodynamic interactions between two colloidal particles. Two microscopic latex beads were held at

varying distances by optical tweezers. The position fluctuations of the beads were measured, from which correlation and cross-correlation functions were calculated (Fig. 6.13). The interesting feature of the experimental data is the presence of a pronounced time-delayed dip in the cross-correlations: the motion of the spheres is anti-correlated. It means that a stationary external potential can impose time-delayed correlations between particles and that one particle does "remember" where the other one was a short time before. The time delay is determined by the natural relaxation time of the harmonic well.

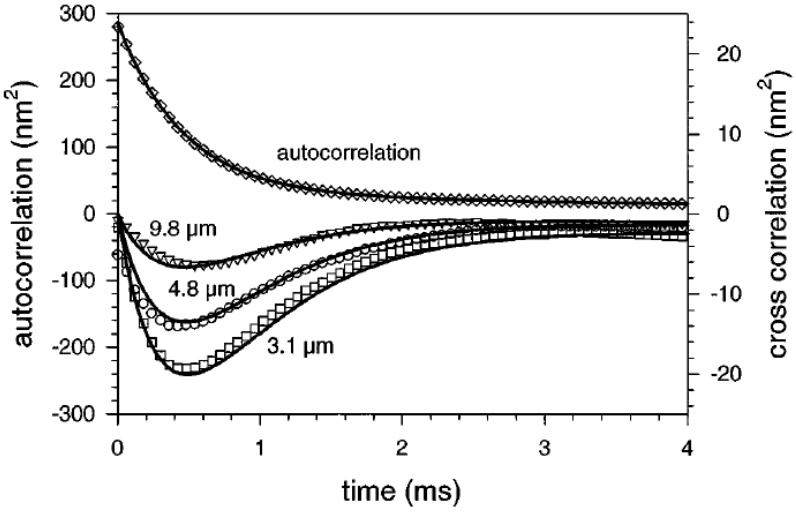

Figure 6.13.: *Longitudinal correlation functions of the position of the two beads in optical traps. The upper curve shows the autocorrelation function of a single bead in its trap, together with a double exponential fit. The lower curves show the cross-correlation functions of two beads held at separations of 9.8, 4.8, and 3.1 µm, respectively, together with the theoretically predicted curves. [84]*

There are Brownian dynamics simulations of such a system [85], with a very good agreement with theory. So it would be very interesting to check, if the hybrid MD/MPC simulations can reproduce these results. The idea was to place two colloidal particles in two MD regions separated by MPC zone with two buffer layers. By calculating the cross-correlation function it is possible to check whether hydrodynamic interaction between two colloidal particles are affected or not. Unfortunately, to simulate the system of the similar size as in the Meiners and Quake's experiment, one would need too much computing time, and simulations with an analogous smaller system didn't show any correlations.

7. Conclusions and outlook

In soft matter physics there is a variety of systems where phenomena occur on different time- and length scales which are inherently coupled. Examples of such systems are colloidal suspensions, polymer solutions and biological macromolecules. Hydrodynamic interactions play a fundamental role in the dynamics of such complex fluids. Therefore, simulations of such systems require a proper inclusion of solvent dynamics. On the other hand, it is important to describe microscopic interactions between atoms of solute and solvent. The full atomistic simulations would require too much computer time. Mesoscale methods are also not suited because they are not able to resolve microscopic interactions. To solve this problem, hybrid methods are being intensively developed, which combine the required features of the two representations.

The necessity to bridge the length- and time-scale gap between the solvent and solute molecules caused the development of a number of mesoscale simulation techniques. The mesoscale model of the solvent allows to take into account the influence of hydrodynamics on solute dynamics properly, but a reasonable description of the atomistic interaction between the solute and solvent molecules is still missing. The particle-based multi-scale simulation approach presented in this work, which couples Molecular Dynamics and Multi-Particle Collision dynamics simulations solves this problem. It allows to change the representation of the molecules composing the fluid "on the fly", taking into account the atomistic details where it is needed, while keeping the description of the rest of the fluid on the mesoscale level. Due to the application of the coarse-grained method, which is demanding less computational effort, it is possible to simulate larger systems for longer times. The capability to reach large length and long time scales is crucial for the study of complex molecular systems if hydrodynamics is of interest.

The coupling in the present approach is realized via a buffer layer separating the MD and MPC regions, which can freely exchange particles (chapter 3). While propagating from one region to another, a particle changes its "identity". For such a scheme there are two possibilities to construct the coupling: energy-based and force-based. Virtues and shortcoming of them were discussed, in a present work the force-based approach has been chosen. It was shown that the transport characteristics of the MPC fluid can be matched to those of the MD fluid by adjusting MPC parameters. It was found that due to the fundamental differences between MD and MPC methods it is impossible to achieve equilibrium between two representations. The different values of pressure and chemical potential cause a particle flux from the MD to the MPC region. Two possible

solutions of this problem are indicated. First, the MPC algorithm can be modified, making the MPC fluid non-ideal. Second, an external restraining force in the buffer zone can be introduced. Although the first possibility would be more "natural" and therefore more preferable, all tries to extend an MPC algorithm failed, that is why the second approach was adopted in the present work. Three ways to derive a restraining force are presented: using the pressure gradient in the buffer region, using the chemical potential gradient or through an iteration process, using the density gradient. All three restraining forces are shown to be able to prevent the MD particles from leaving the MD region. The restraining force derived by iteration also yields a desirable uniform density profile throughout the whole hybrid system.

The main goal of this work is to construct a coupling in such a way that the hydrodynamic interactions remain intact. To reveal the hydrodynamic properties of the hybrid fluid, several correlation functions for various systems consisting of particles with "mixed" identity (chapter 4) were calculated. It was found that transverse current correlation functions and long time tail of the velocity correlation function are equal for all such systems, i.e. "pure" MD, "pure" MPC and all "mixed identity" systems. Since these correlation functions are strongly related to the viscosity and diffusion coefficient, these results show that the transport properties of the fluid are not altered throughout the hybrid fluid.

Due to the principle differences between the two coupled fluid models, there are some fluid characteristics which cannot be matched. The MPC fluid has no excluded volume and has higher compressibility than the MD one. Because of that, the pair distribution functions, dynamic structure factors, longitudinal current correlation functions, and values for sound velocities are different for the systems consisting of particles with different "mixed" identities.

The hybrid nature of the system implies some specific features of the implementation (chapter5). The MP2C program was modified to assure a smooth transition of the MPC particles to the buffer region. Otherwise the new arrived particle can happen to appear too close to its neighbors, which would cause inconsistently large repulsive forces. The MD/MPC hybrid scheme can be parallelized. The parallelization of the program is based on a three-dimensional domain-decomposition approach, where particles are sorted onto processors according to their spatial coordinates. The program is written in module-oriented Fortran 90. Message passing between processors is realized with the MPI standard.

In order to probe, whether hydrodynamics is maintained in the hybrid system, several test simulations were performed (chapter 6). The transverse current correlation functions for the hybrid system are found to be in good agreement with theoretical predictions. The transverse current correlation functions calculated for the MD, MPC and

buffer regions separately show deviations from the expected values for some transversal modes with small wave vectors. It was shown that these deviations arise not from the inconsistencies of the hybrid scheme but from the way of calculating the correlation function only for part of the system. Also several simple flow simulations, such as Poiseuille flow, shear flow and Couette flow were performed. It was shown that the behavior of the hybrid system under flow parallel to the boundaries between the MD, MPC and buffer regions resembles that of a fluid modeled by a monoscale methods. For the Poiseuille and shear flows, the deviation of the velocity profile from the expected one is less than 2%. Also simulations with the hybrid system under the Poiseuille flow in the direction perpendicular to the buffer layer is performed. The velocity profiles for the MD, MPC and buffer regions were calculated separately. All show noticeable deviations from the expected theoretical curve.

The MD/MPC hybrid scheme and its presented implementation offers a wide range of possibilities for future enhancements. The coupling algorithm has to be extended to three dimensions, i.e. the MD region should be a sphere surrounded by the buffer shell. Since MD region will be represented by a sphere, it will be able to move within the system and meet other MD "spheres". Therefore, the algorithm of merging and dissociation of the MD zones should be proposed. The domain decomposition should not be static. Since the MD calculations are much more time-consuming than MPC ones, the domains should be able to adjust its boundaries depending on representation of the particles sorted to this domain.

Although the full thermodynamic equilibrium is impossible due the fundamental differences between MD and MPC methods, the hybrid MD/MPC scheme presented in this work is proved to be the very promising approach for simulation of the complex fluids. By applying the restraining force in the buffer zone it is possible to maintain dynamical equilibrium throughout the hybrid system. It was shown that the transport properties of the hybrid fluid remain the same across the buffer zone, allowing the consistent description of the hydrodynamics in the system. By changing the representation of the molecules "on the fly", the hybrid MD/MPC approach allows to couple within a single simulation atomistic and mesoscale representation of the fluids, providing a valuable tool for many problems in soft matter science.

A. Appendix

A.1. Collision rules for the non-ideal 3D MPC fluid

For the direction ζ_1:

$$\begin{cases} v_{i,x}(t+\Delta t) &= 2u_x - v_{i,x}(t) \\ v_{i,y}(t+\Delta t) &= v_{i,y}(t) \\ v_{i,z}(t+\Delta t) &= v_{i,z}(t) \end{cases}, \tag{A.1}$$

for the direction ζ_2:

$$\begin{cases} v_{i,x}(t+\Delta t) &= v_{i,x}(t) \\ v_{i,y}(t+\Delta t) &= 2u_y - v_{i,y}(t) \\ v_{i,z}(t+\Delta t) &= v_{i,z}(t) \end{cases}, \tag{A.2}$$

for the direction ζ_2:

$$\begin{cases} v_{i,x}(t+\Delta t) &= v_{i,x}(t) \\ v_{i,y}(t+\Delta t) &= v_{i,y}(t) \\ v_{i,z}(t+\Delta t) &= 2u_z - v_{i,z}(t) \end{cases}, \tag{A.3}$$

for the direction ζ_3:

$$\begin{cases} v_{i,x}(t+\Delta t) &= v_{i,x}(t) \\ v_{i,y}(t+\Delta t) &= v_{i,y}(t) \\ v_{i,z}(t+\Delta t) &= 2u_z - v_{i,z}(t) \end{cases}, \tag{A.4}$$

for the direction ζ_4:

$$\begin{cases} v_{i,x}(t+\Delta t) &= u_x + u_y - v_{i,y}(t) \\ v_{i,y}(t+\Delta t) &= u_x + u_y - v_{i,x}(t) \\ v_{i,z}(t+\Delta t) &= v_{i,z}(t) \end{cases}, \tag{A.5}$$

for the direction ζ_5:

$$\begin{cases} v_{i,x}(t+\Delta t) &= u_x + u_z - v_{i,z}(t) \\ v_{i,y}(t+\Delta t) &= v_{i,y}(t) \\ v_{i,z}(t+\Delta t) &= u_x + u_z - v_{i,x}(t) \end{cases}, \tag{A.6}$$

for the direction ζ_6:

$$\begin{cases} v_{i,x}(t+\Delta t) &= v_{i,x}(t) \\ v_{i,y}(t+\Delta t) &= u_y + u_z - v_{i,z}(t) \\ v_{i,z}(t+\Delta t) &= u_y + u_z - v_{i,y}(t) \end{cases}, \tag{A.7}$$

for the direction ζ_7:

$$\begin{cases} v_{i,x}(t+\Delta t) &= u_x - u_y + v_{i,y}(t) \\ v_{i,y}(t+\Delta t) &= -u_x + u_y + v_{i,x}(t) \\ v_{i,z}(t+\Delta t) &= v_{i,z}(t) \end{cases}, \tag{A.8}$$

for the direction ζ_8:

$$\begin{cases} v_{i,x}(t+\Delta t) &= u_x - u_z + v_{i,z}(t) \\ v_{i,y}(t+\Delta t) &= v_{i,y}(t) \\ v_{i,z}(t+\Delta t) &= -u_x + u_z + v_{i,x}(t) \end{cases}, \tag{A.9}$$

for the direction ζ_9:

$$\begin{cases} v_{i,x}(t+\Delta t) &= v_{i,x}(t) \\ v_{i,y}(t+\Delta t) &= u_y - u_z + v_{i,z}(t) \\ v_{i,z}(t+\Delta t) &= -u_y + u_z + v_{i,y}(t) \end{cases}. \tag{A.10}$$

A.2. Data structures

```
type, public   ::  solvent
     sequence
     ! mass
     real  (kind $=$ real_typ)    ::   m
     ! spacial coordinates
     real  (kind $=$ real_typ),dimension(dim)    ::   x
     ! velocity
     real  (kind $=$ real_typ),dimension(dim)    ::   v
     real  (kind $=$ real_typ),dimension(dim)    ::   v_rel
     ! absolute index of particle
     integer  :: i

type, public   ::  solute
     sequence
     ! mass
     real  (kind $=$ real_typ)    ::   m
     ! spacial coordinates
     real  (kind $=$ real_typ),dimension(dim)    ::   x
     ! velocity
     real  (kind $=$ real_typ),dimension(dim)    ::   v
     real  (kind $=$ real_typ),dimension(dim)    ::   v_rel
     ! force
     real  (kind $=$ real_typ),dimension(dim)    ::   v
     ! absolute index of particle
     integer  :: i
```

A.3. Force-shifted LJ potential

$$U^{fs}(r) = \begin{cases} br^3 + ar + q & , \quad r < r_a \\ 4\epsilon\left(\left(\frac{\sigma}{r_{ij}}\right)^{12} - \left(\frac{\sigma}{r_{ij}}\right)^{6}\right) + c(r - r_c) + d & , \quad r_a < r \\ 0 & , \quad r > r_c \end{cases} \tag{A.11}$$

and

$$\vec{f}^{fs}(\vec{r}) = \begin{cases} -3br\vec{r} - a\frac{\vec{r}}{r} & , \quad r < r_a \\ 48\epsilon\frac{\vec{r}}{r^2}\left(\left(\frac{\sigma}{r_{ij}}\right)^{12} - 0.5\left(\frac{\sigma}{r_{ij}}\right)^{6}\right) - c\frac{\vec{r}}{r} & , \quad r_a < r \\ 0 & , \quad r > r_c \end{cases} \tag{A.12}$$

where

$$c = 48\frac{\epsilon}{r_c}\left[\left(\frac{\sigma}{r_c}\right)^{12} - 0.5\left(\frac{\sigma}{r_c}\right)^{6}\right], \tag{A.13}$$

$$d = -4\epsilon\left[\left(\frac{\sigma}{r_c}\right)^{12} - \left(\frac{\sigma}{r_c}\right)^{6}\right], \tag{A.14}$$

$$b = 8\frac{\epsilon}{r_a^3}\left[13\left(\frac{\sigma}{r_a}\right)^{12} - 3.5\left(\frac{\sigma}{r_a}\right)^{6}\right], \tag{A.15}$$

$$a = c - 3br_a^2 - 48\frac{\epsilon}{r_a}\left[\left(\frac{\sigma}{r_a}\right)^{12} - 0.5\left(\frac{\sigma}{r_a}\right)^{6}\right], \tag{A.16}$$

$$q = 4\epsilon\left[\left(\frac{\sigma}{r_a}\right)^{12} - \left(\frac{\sigma}{r_a}\right)^{6}\right] + c(r_a - r_c) + d - br_a^3 - ar_a. \tag{A.17}$$

Here r_a is a point, where the Lennard-Jones potential function connect the polynomial function and can be chosen quite freely, it is 0.8σ in our simulation.

A.4. Transverse current correlations for hybrid system

$$
\begin{aligned}
J_t^{wh.sys.}(k,t) &= \frac{1}{N}\left\langle \sum_l^N v_{l,t}(0)e^{-i\mathbf{k}\mathbf{R}_l}(0) \sum_l^N v_{l,t}(t)e^{i\mathbf{k}\mathbf{R}_l}(t) \right\rangle \\
&= \frac{1}{N}\left\langle \left[\sum_l^{N_1} v_{l,t}(0)e^{-i\mathbf{k}\mathbf{R}_l}(0) + \sum_l^{N_2} v_{l,t}(0)e^{-i\mathbf{k}\mathbf{R}_l}(0) \right] \right. \\
&\quad \left. \cdot \left[\sum_l^{N_1} v_{l,t}(t)e^{i\mathbf{k}\mathbf{R}_l}(t) + \sum_l^{N_2} v_{l,t}(t)e^{i\mathbf{k}\mathbf{R}_l}(t) \right] \right\rangle \\
&= \frac{1}{N}\left\langle \left[j_t^{part1*}(k,0) + j_t^{part2*}(k,0) \right] \cdot \left[j_t^{part1}(k,t) + j_t^{part2}(k,t) \right] \right\rangle \qquad \text{(A.18)} \\
&= \frac{1}{N}\left\langle j_t^{part1*}(k,0) j_t^{part1}(k,t) + j_t^{part1*}(k,0) j_t^{part2}(k,t) \right. \\
&\quad \left. + j_t^{part2*}(k,0) j_t^{part1}(k,t) + j_t^{part2*}(k,0) j_t^{part2}(k,t) \right\rangle \\
&= \frac{\langle N_1 \rangle}{N} J_t^{part1}(k,t) + \frac{\langle N_2 \rangle}{N} J_t^{part2}(k,t) \\
&\quad + \frac{1}{N} J_t^{cross12}(k,t) + \frac{1}{N} J_t^{cross21}(k,t),
\end{aligned}
$$

Bibliography

[1] D.Frenkel and B.Smit *Understanding Molecular Simulation* (Academic press, San Diego, 2002)

[2] P.A.Egelstaff *"An introduction to the Liquid State* (Clarendon press, Oxford, 1992)

[3] P.Resibois and M. DeLeener *"Classical Kinetic Theory of Fluids"* (Wiley, New York, 1977)

[4] J.P.Boon and S.Yip *"Molecular Hydrodynamics"* (McGraw-Hill, New York, 1980)

[5] U.Balucani and Marco Zoppi *"Dynamics of the Liquid State"* (Clarendon press, Oxford, 1994)

[6] M.P. Allen, D.J.Tildesley *"Computer Simulation of Liquids"* (Clarendon Press, Oxford, 1989)

[7] J.P.Hansen and I.R.McDonald *"Theory of Simple Liquids"* (Elsevier, Amsterdam, 2006)

[8] D.J.Tritton *"Physical Fluid Dynamics"* (Clarendon Press, Oxford, 1988)

[9] MPI Forum, *A Message-Passing Interface Standand*, Version 2.2 (2009)

[10] B.J.Adler and T.E.Wainwright *"Phase transition for a hard sphere system"*, J.Chem.Phys. **27**, 1208 (1957)

[11] A.Rahman *"Correlations in the motion of atoms in liquid argon"*, Phys.Rev. **136**, A405 (1964)

[12] W. C. Swope, H. C. Andersen, P. H. Berens, and K. R. Wilson *"A computer simulation method for the calculation of equilibrium constants for the formation of physical clusters of molecules: Application to small water clusters"* J.Chem.Phys. **76**, 637 (1982)

[13] U.Frisch, B.Hasslacher, and Y.Pomeau *"Lattice Gas Automata for the Navier-Stokes equation"*, Phys. Rev. Lett. **56**, 1505 (1986)

[14] J.M.V.A.Koelman *"Cellular-automaton-based simulation of 2D polymer dynamics"*, Phys. Rev. Lett. **64**, 1915 (1990)

[15] G.R.McNamara and G.Zanetti *"Use of the Soltzmann equation to simulate Lattice-Gas Automata"*, Phys. rev. Lett. **61**, 2332 (1988)

[16] P.Lallemand and L.S.Luo *"Theory of the Lattice Boltzmann method: dispersion, dissipation, isotropy, galilean invariance, and stability"*, Phys. Rev. E **61**, 6546 (2000)

[17] R.Gingold and J. Monaghan *"Smoothed-Particle Hydrodynamics: theory and application to non-spherical stars"*, Mon. Not. R. Astron. Soc. **181**, 375 (1977)

[18] O.Kum, W.G.Hoover, and H.A.Posch *"Viscous conducting flows with smooth-particle applied mechanics"*, Phys. Rev. E **52**, 4899 (1995)

[19] P.J.Hoogerbrugge and J.M.V.A.Koelman *"Simulating microscopic hydrodynamic phenomena with Dissipative Particle Dynamics"*, Europhys. Lett. **19**, 155 (1992)

[20] P.Espanol and P.Warren *"Statistical mechanics of Dissipative Particle Dynamics"*, Europhys. Lett. **30**, 191 (1995)

[21] R.D.Groot and P.B.Warren *"Dissipative particle dynamics: bridging the gap between atomistic and mesoscopic simulation"*, J. Cem. Phys. **107**, 4423 (1997)

[22] N.Metropolis, A.W.Rosenbluth, M.N. Rosenbluth, A.H. Teller, and E.Teller *"Equation of state calculations by fast computing machines"*, J. Chem. Phys. **21**, 1087 (1953)

[23] G.A.Bird *"Approach to translational equilibrium in a rigid sphere gas"*, Phys. Fluids **6**, 1518 (1963)

[24] G.A.Bird *"Direct simulation and the Boltzmann equation"*, Phys. Fluids **13**, 2676 (1970)

[25] H.Tanaka and T.Araki *"Simulation method of colloidal suspensions with hydrodynamic Interactions: fluid particle dynamics"*, Phys. Rev. Lett. **85**, 1338 (2000)

[26] A.Malevanets and R.Kapral *"Mesoscopic model for solvent dynamics"*, J. Chem. Phys. **110**, 8605 (1999)

[27] A.Malevanets and R.Kapral *"Solute Molecular Dynamics in a mesoscale solvent"*, J. Chem. Phys. **112**, 7260 (2000)

[28] T.Ihle and D.M. Kroll *"Stochastic rotation dynamics: A Galilean-invariant mesoscopic model for fluid flow"*, Phys. Rev. E **63**, 020201 (2001)

[29] A.Lamura, G.Gompper, T.Ihle and D.M.Kroll *"Multi-Particle Collision dynamics: Flow around a circular and a square cylinder"*, Europhys. Lett. **56** (3), 319 (2001)

[30] T.Ihle and D.M. Kroll *"Stochastic rotation dynamics. I. Formalism, Galilean invariance, and Green-Kubo relations"*, Phys. Rev. E **67**, 066705 (2003)

[31] T.Ihle and D.M. Kroll *"Stochastic rotation dynamics. II. Transport coefficients, numerics, and long-time tails"*, Phys. Rev. E **67**, 066706 (2003)

[32] N.Kikuchi,C.M.Pooley,J.F.Ryder and J.MYeomans *"Transport coefficients of a mesoscopic fluid dynamics model"*, J.Chem. Phys. **119**, 6388 (2003)

[33] E. Tützel, M.Strauss, T.Ihle, and D.M.Kroll *"Transport coefficients for stochastic rotation dynamics in three dimensions"*, Phys. Rev. E **68**, 036701 (2003)

[34] M.Ripoll, K.Mussawisade, R.G.Winkler and G.Gompper *"Low-Reynolds-number hydrodynamics of complex fluids by Multi-Particle Collision dynamics"*, Europhys. Lett. **68** (1), 106 (2004)

[35] T.Ihle, E. Tützel, and D. M. Kroll *"Resummed Green-Kubo relations for a fluctuating fluid-particle model"*, Phys. Rev. E **70**, 035701 (2004)

[36] C.M.Poley and J.M.Yeomans *"Kinetic Theory Derivation of the Transport Coefficients of Stochastic Rotation Dynamics"*, J. Phys. Chem. B **109**, 6505 (2005)

[37] M.Ripoll, K.Mussawisade, R.G.Winkler and G.Gompper *"Dynamic regimes of fluids simulated by Multi-Particle Collision dynamics"*, Phys. Rev. E **72**, 016701 (2005)

[38] T. Ihle, E. Tützel, and D. M. Kroll *"Equilibrium calculation of transport coefficients for a fluid-particle mode"*, Phys. Rev. E **72**, 046707 (2005)

[39] E.Tüzel, T.Ihle, D.M.Kroll *"Dynamic correlations in stochastic rotation dynamics"*, Phys. Rev. E **74**, 056702 (2006)

[40] H.Noguchi, N.Kikuchi, and G.Gompper *"Particle-based mesoscale hydrodynamic techniques"* Europhys. Lett **78**, 10005 (2007)

[41] H.Noguchi and G.Gompper *"Transport coefficients of off-lattice mesoscale-hydrodynamics simulation techniques"*, Phys. Rev. E **78**, 016706 (2008)

[42] R.G.Winkler and C.C.Huang *"Stress tensors of multiparticle collision dynamics fluids"*, J. Phys. Chem. **130**, 074907 (2008)

[43] G. Gompper, T. Ihle, D. M. Kroll, and R. Winkler *"Multi-Particle Collision dynamics: a particle-based mesoscale simulation approach"*, Adv. in Polym. Sci **221**, 1-87 (2009)

[44] C.C.Huang, G.Gompper, and R.G.Winkler *"Hydrodynamic correlations in Multi-Particle Collision dynamics fluids"*, Phys. Rev. E **86**, 056711 (2012)

[45] E.Tüzel, T.Ihle, D.M.Kroll *"Consistent particle-based algorithm with a non-ideal equation of state"*, Europhys. Lett. **73**, 5, 664 (2006)

[46] T.Ihle *"Transport coefficients of Multi-Particle Collision algorithms with velocity-dependent collision rules"*, J.Phys. Cond. Matt. **20**, 235224 (2008)

[47] E.Tüzel, T.Ihle *"Static and dynamic properties of a particle-based algorithm for non-ideal fluids and binary mixtures"*, Prog. Comp. Fluid Dyn. **8,** 138 (2008)

[48] H. J. C. Berendsen, J. P. M. Postma, W. F. van Gunsteren, A. DiNola, and J. R. Haak *"Molecular dynamics with coupling to an external bath"*, J. Chem. Phys. **81**, 3684 (1984)

[49] H.C.Andersen *"Molecular dynamics simulations at constant pressure and/or temperature"*, J. Chem. Phys. **72**, 2384 (1980)

[50] E.Allahyarov and G.Gompper, *"Mesoscopic solvent simulations: Multiparticle-collision dynamics of three-dimensional flows"* Phys. Rev. E **66**, 036702 (2002)

[51] S. J. Zhou, D. M. Beazley, P. S. Lomdahl, and B. L. Holian *"Large-scale Molecular Dynamics simulations of three-dimensional ductile failure"*, Phys. Rev. Lett. **78**, 479 (1996)

[52] R. Schulz, B. Lindner, L. Petridis, and J. C Smith *"Scaling of multimillion-atom biological Molecular Dynamics simulation on a petascale supercomputer"*, J. Chem. Theor. and Comp. **5**, 2798 (2009)

[53] A.Warshel and M.Levitt *"Theoretical studies of enzymic reactions: Dielectric, electrostatic and steric stabilization of the carbonium ion in the reaction of lysozyme"*, J. Mol. Biol. **103**, 227 (1976)

[54] H.M.Senn and W.Thiel *"QM/MM Methods for Biomolecular Systems"*, Angew. Chem. Int. Ed. **48**, 1198 (2009)

[55] S.Kohlhoff, P.Gumbsch, and H.F.Fischmeister *"Crack propagation in b.c.c. crystals studied with a combined finiteelement and atomistic model"*, Phil. Mag. A **64**, 851 (1991)

[56] V.B.Shenoy, R.Miller, E.B.Tadmor, R.Phillips, and M.Ortiz *"Quasicontinuum models of interfacial structure and deformation"*, Phys. Rev. Lett. **80**, 742 (1998)

[57] R.Miller, M.Ortiz, R.Phillips, V.B.Shenoy, and E.B.Tadmor *"Quasicontinuum models of fracture and plasticity"*, Eng. Fract. Mech. **61**, 427 (1998)

[58] J.B.Bell, A.Garcia, and S.A.Williams *"Algorithm refinement for fluctuating h ydrodynamics"*, Multiscale Model. Simul. **6**, 1256 (2008)

[59] A.Donev, J.B.Bell, A.L.Garcia, and B.J.Alder *" A hybrid particle-continuum method for hydrodynamics of complex fluids"*, Multiscale Model. Simul. **8**, 871 (2010)

[60] M.Bckmann, D.Narx, C.Peter, L.Delle Site, K.Kremer, and N.LDoltsinis *"Multi-scale modelling of mesoscopic phenomena triggered by quantum events: light-driven azo-materials and beyond"*, Phys. Chem. Chem. Phys. **17**, 7604 (2011)

[61] M.Praprotnik, L. Delle Site, and K.Kremer *"Adaptive resolution molecular-dynamics simulation: Changing the degrees of freedom on the fly"*, J. Chem. Phys. **123**, 224106 (2005)

[62] M.Praprotnik, K.Kremer, and L. Delle Site *"Adaptive molecular resolution via a continuous change of the phase space dimensionality"*, Phys. Rev. E **75**, 017701 (2007)

[63] L. Delle Site *"Some fundamental problems for an energy-conserving adaptive-resolution Molecular Dynamics scheme"*, Phys. Rev. E **76**, 047701 (2007)

[64] S.Poblete, M.Praprotnik, K.Kremer, and L.Delle Site *"Coupling different levels of resolution in molecular simulations"*, J. Chem. Phys. **132**, 114101 (2010)

[65] R.Potestio, S.Fritsch, P.Espanol, R. Delgado-Buscalioni, K.Kremer, R.Everaers, and D.Donaldio *"Hamiltonian adaptive resolution simulation for molecular liquids"*, Phys. Rev. Lett. **110**, 108301 (2013)

[66] M.K.Petersen, J.B.Lechman, S.J.Plimpton, G.S.Grest, P.J. in't Veld, and P.R.Schunk *"Mesoscale hydrodynamics via stochastic rotation dynamics: Comparison with Lennard-Jones fluid"*, J. Chem. Phys. **132**, 174106 (2010)

[67] M.Shoen and C.Hoheisel *"The shear viscosity of a Lennard-Jones fluid calculated by equilibrium Molecular Dynamics"*, Mol. Phys. **56**, 3, 653 (1985)

[68] R.L.Rowley and M.M.Painter *"Diffusion and viscosity equations of state for a Lennard-Jones fluid obtained from Molecular Dynamics simulations"*, Int. J. Therm. **18**, 5, 1109 (1997)

[69] B.J.Alder and T.E.Wainwright *"Decay of the Velocity Autocorrelation Function*"*, Phys. Rev. A **1**, 18 (1970)

[70] R.Zwanzig and M.Bixon *"Hydrodynamic Theory of the Velocity Correlation Function*"*, Phys. Rev. A **2**, 2005 (1970)

[71] M.H.Ernst, E.H.Hauge, and J.M.J. van Leeuwen *"Asymptotic time behavior of correlation functions. I. Kinetic terms"*, Phys. Rev. A **4**, 2055 (1971)

[72] J.R.Dorfman and E.G.D.Cohen *"Velocity-correlation functions in two and three dimensions: Low density"*, Phys. Rev. A **6**, 776 (1972)

[73] J.R.Dorfman and E.G.D.Cohen *"Velocity-correlation functions in two and three dimensions. II. Higher density"*, Phys. Rev. A **12** , 292(1975)

[74] Y.Pomeau *"Low-frequency behavior of transport coefficients in fluids"*, Phys. Rev. A **5**, 2569 (1972)

[75] D.Levesque and W.T.Ashurst *"Long-time behavior of the velocity autocorrelation function for a fluid of soft repulsive particles"*, Phys. Rev. Lett **33**, 277 (1974)

[76] G.L.Paul and P.N.Pusey *"Observation of a long-time tail in Brownian motion"*, J. Phys. A **14**, 3301 (1981)

[77] A.McDonough, S.P.Russo and I.K.Snook *"Long-time behavior of the velocity autocorrelation function for moderately dense, soft-repulsive, and Lennard-Jones fluids"*, Phys. Rev E **63**, 026109 (2001)

[78] G. Sutmann, L. Westphal, and M. Bolten *"Particle based simulations of complex systems with MP2C : Hydrodynamics and electrostatics"* AIP Conf. Proc. **1281**, 1768 (2010)

[79] L.Verlet *"Computer "experiments" on classical fluids. I. Thermodynamical properties of Lennard-Jones molecules"*, Phys. Rev. **159**, 98 (1967)

[80] L.Verlet *"Computer "experiments" on classical fluids. II. Equilibrium correlation functions"*, Phys. Rev. **165**, 201(1968)

[81] D.Brown, J.H.R.Clarke, M.Okuda, and T.Yamazaki *"A domain decomposition parallelization strategy for Molecular Dynamics simulations on distributed memory machines"*, Comp. Phys. Comm. **74**, 67 (1993)

[82] C.C.Huang, A.Chatterji, G.Sutmann, G.Gompper, R.G.Winkler *"Cell-level canonical sampling by velocity scaling for Multi-Particle Collision dynamics simulations"*, J. Comp. Phys. **229**, 168 (2010)

[83] M.T.Matthews and J.M.Hill *"On three simple experiments to determine slip lengths"*, Microfluid. Nanofluid. **6**, 611 (2009)

[84] J.-C.Meiners and S.R.Quake *"Direct measurement of hydrodynamic cross correlations between two particles in an external potential"*, Phys. Rev. Lett. **82** (10), 2211 (1999)

[85] M.Reichert *"Hydrodynamic Interactions in Colloidal and Biological Systems"* (Universität Konstanz, 2006)

Acknowledgments

First of all I would like to express my sincere gratitude to my advisors Dr. Godehard Sutmann and Prof. Dr. Roland G. Winkler for their supervision and guidance. They are most responsible for helping me understand intricate features of fluid dynamics and molecular hydrodynamics. Without their help and support this work could not have been accomplished.

A special thanks go to the Dr. I. Kabadshow who seems not only be able to understand and fix any occurring software malfunction but can also always find a few right words to encourage and cheer up people in every situation.

I'm very thankful to the JSC team, which has done an excellent job providing reliable supercomputing resources. I would also like to thank the German Research School for Simulation Sciences for funding my work.